



HAL
open science

Geochemistry of Zr, Hf and REE in extreme water environments: hyperacid, hypersaline and lake waters in hydrothermal systems

Claudio Inguaggiato

► **To cite this version:**

Claudio Inguaggiato. Geochemistry of Zr, Hf and REE in extreme water environments: hyperacid, hypersaline and lake waters in hydrothermal systems. Geochemistry. Université Pierre et Marie Curie - Paris VI; Università degli studi (Palerme, Italie), 2016. English. NNT : 2016PA066007 . tel-01356129

HAL Id: tel-01356129

<https://theses.hal.science/tel-01356129>

Submitted on 7 Jul 2017

HAL is a multi-disciplinary open access archive for the deposit and dissemination of scientific research documents, whether they are published or not. The documents may come from teaching and research institutions in France or abroad, or from public or private research centers.

L'archive ouverte pluridisciplinaire **HAL**, est destinée au dépôt et à la diffusion de documents scientifiques de niveau recherche, publiés ou non, émanant des établissements d'enseignement et de recherche français ou étrangers, des laboratoires publics ou privés.



UNIVERSITÀ
DEGLI STUDI
DI PALERMO

UPMC
SORBONNE UNIVERSITÉS



UNIVERSITÉ
FRANCO
ITALIENNE

UNIVERSITÀ
ITALO
FRANCESE

Università degli Studi di Palermo (Palermo, Italy)
Dipartimento di Scienze della Terra e del Mare (DiSTeM)

Université Pierre et Marie Curie-Sorbonne Universités (Paris, France)
Institut des Sciences de la Terre de Paris (ISTeP)

Co-supervision PhD in Geochemistry

DOTTORATO DI RICERCA IN SCIENZE DELLA TERRA – GEOCHIMICA XXVI° CICLO (GEO/08)
ECOLE DOCTORALE: GEOSCIENCES, RESSOURCES NATURELLES ET ENVIRONNEMENT (ED 398)
DISCIPLINE GEOCHIMIE

Geochemistry of Zr, Hf and REE in extreme water environments: hyperacid, hypersaline and lake waters in hydrothermal systems

PhD thesis by

Claudio Inguaggiato

Supervisors:

Prof. Paolo Censi
(Università degli Studi di Palermo)

Prof. Pierpaolo Zuddas
(Université Pierre et Marie Curie)

Dr. Walter D'Alessandro
(Istituto Nazionale di Geofisica e Vulcanologia)

PhD Coordinators:

Prof. Francesco Parello
(Università degli Studi di Palermo)

Prof. François Baudin
(Université Pierre et Marie Curie)



UNIVERSITÀ
DEGLI STUDI
DI PALERMO

UPMC
SORBONNE UNIVERSITÉS



UNIVERSITÉ
FRANCO
ITALIENNE

UNIVERSITÀ
ITALO
FRANCESE

Università degli Studi di Palermo (Palermo, Italy)
Dipartimento di Scienze della Terra e del Mare (DiSTeM)

Université Pierre et Marie Curie-Sorbonne Universités (Paris, France)
Institut des Sciences de la Terre de Paris (ISTeP)

Co-supervision PhD in Geochemistry

DOTTORATO DI RICERCA IN SCIENZE DELLA TERRA – GEOCHIMICA (XXVI° CICLO)
ECOLE DOCTORALE GEOSCIENCES, RESSOURCES NATURELLES ET ENVIRONNEMENT (ED 398)
DISCIPLINE GEOCHIMIE

***Geochemistry of Zr, Hf and REE in extreme water environments: hyperacid,
hypersaline and lake waters in hydrothermal systems***

PhD thesis by
Claudio Inguaggiato

Supervisors:

Prof. Paolo Censi
(Università degli Studi di Palermo)
Prof. Pierpaolo Zuddas
(Université Pierre et Marie Curie)
Dr. Walter D'Alessandro
(Istituto Nazionale di Geofisica e Vulcanologia)

PhD Coordinators:

Prof. Francesco Parello
(Università degli Studi di Palermo)
Prof. François Baudin
(Université Pierre et Marie Curie)

Reviewers:

Prof. Yuri Taran (Universidad Nacional Autónoma de México)
Prof. Franco Tassi (Università degli Studi di Firenze)
Prof. Johan C. Varekamp (Wesleyan University)

Board of Examiners:

Prof. Paolo Censi (Università degli Studi di Palermo)
Prof. Mariano Valenza (Università degli Studi di Palermo)
Prof. Orlando Vaselli (Università degli Studi di Firenze)
Prof. Pierpaolo Zuddas (Université Pierre et Marie Curie)
Prof. Christian Gorini (Université Pierre et Marie Curie)
Prof. Sylvain Huon (Université Pierre et Marie Curie)

ABSTRACT

This PhD thesis concerns the geochemistry of Zr, Hf and REE in extreme water environments characterized by a wide spectrum of chemical physical-parameters and compositions. The investigations were carried out in hypersaline waters covering a wide range of Eh values along Dead Sea Fault (Israel), in hyperacid waters circulating in Nevado del Ruiz volcano-hydrothermal system (Colombia) and in CO₂-rich waters belonging to the Pantelleria volcano-hydrothermal system (Italy), including the alkaline lake “Specchio di Venere” formed within a calderic depression. The wide spectrum of chemical-physical conditions and various water chemical compositions interacting with different solid phases allowed to depict a scenario where Zr, Hf and REE are ruled by different processes, filling the still missing geochemical aspects.

The important role of the pH (from 1 to 8.8) and the water chemical composition in regard to the distribution of Zr, Hf and REE was mainly investigated in the Nevado del Ruiz volcano-hydrothermal system. The pH rules the precipitation of authigenic Fe-, Al-oxyhydroxides producing changes in Zr, Hf and REE abundances and strong cerium anomaly. Significant LREE (Light Rare Earth elements) depletion was found in acidic sulphate waters, where the formation of alunite and jarosite was recognized. Sub-chondritic Zr/Hf ratios (lower than magmatic local rocks) and chondritic Y/Ho ratios (close to the local magmatic rocks) are shown in acidic sulphate waters ($1 < \text{pH} < 3.6$). Zr/Hf ratio increases as Cl/SO₄ ratio increases, suggesting a different behaviour of Zr and Hf as function of complexing ligands in solution. Differently to the acid waters, the same fractionation of Y-Ho and Zr-Hf was found in near neutral waters where Al-, Fe-oxyhydroxides were found. The twin pairs show Y/Ho and Zr/Hf ratios increasing towards super-chondritic values due to the preferential removal of Ho and Hf compared to Y and Zr by Al-, Fe-oxyhydroxides.

Pantelleria hydrothermal waters are dominated by Na and Cl ions with variable HCO₃⁻ enrichments due to the interaction with deep-seated CO₂. Different behaviour of Zr, Hf and REE

was found in the alkaline lake “Specchio di Venere” with respect to the CO₂-rich thermal waters circulating in the Pantelleria volcano-hydrothermal system. Shale-normalised REE (relative to Post Archean Australian Shale, PAAS) in CO₂-rich waters showed the same pattern increasing along the REE series, with the elemental speciation dominated by carbonate ligands. Zr, Hf and REE show higher concentrations in lake “Specchio di Venere” with intermediate REE (MREE) enrichments and positive Ce anomaly. Similar features (MREE enriched and positive Ce anomaly) were found in the settling dust and in the Desert Varnish, mainly constituted by Fe-, Mn-oxyhydroxides and clay minerals. Moreover, Y/Ho and Zr/Hf molar ratios in “Specchio di Venere” lake (35.37 and 76.30, respectively) show also a Desert Varnish signature. These latter data, coupled with the MREE enrichments and the presence of Fe-oxyhydroxides and phyllosilicates in the shallowest water layer of “Specchio di Venere”, testify for an aeolian input from the nearby Sahara desert demonstrating that Zr, Hf and REE are useful tracers to identify the contribution of atmospheric particle in open water bodies.

The key role of the Eh values and the water composition towards the distribution of Zr, Hf and REE was mainly evaluated in waters along the Dead Sea Fault. Here, both cold and hot waters fall within a wide range of salt contents (from 0.3 to 193.5 g l⁻¹) and Eh values (from -400 to 256 mV). These waters are mainly NaCl dominated with variable enrichments in SO₄, HCO₃ and Ca due to water rock-interactions. The investigated waters are oversaturated with respect to carbonate minerals, Fe-, Mn-oxyhydroxides and pyrite, and always undersaturated in gypsum and halite. The REE distribution shows MREE enrichments, due to the dissolution of evaporitic minerals characterized by MREE enrichments. The redox conditions influence the amplitude of Ce and Eu anomalies. Oxidized waters show negative Ce anomalies related to the oxidative Ce scavenging, whereas positive Eu anomalies are found in waters characterised by Eh values < -100 mV consistently with the Eu occurrence as the dissolved Eu²⁺. This condition enhances the Eu stability in dissolved phase relatively to its trivalent neighbours along the REE series. Since dissolved Zr/Hf

molar ratio is sensitive to the occurrence of solid Fe-oxyhydroxide surfaces where Hf is preferentially scavenged, redox conditions influence the Zr/Hf signature in these waters despite neither Zr nor Hf are redox sensitive elements. Therefore, the Zr and Hf in waters oversaturated with respect to Fe-oxyhydroxides show superchondritic Zr/Hf values due to the preferential Hf scavenging onto solid surfaces whereas the waters oversaturated relative to pyrite show chondritic Zr/Hf signatures.

RIASSUNTO

Questa tesi di dottorato è incentrata sullo studio del comportamento geochimico di Zr, Hf e Terre Rare in ambienti acquosi estremi, caratterizzati da un ampio spettro di parametri chimico-fisici e di composizione chimica delle acque. Gli studi sono stati condotti in differenti sistemi naturali ognuno dei quali aventi delle specifiche caratteristiche: i) acque ipersaline lungo la faglia del Mar Morto (Israele) dove esiste un ampio range di valori di Eh, ii) acque iperacide circolanti nel sistema vulcanico-idrotermale del Nevado del Ruiz (Colombia) e iii) acque ricche in CO₂ circolanti nel sistema vulcanico-idrotermale dell'Isola di Pantelleria, includendo il lago alcalino "Specchio di Venere". L'ampio spettro di condizioni chimico-fisiche e la diversa composizione delle acque interagenti con le fasi solide di diversa natura, hanno permesso di investigare il comportamento geochimico di Zr, Hf e Terre Rare in fase acquosa, colmando gli aspetti geochimici ancora oggi mancanti.

L'importante ruolo svolto dal pH (1-8.8) e dalla composizione chimica dell'acqua nei confronti della distribuzione di Zr, Hf e Terre Rare è stato studiato principalmente nel sistema vulcanico-idrotermale del Nevado Del Ruiz. Il pH gioca un ruolo fondamentale riguardo alla precipitazione degli ossidrossidi di ferro e alluminio, inducendo variazioni delle concentrazioni di Zr, Hf e Terre rare e significative anomalie positive di cerio. Elevati impoverimenti in Terre rare leggere sono stati riscontrati nelle acque acide solfato dominante dove è stata riconosciuta la formazione di alunite e jarosite. Le acque solfato acide ($1 < \text{pH} < 3.6$) sono caratterizzate da rapporti di Zr/Hf sub-condritici (inferiori rispetto alle rocce locali) e rapporti condritici di Y/Ho (simili ai rapporti delle rocce locali). I rapporti molari di Zr/Hf mostrano valori crescenti al crescere del rapporto Cl/SO₄ suggerendo un differente comportamento di Zr e Hf in funzione della loro complessazione ionica al variare del rapporto dei leganti ionici presenti in soluzione. Differentemente alle acque acide, i rapporti di Y/Ho e Zr/Hf nelle acque vicino alla neutralità crescono verso valori sempre più super-

condritici, a causa della rimozione preferenziale di Hf e Ho rispetto a Zr e Y da parte degli ossidrossidi di ferro e alluminio.

Le acque idrotermali di Pantelleria hanno una composizione chimica dominata da Na e Cl, con concentrazioni variabili di HCO_3 dovute all'interazione della CO_2 (principalmente di origine magmatica) con le acque del sistema idrotermale. E' stato riscontrato un differente comportamento di Zr, Hf e Terre Rare nell'acqua del lago Specchio di Venere rispetto alle acque circolanti nel sistema idrotermale. Le Terre Rare normalizzate al PAAS (Post Archean Australian Shale) mostrano degli andamenti progressivamente crescenti dal La al Lu e sono principalmente complessate dalle specie carbonatiche. Il lago Specchio di Venere comparato con le acque idrotermali, mostra delle concentrazioni maggiori di Zr, Hf e Terre Rare, con un arricchimento in Terre rare intermedie e anomalia positiva di Ce. Caratteristiche simili sono state trovate nel Desert Varnish (fase solida presente in ambienti aridi) costituito principalmente da minerali argillosi e ossidrossidi di Fe e Mn. I rapporti molari di Y/Ho e Zr/Hf nello Specchio di Venere (35.37 e 76.30, rispettivamente) sono caratterizzati da valori molto simili a quelli trovati nel Desert Varnish. La distribuzione del pattern delle Terre Rare, insieme ai rapporti di Y/Ho e Zr/Hf e alla presenza di fillosilicati e ossidrossidi di Fe nello strato più superficiale dello Specchio di Venere, testimoniano l'interazione tra il particolato atmosferico proveniente dal vicino deserto del Sahara e il lago Specchio di Venere, dimostrando che Zr, Hf e Terre Rare sono degli utili traccianti in grado di identificare il contributo del particolato atmosferico nei corpi idrici superficiali.

Il ruolo chiave svolto dalle variazioni di Eh nei confronti della distribuzione di Zr, Hf e Terre Rare è stato principalmente valutato nelle acque presenti lungo la faglia del Mar Morto, caratterizzate da un ampio range di valori di Eh (da -400 a 390 mV) e da un contenuto in sali disciolti tra 0.3 e 193.4 g l^{-1} . Le acque hanno contenuti di Na e Cl dominanti con variabili arricchimenti in SO_4 , HCO_3 e Ca, causati dall'interazione delle acque con le rocce locali. Inoltre, le acque sono sovrassature in minerali carbonatici, pirite e ossidrossidi di Fe e Mn, mentre sono sottosature rispetto a gesso e

alite. Alcune acque mostrano arricchimenti in Terre rare intermedie, principalmente causati dalla dissoluzione di minerali evaporitici. Le grandi variazioni redox riscontrate in questo sistema idrotermale sono la causa delle anomalie di Eu e Ce riconosciute nelle acque. Le acque ossidate mostrano anomalie negative di cerio dovute allo scavenging ossidativo, mentre anomalie positive di europio sono presenti nelle acque caratterizzate da valori di $E_h < -100$ mV dovute alla presenza dell' Eu^{2+} in fase disciolta. Queste condizioni estremamente riducenti aumentano la stabilità dell' Eu^{2+} rispetto agli elementi vicini (con stato di ossidazione 3+) lungo la serie delle Terre Rare. Il rapporto Zr/Hf è sensibile alla presenza di ossidrossidi di ferro che causano la principale rimozione di Hf rispetto a Zr sulle superfici dei minerali. Sebbene Zr e Hf non siano elementi sensibili alle variazioni redox del sistema, il rapporto Zr/Hf è influenzato dalle variazioni di E_h che inducono variazioni della stabilità degli ossidrossidi di ferro. Pertanto, il rapporto Zr/Hf nelle acque sovrassature in ossidrossidi di ferro mostrano valori super-condritici causati dalla preferenziale rimozione di Hf sulle superfici dei solidi, mentre le acque sovrassature in pirite mostrano rapporti Zr/Hf simili ai valori condritici.

RÉSUMÉ

Cette thèse de doctorat traite du comportement géochimique de Zr, Hf et Terres Rares dans des environnements aqueux extrêmes, caractérisés par une grande variété de paramètres chimiques et physiques et de composition chimique de l'eau. Les études ont été effectuées dans des systèmes naturels différents dont chacun ayant des caractéristiques spécifiques: dans les eaux hyper-salines long de la faille de la Mer Morte (Israël), caractérisée par une large gamme de valeurs d'Eh, les eaux hyper-acides qui circulent dans le système volcanique hydrothermal du Nevado del Ruiz (Colombie) et les eaux riches en CO₂ du système volcanique hydrothermal de l'île de Pantelleria, en comprenant le lac alcalin "Specchio di Venere". Le large éventail de conditions physico-chimiques et la composition différente des eaux en interaction avec les phases solides de nature différente, ont permis d'étudier Zr, Hf et les Terres rares dans un scénario complet, en mettant en évidence les aspects géochimiques encore absents pour ce qui concerne le comportement de ces éléments dans la phase aqueuse.

Le rôle important joué par le pH (1 à 8.8) et par la composition chimique de l'eau par apport à la distribution de Zr, Hf et Terre Rares a été étudié principalement dans le système volcanique hydrothermal du Nevado del Ruiz. Le pH joue un rôle fondamental en ce qui concerne la précipitation des oxyhydroxydes de fer et d'aluminium, ce qui induit des variations des concentrations de Zr, Hf et Terres rares et considérables anomalies positives de cérium. Haute appauvrissement en Terres Rares légères ont été trouvés dans les eaux acide dominées par le sulfate où on a reconnu la formation d'alunite et jarosite. Les eaux sulfates acides ($1 < \text{pH} < 3.6$) se caractérisent par des relations de Zr/Hf sous-condritique (inférieur aux roches locales) et des relations condritique de Y/Ho (semblables aux valeurs des roches locales). Les rapports molaires de Zr/Hf augment à l'augmentation du rapport Cl/SO₄ en suggérant un comportement différent de Zr et Hf qui pourrait dépendre de la complexation des ions en solution. Contrairement aux eaux acides,

les relations de Y/Ho et Zr/Hf dans les eaux proches de la neutralité, augmentent vers des valeurs super-condritiques, en raison de l'élimination préférentielle par les oxyhydroxydes de fer et d'aluminium de l'Hf et Ho que de Zr et Y.

Les eaux hydrothermales de Pantelleria ont une composition chimique dominée par Na et Cl, avec des concentrations variables de HCO_3 due à l'interaction de CO_2 (principalement d'origine magmatique) avec les eaux du système hydrothermal. On a constaté un comportement différent de Zr, Hf et Terres Rares dans l'eau du lac "Specchio di Venere" par rapport aux eaux thermales qui circulent dans le système hydrothermal. Les Terres Rares normalisées à PAAS (Post Archean Australian Shale) croissent du La au Lu et sont complexées par les espèces carbonatées. Le lac "Specchio di Venere" comparé aux eaux hydrothermales, montre des concentrations plus élevées en Zr, Hf et de Terres Rares, ainsi qu'un enrichissement de Terres Rares intermédiaires et une anomalie positive de Ce. Caractéristiques similaires se retrouvent dans les poudres du Desert Varnish (phase solide présente dans les environnements arides) composé principalement de minéraux argileux et oxyhydroxydes de Fe et Mn. Les rapports molaires de Y/Ho et Zr/Hf du "Specchio di Venere" (respectivement, 35.37 et 76.30) sont proches des valeurs trouvés dans les poudres du Desert Varnish. La distribution des Terres Rares, avec les rapports de Y/Ho et Zr/Hf et la présence de phyllosilicates et oxyhydroxydes de fer dans la couche superficielle du "Specchio di Venere" montrent l'interaction entre les particules atmosphériques qui provient du désert du Sahara et le lac "Specchio di Venere", démontrent que Zr, Hf et terres rares sont de traceur utiles, capables d'identifier la contribution des particules atmosphériques dans les bassins.

Le rôle crucial joué par les changements de Eh par rapport à la distribution de Zr, Hf et Terres Rares a été évalué principalement dans les eaux étudiées le long la faille de la Mer Morte. Ces eaux sont caractérisées par une large gamme de contenu en sel (de 0.3 à 193.4 g l⁻¹) et de valeurs de Eh (de -400 à 390 mV). Les eaux sont caractérisées principalement par le contenu de Na et Cl dominants avec enrichissement variable dans SO_4 , HCO_3 et Ca, provoqués par l'interaction de l'eau

avec les roches locales. Les eaux sont sursaturées en minéraux carbonatés, pyrite et oxyhydroxydes de Fe et Mn, tandis que toujours soussaturées en gypse et halite. Certaines eaux montrent des enrichissements en Terres Rares intermédiaire, principalement causés par la dissolution des minéraux évaporitiques. Les grandes variations redox observées dans ce système hydrothermal sont la cause des anomalies de Eu et Ce reconnues dans les eaux. Les eaux oxydés montrent des anomalies négatives de cérium en raison du *scavenging* oxydatif, tandis que des anomalies positives de l'euprium sont présents dans les eaux caractérisées par des valeurs de Eh <-100mV en raison de la présence du Eu^{2+} dans la phase dissoute. Ces conditions extrêmement réductrices augmentent la stabilité du Eu^{2+} par rapport aux éléments proches (à l'état d'oxydation 3+) tous le long de la série des Terres Rares. Le rapport Zr/Hf est sensible à la présence d'hydroxydes de fer qui provoquent l'enlèvement principal de Hf par rapport à Zr sur les surfaces des minéraux. Bien que Zr et Hf ne sont pas de éléments sensibles aux variations redox du système, le rapport Zr/Hf est influencée par les changements de Eh qui induisent des changements dans la stabilité des oxyhydroxydes de fer. En conséquence, le rapport Zr/Hf dans les eaux sursaturées d'oxyhydroxydes de fer présentent des valeurs sur-condritiques provoqués par l'élimination préférentielle de Hf sur les surfaces des solides, tandis que les eaux sursaturées de pyrite montrent des rapports Zr/Hf semblables aux valeurs condritiques.

ACKNOWLEDGEMENTS

I would like to thank my supervisors Prof. Paolo Censi, Prof. Pierpaolo Zuddas and Dr. Walter D'Alessandro for their willingness to help me at any time, for providing me with ideas that allowed me to carry out this PhD in a remarkable way. I am glad and honoured that they shared with me their scientific knowledge that they acquired during their career, providing me with the “tools” to start new scientific researches in the near future.

I am grateful to the INGV (Istituto Nazionale di Geofisica e Vulcanologia-Palermo) and their staff for the analytical support and the constructive discussion. In particular, I thank Salvatore Francofonte, Lorenzo Brusca, Sergio Bellomo, Mariano Tantillo, Aldo Sollami, Dr. Ygor Oliveri and Francesco Salerno who were always helpful at any time.

I would like to thank the “Università Italo-Francese” for funding part of the study carried out in Université Pierre et Marie Curie (Paris). Moreover, I thank the Geological Survey of Israel (Jerusalem) and the Servicio Geologico Colombiano (Observatorio Vulcanologico y Sismologico de Manizales) to help me in organizing the field trips and for the scientific discussions and their suggestions.

I thank my parents Salvatore and Rosaria for supporting me morally and economically, spending their time and money to make sure I could grow up in the best way, both personally and academically. They took care of me in the most difficult moments during my young life. One of the most important that lessons my parents taught me was to remember the importance of the equilibrium between work and everyday life, considering the latter mainly based on moral values, family and friends, which are fundamental to live life to the fullest.

I thank my brother who was able to make me laugh during the few moments of tiredness with his positivity and his unique and ironic approach to life.

Special thanks to my father who since I was child, showed me the beauties of nature,

unconsciously enhanced in me the love and the curiosity for the earth science. He took me with him during many field trips in volcanic systems, showing me wonderful natural places that I will remember forever. Moreover, he taught me so much about geochemistry, stimulating my ideas and curiosity about the research.

I want to thank my girlfriend Simona who supported me during the last year I apologize because I could not spend as much time as I wanted with her lately; I hope to spend more time with her in the near future. Moreover, I think that, hearing my scientific discussions and looking with curiosity at the articles that I wrote during the past three years, she has learned unconsciously a little bit of geochemistry.

Last but not least, I want to thank my friends with whom I shared the relaxed moments during these three years; in particular, I would like to thank Mario, Luigi, Benedetto and Alessio.

CONTENTS

ABSTRACT.....	I
RIASSUNTO	IV
RÉSUMÉ	VII
ACKNOWLEDGEMENTS	X
CONTENTS.....	XII
LIST OF FIGURES	XV
PREFACE	1
CHAPTER 1 Introduction.....	3
1.1 General aspects and aim of the work	3
1.2 The aqueous geochemistry of REE.....	6
1.3 The normalization of REE	8
1.4 The aqueous geochemistry of zirconium and hafnium	9
CHAPTER 2 Investigated areas and background information	11
2.1 Nevado del Ruiz.....	11
2.2 Pantelleria Island.....	13
2.3 Dead Sea Fault area.....	16
CHAPTER 3 Materials and methods	20
3.1 Sampling and analytical methods	20
3.2 Method to determine Zr, Hf and REE in Dead Sea Fault and Pantelleria waters.....	21
3.3 Speciation calculations and saturation indexes.....	22
3.4 Equation to determine anomalies of REE	22
CHAPTER 4 Geochemistry of Zr, Hf and REE in a wide range of pH and water composition: The Nevado del Ruiz volcano-hydrothermal system (Colombia).....	23

4.1	RESULTS	23
4.1.1	General aspects	23
4.1.2	REE, Zr and Hf	28
4.2	DISCUSSION	31
4.2.1	REE behaviour	31
4.2.2	The behaviour of twin pairs (Y-Ho; Zr-Hf)	36
4.3	CONCLUDING REMARKS	38
CHAPTER 5 Zr-Hf and REE signatures discriminating the effect of atmospheric fallout from the hydrothermal input in volcanic lake waters		
		40
5.1	RESULTS	40
5.1.1	General aspects	40
5.1.2	REE, Zr and Hf	45
5.2	Discussions.....	48
5.2.1	Aqueous speciation	48
5.2.2	REE behaviour in springs and wells	49
5.2.3	Ce anomaly	52
5.2.4	Y/Ho and Zr/Hf fractionation in spring and wells	53
5.2.5	The source of REE, Zr and Hf in “Specchio di Venere”	55
5.3	Concluding remarks	57
CHAPTER 6 Geochemistry of Zr, Hf and REE in a wide spectrum of Eh and water composition: The case of the Dead Sea Fault system (Israel)		
		59
6.1	RESULTS	59
6.1.1	General aspects	59
6.1.2	REE, Zr and Hf	65
6.2	DISCUSSION	68

6.2.1	Zirconium and hafnium.....	68
6.2.2	Yttrium and Holmium.....	71
6.2.3	REE distribution.....	71
6.3	CONCLUDING REMARKS.....	73
CHAPTER 7	General conclusions.....	75
CHAPTER 8	Geochemical characterisation of gases along the Dead Sea Rift: Evidences of mantle-CO ₂ degassing.....	78
8.1	INTRODUCTION.....	79
8.2	MATERIALS AND METHODS.....	81
8.3	RESULTS AND DISCUSSION.....	83
8.3.1	Mantle derived helium along Dead Sea Fault.....	89
8.3.2	Origin of CO ₂	93
8.4	IMPLICATIONS.....	97
8.5	CONCLUNDING REMARKS.....	98
CHAPTER 9	References.....	100
APPENDIX	113

LIST OF FIGURES

Fig. 1.1 - Stability complexes for the formation of lanthanides complexes (Millero, 1992).....	8
Fig. 1.2 – The distribution of REE (ppm) in Chondrite, PAAS and UCC (Data from: Taylor and McLennan 1985; 1995; McDonough and Sun 1995).....	9
Fig. 2.1 – Location map of Nevado del Ruiz volcano. Active subduction of Nazca Plate below the South American plate, generating the volcanism along the chain of the Andes.....	11
Fig. 2.3 – Location map of Pantelleria volcanic island. Main tectonic features of Strait of Sicily (Esperança e Crisci 1993).	13
Fig. 2.4 – Geologic map of Pantelleria volcanic island (Orsi, 2003).....	14
Fig. 2.5 - Photo representing an overview of “Specchio di Venere” alkaline lake.....	16
Fig. 2.7 – Photo representing an overview of Dead Sea.	19
Fig. 4.1 - Location map of sampled waters.....	23
Fig. 4.3 - SEM-EDS observations of SPM showing: in Group 1a Al-, Fe- oxyhydroxides encrusting amorphous silica (a); in Group 2a, silica sphere probably encrusting biological matter (b), Fe (partially Ca) rich solids (probably sulphates) onto amorphous silica (c), Fe-, Al-, rich solids.	26
Fig. 4.4 - Isosol diagram is a log-log compositional plot, with the average volcanic rock composition versus the water composition. Isosol lines represent the equal amount of rock dissolved for the element considered. The plot shows the near-congruent dissolution of Group 2b (acid waters) and the depletion in K, Na, Fe, Al, in Group 2a (acid waters). The Group 2 shows a rock dissolution ranging between 5 and 10 g/l. Group 1 (near-neutral pH) is strongly depleted in Fe, Al reflecting the precipitation of Fe, Al- oxyhydroxides. (probably sulphates) onto amorphous silica (d).....	27
Fig. 4.5 - Variations of total REE dissolved in water as a function of pH. Symbols as in Fig. 4.2...	28

Fig. 4.6 - Average local rock-normalized REE patterns dissolved in water.....	30
Fig. 4.7 - Zr/Hf and Y/Ho (molar ratios). Symbols as in Fig. 4.2, blue circle represent Y/Ho and Zr/Hf (molar ratios) in average local rock.	31
Fig. 4.8 - Total amount of REE versus Fe, Al dissolved in waters. Symbols as in Fig. 4.2.....	32
Fig. 4.9 - Variations of total REE dissolved in water as a function of pH. Symbols as in Fig. 4.2...36	
Fig. 4.10 - Zr/Hf versus Cl/SO ₄ (molar ratios) in acidic waters (Group 2). Symbols as in Fig. 4.2. 38	
Fig. 5.1 – Location map of sampled waters.	41
Fig. 5.2 – a) Triangular plot of major anions dissolved in waters. b) Triangular plot of major cations dissolved in waters.	42
Fig. 5.3 - The binary graph (Na vs. Cl) shows higher Na/Cl molar ratios with respect to the Na/Cl molar ratio in seawater (dashed line). Na enrichments in waters are due to the water-rock interaction with the Na-alkaline hosting rock.	43
Fig. 5.4 - Triangular plot, relative abundance of CO ₂ , N ₂ and O ₂ dissolved in waters. The ASSW (air saturated seawater) values is reported for comparison. The dashed line represents the theoretical mixing between air dominated system and CO ₂ -rich fluids.	44
Fig. 5.5 - Nature of suspended particulates in “Specchio di Venere” lake water and Polla 3 thermal-spring feeding the lake [a]. Fe-oxyhydroxides [b] and phyllosilicates [c] from the shallowest water layer, as recognised by X-ray spectra [d] and [e], respectively. On the contrary, suspended particulates from the hydrothermal Polla 3 mainly consist of amorphous silica [f] as indicated by the reported x-ray maps for oxygen and silicon.	45
Fig. 5.6 - REE dissolved in waters normalised to the PAAS. The average seawater (Censi et al., 2007) was plotted for comparison.....	46
Fig. 5.7 - (LREE/HREE) _N vs. (MREE/HREE) _N showing values <1, except lake waters characterized by (MREE/HREE) _N ratios >1. The seawater is reported for comparison.	47
Fig. 5.8 - Relative abundance (percentage) of the REE complexes in the investigated waters. REE	

aqueous speciation was performed with Phreeqc software (LLNL database).....	49
Fig. 5.9 - No correlation was found between Eu and Ce anomalies, showing a different chemical behaviour. Positive Eu anomalies identify the interaction of waters with the less evolved hosting rocks.	51
Fig. 5.10 - Ce/Ce* displays to be function of the Eh values, showing negative anomalies increasing the Eh values. Buvira Rizzo sample has an anomalous behaviour, probably due to the higher organic carbon concentration that enhanced the stability of Ce in the dissolved phase. The highest values of Ce anomalies are caused by the interaction of water with the atmospheric fallout enriched in Ce.	53
Fig. 5.11 - Changes of Y/Ho and Zr/Hf molar ratios in waters. The coloured band in the graph represents the range of Y/Ho and Zr/Hf ratios in Desert Varnish (Thiagarajan et al., 2004).	55
Fig. 5.12 - PAAS-normalised REE in lake waters (from top and bottom), average Desert Varnish and settling dust (values from: Thiagarajan and Aeolus Lee, 2004; Goldsmith et al., 2014).	57
Fig. 6.1 - Location of sampling sites.....	60
Fig. 6.2 - a) Triangular plot of major anions dissolved in water. The red arrow indicates SO ₄ enrichments probably due to the gypsum dissolution. b) Triangular plot of major cation dissolved in water. The red arrow indicates Ca enrichments probably due to the gypsum dissolution.	62
Fig. 6.3 – Carbonate minerals and Fe-, Mn-oxyhydroxides in SPM collected from water of Group 1; Pyrite in SPM collected from water of Group 2.	64
Fig. 6.4 - Zr-Hf and Y-Ho molar ratios. The coloured bands indicate the chondritic Y/Ho and Zr/Hf molar ratios.	65
Fig. 6.5 - Relative abundances (percentage) of the REE complexes in the investigated waters.	66
Fig. 6.6 - PAAS-normalized REE patterns dissolved in water.	68
Fig. 6.7 - Zr/Hf molar ratios versus Eh values.....	69

Fig. 6.8 - a) Zr/Hf molar ratios vs. saturation indexes of Fe-oxyhydroxides. b) Zr/Hf molar ratios vs. saturation indexes of pyrite.	70
Fig. 6.9 - Relationship between Eu anomalies and Ce anomalies.	73
Fig. 8.1 - Location map of sampled waters along Dead Sea Fault area.....	82
Fig. 8.2 - a) Triangular plot, relative pressure of CO ₂ , N ₂ and O ₂ . The air values are also reported for comparison; the straight line represents the theoretical mixing between air dominated system and CO ₂ -rich fluids. b) Triangular plot, relative pressure of CO ₂ , N ₂ and CH ₄	85
Fig. 8.3 - He vs. CO ₂ contents (cc l ⁻¹ STP) of dissolved gases in the sampled waters. The ASSW values are also reported for comparison.	86
Fig. 8.4 - Changes in ⁴ He and CO ₂ dissolved in waters (cc l ⁻¹ STP) with respect to the temperature values of the waters 4b) Changes in CO ₂ dissolved in waters (cc l ⁻¹ STP) with respect to the temperature values of the waters.....	88
Fig. 8.5 - R/Ra values vs. ⁴ He/ ²⁰ Ne ratios diagram. Air Saturated Water (ASW), Mid-Ocean Ridge Basalts (MORB) and Radiogenic fields are reported as reference.	89
Fig. 8.6 - Geographical distribution of mantle source. The percentage of mantle source was calculated using the equation of Sano and Waikita (1985).....	91
Fig. 8.7 - CO ₂ / ³ He plotted vs. R/Ra shows a different proportion of mixing between fluids of crust and mantle origins. Mid-Ocean Ridge Basalts (MORB) and crust fields are reported as reference. The black circle represents the bubbling gas collected to H. Gader, showing a fractionation process of CO ₂ and He with respect to the dissolved gases.	92
Fig. 8.8 - Co-variation of δ ¹³ C (TDIC) and dissolved CO ₂ (cc l ⁻¹ STP). The arrows indicate the different processes involving CO ₂ in the investigated waters.....	94
Fig. 8.9 - CO ₂ / ³ He plotted vs. δ ¹³ C _{CO2} shows a different proportion of CO ₂ mixing between fluids of crust and mantle origins. Mantle carbon (M), Marine limestone (L) and Organic sediment (S) fields are reported as reference.	96

LIST OF TABLES

Tab. 4.1 - Chemical composition of the studied waters expressed in mmol/l.	25
Tab. 4.2 - Saturation indexes of studied waters.	25
Tab. 4.3 - REE, Zr and Hf dissolved in waters expressed in nmol/l.	29
Tab. 5.1 - Chemical composition of cold and thermal waters. The chemical composition of major ions is expressed in mmol l ⁻¹ , while dissolved gases are expressed in cc l ⁻¹ (STP).	42
Tab. 5.2 REE, Zr and Hf dissolved in waters expressed in pmol l ⁻¹	46
Tab. 6.1 - Chemical composition of the studied waters expressed in mmol/l.	61
Tab. 6.2 - Saturation indexes of studied waters.	63
Tab. 6.3 - REE, Zr and Hf dissolved in waters expressed in pmol l ⁻¹	67
Tab. 8.1 - Total Dissolved Salts (TDS) is expressed in g l ⁻¹ . Chemical composition of dissolved gases (values expressed in cc l ⁻¹ STP), bubbling gases (values of O ₂ , N ₂ and CO ₂ are expressed in % vol, while the values of He, H ₂ , CO, CH ₄ are expressed in p.p.m vol). The isotopic composition of C gas ($\delta^{13}\text{C}_{\text{TDIC}}$) is expressed in ‰ PDB standard. Isotopic composition of Helium is expressed as R/Ra, ³ He/ ⁴ He ratios normalized to the atmospheric ratio (Ra=1.39×10 ⁻⁶). While, R/Rac represent R/Ra corrected for the atmospheric contamination. Percentage of Radiogenic (R), Magmatic (M) and Atmospheric (A) represent the contribution of different He source calculated following the description of Sano et al. (1985) Percentage of Mantle carbon (M), Marine limestone (L) and organic Sediment (S) fields represent the CO ₂ contribution from different sources calculated following the description of Sano and Marty (1995). The kinds of samples are: Spring (S), Well (W), Lake (L) and Bubbling gas (B).	85

PREFACE

This PhD thesis concerns the geochemistry of Zr, Hf and REE never studied in extreme environments, in order to evaluate the main processes involving these elements in hyperacid, hypersaline and lake systems. This thesis consists of an introduction presented in Chapter I; the description of the investigated areas in Chapter II; materials and methods in Chapter III; results, discussions and conclusions of each case of study are presented from Chapters IV to VI. The general conclusions regarding the geochemistry of Zr, Hf and REE are presented in Chapter 7. Chapter 8 is an additional study concerning the chemical and isotopic composition of dissolved gases in waters along Dead Sea Fault area. The aim of this last study is to characterise the source of volatiles (carbon dioxide and helium) and to investigate their relationship with the main tectonic framework. The paragraphs “Introduction” and “Materials and methods” related to this last study are included in Chapter VIII. The references relative to the chapters are in Chapter IX.

The case studies presented in this work are the results, discussions and conclusions of the articles prepared by the author of the thesis. The articles are already published, accepted or under review in international journals. The papers already published are also included in the appendix (Chapter X).

ARTICLES

1. **Inguaggiato C.**, Censi P., Zuddas, P., Londoño, J. M., Chacón Z., Alzate D., Brusca L., D'Alessandro, W., 2015 "Geochemistry of REE, Zr and Hf in a wide range of pH and water composition: The Nevado del Ruiz volcano-hydrothermal system (Colombia)" *Chemical Geology* 417, 125-133.
2. **Inguaggiato C.**, Censi P., Zuddas P., D'Alessandro W., Brusca L., Pecoraino G., Bellomo, S. "Zr-Hf and Rare Earths signatures discriminating the effect of atmospheric fallout from the hydrothermal input in volcanic lake waters" (under review for *Chemical Geology*).
3. **Inguaggiato C.**, Censi, P., D'Alessandro, W., Zuddas, P., "Geochemical characterisation of gases along Dead Sea Rift: Evidences of Mantle CO₂ degassing" (in review for *Journal of Volcanology and Geothermal Research*).
4. Censi P., Raso M., Yechieli Y., Ginat H., Saiano F., Zuddas P., Brusca L., D'Alessandro W., **Inguaggiato C.** "Geochemistry of Zr, Hf and REE in a wide spectrum of Eh and water composition: The case of Dead Sea Fault system (Israel)" (in review for *Geochimica et Cosmochimica Acta*).

CONFERENCE PAPERS

1. **Inguaggiato C.**, Censi P., Zuddas P., Brusca L., D'Alessandro, W., Pecoraino, G., Bellomo, S. "Zr, Hf and Rare Earths Elements signatures discriminating the effect of atmospheric fallout from the hydrothermal input in volcanic lake waters: The case study of lake "Specchio di Venere" (Pantelleria, Italy)" (Abstract) IAVCEI-CVL9 Workshop, Yaoundé, Cameroon, 13-20 March 2016.
2. **Inguaggiato C.**, Censi P., Zuddas P., Brusca L., D'Alessandro, W., Pecoraino, G. "Water-rock interaction in Pantelleria hydrothermal system (Italy). The behaviour of Zr, Hf and REE" (Abstract and oral presentation) Goldschmidt 2015, Prague, Czech Republic, 16-21 August.
3. Censi P., **Inguaggiato C.**, Zuddas P., Sposito F., Inguaggiato S. "Zr, Hf and REE Behaviour in River Waters. A Consequence of Dissolution of Fe-Oxyhydroxides and Evaporites" (Abstract and poster) Goldschmidt 2015, Prague, Czech Republic, 16-21 August.
4. **Inguaggiato C.**, Censi P., Zuddas P., Londoño, J. M., Chacón Z., Alzate D., Brusca L., D'Alessandro, W. "The behaviour of REE and Zr-Hf fractionation in the volcanic waters of Nevado del Ruiz system (Colombia)" (Abstract and poster) European Geosciences Union General Assembly 2015 Vienna, Austria, 12 – 17 April 2015.

AWARD

1. Award "Premio Vinci 2013", grant for the mobility between Italy and France (PhD research under joint supervision). Università Italo-Francese, Torino, Italy (25/06/2013).

CHAPTER 1

INTRODUCTION

1.1 General aspects and aim of the work

The REE (Rare Earth Elements; lanthanides and yttrium) are resources economically important with an increasing exploitation due to the continuous using of these metals in the production of electronic devices. Previously, Zr, Hf and REE were considered immobile, free from geochemical fractionations during water-rock interaction. Starting from 80' years, with the improvement of analytical techniques, the Zr, Hf and REE have been progressively investigated in dissolved phase. Here, a geochemical behavior of REE controlled by their external electronic configuration rather than their charge-to-radius ratio was recognised. In the last 30 years, an extensive literature has been developed about the distribution of REE and the Y/Ho ratios during interaction processes between different phases while very limited investigations were carried out about the Zr and Hf geochemistry. The study of Zr and Hf distributions in natural waters started about 20 years ago and was mainly focused on seawater (Bau et al. 1996; Godfrey et al., 1996; 2008; Firdaus et al., 2011; Frank, 2011).

A special attention was focused on the capability of the REE to provide insights into geochemical processes occurring in natural environments (Bau, 1996; 1999; Bau and Dulski, 1999; Fulignati et al., 1999; Wood et al., 2003 and references therein; Censi et al., 2007; Piper and Bau, 2013; Censi et al., 2014; 2015; Inguaggiato et al., 2015). The Zr, Hf and REE behaviour in geothermal fluids depends from their chemical-physical characters, rock-water interactions, the deposition of authigenic minerals and speciation (Wood, 1990a; 2003; Lewis et al., 1997, 1998; Gammons et al., 2005; Bao et al., 2008; Peiffer et al., 2011; Varekamp et al., 2015). The input of atmospheric fallout was recognized as responsible for the mobilization of the REE and the changes of seawater composition (Greaves et al., 1994; 1999), mainly in an epicontinental basin like the

Mediterranean Sea. Here, the effects of the dissolution of atmospheric fallout influence the dissolved REE distribution along the water column (Greaves et al., 1991; Censi et al., 2004; 2007), whereas Zr and Hf behaviour is not known.

The geothermal waters with very acidic pH values have higher contents of REE dissolved in waters up to 10^4 times compared to seawater. The REE contents in hydrothermal waters change as function of pH values increasing as the acidity of solution increases, independently from the temperature and the type of local rock (Michard, 1989). The geothermal systems are characterized by a large variety of REE patterns. In particular, the acid sulphate waters have high REE contents sometimes with Light Rare Earth Elements (LREE) strongly depleted with respect to the local rocks (Wood, 2003 and references therein). During the mixing between reduced fluids discharged from the hydrothermal vent at the marine floor and oxidized seawater, the REE are scavenged by the formation of Fe and Mn oxyhydroxides (Bau, 1999, Wood et al., 2003 and references therein).

The knowledge of the REE behaviour in alkaline lakes is limited (Johannesson and Lyons, 1994) and only few studies have been carried out on acid volcanic lakes (Ayers, 2012; Varekamp, 2015 and references therein) whereas the dissolved Zr and Hf geochemistry under these conditions is unknown.

The concentration of total dissolved REE in near neutral pH waters and in seawater is low and their dissolved species are dominated by carbonate complexes (Luo and Byrne, 2004) whereas the latter species and hydroxides could be considered negligible in acidic waters. In seawater, the shale-normalized REE patterns progressively increase along the REE series showing negative Ce anomalies consistently with the oxidative scavenging of CeO_2 (Censi et al., 2007; Seto et al., 2008; Piper et al., 2013 and references therein).

Recent studies investigated isovalent elements Zr-Hf, Y-Ho in waters and their fractionation in processes involving solid phases (Godfrey et al., 2008; Firdaus et al., 2011; Frank 2011; Schmidt et al., 2014). A different behaviour of Y-Ho and Zr-Hf geochemical twins has been evidenced in

aqueous solution in contrast to the negligible fractionation of Y-Ho and Zr-Hf occurring at high temperature in pure silicate melts, where the processes are mainly controlled by the ion charge and radius (Bau, 1996). Y/Ho and Zr/Hf ratios in aqueous solutions deviate from the chondritic ratio, due to the fractionation processes ruled by the electronic configurations of elements (Bau, 1996). In seawater, the continental material has been recognised as the main source of Zr and Hf. A larger removal of Hf with respect to Zr was found in seawater, due to the different sorption of these elements onto Fe-, Mn-oxyhydroxides (Godfrey et al., 1996; 2008; Firdaus et al., 2011; Frank et al. 2011; Schmidt et al., 2014). In the water column of the Pacific Ocean, the Zr/Hf molar ratio ranges from 100 to 600 (Firdaus et al., 2011), whereas in Atlantic coastal waters Zr/Hf molar ratio spans between 100 and 200 (Godfrey et al., 1996; 2009). Censi et al., (2014) investigated the sediments collected from deep-sea brines in the eastern part of Mediterranean Sea basin, showing sub-chondritic Y/Ho and Zr/Hf ratios in authigenic carbonates and lack of Zr/Hf fractionation during halite precipitation. In the last years, the scientific community focused the attention through the Zr-Hf and Nb-Ta (geochemical pairs) in the ocean, recognizing them as a useful geochemical tool for tracing water masses in the ocean (Bau, 1996; Firdaus et al., 2011; Frank, 2011). However, the behaviour of Zr and Hf has never been studied in extreme environments: strong acidic waters linked to volcanic system, lakes where the interaction between the water body and the atmospheric fallout contribution from the nearby desert occurs and waters characterized by high TDS values and very low Eh values.

This PhD research investigated the geochemistry of Zr, Hf and REE in waters circulating within the Nevado del Ruiz (Colombia) and Pantelleria (Italy) volcano-hydrothermal systems, in the alkaline lake formed in the calderic depression of Pantelleria volcanic island and in the hypersaline waters with variable Eh values collected along the Dead Sea Fault (Israel). These natural systems were considered as natural laboratories for better understanding the processes involving the elements previous mentioned within a wide range of pH, Eh, TDS and water chemical composition.

In particular the attention was focused on:

1. The geochemistry of Zr, Hf and REE in waters of Nevado del Ruiz, covering a range of pH from 1 to 8.8; with special attention on the acid sulphate-chlorine waters with pH included between 1 and 3.6.
2. The geochemistry of Zr, Hf and REE in CO₂-rich waters of Pantelleria Island, covering a range of pH from 6 to 9; with special attention on the source of Zr, Hf and REE in the alkaline lake “Specchio di Venere”.
3. The geochemistry of Zr, Hf and REE in waters circulating along the Dead Sea fault area; with special attention on the different Zr and Hf affinity with respect to the authigenic mineral surfaces in waters covering a wide range of Eh and TDS values.

1.2 The aqueous geochemistry of REE

Lanthanides are a group of 15 elements belonging to the f-block, usually split in 3 groups: light (La, Ce, Pr, Nd, (Pm)), middle (Sm, Eu, Gd, Tb, Dy) and heavy (Ho, Er, Tm, Yb Lu). Promethium (Pm) is a radioactive lanthanide outside the focus of this study. The external electronic configuration changes from La to Lu with the filling of inner 4f orbitals giving to these elements quite similar chemical properties. However, the progressive filling of 4f orbitals closest to the nucleus induces a phenomenon well known as “Lanthanide Contraction”, consisting in the progressive decrease of ionic radius increasing the atomic number (Shannon, 1976). In natural waters, the lanthanides are predominant in solution with the trivalent oxidation state, whereas tetravalent cerium and bivalent europium occur in oxidized condition and extreme reduced condition, respectively. Although Y has not f-electrons it is included with the HREE, because it is characterized by similar ionic radius and the same oxidation state (+3) compared to Ho. Sometimes some REE normalized pattern or sequences of distribution coefficients of REE can be splitted into four different curves called tetrads explained according to the Refined Spin Pairing energy theory (Reisfeld and Jorgensen, 1977; Jorgensen, 1979 and cited references).

The REE form strong complexes with different inorganic ligands: carbonate, hydroxide, sulphate, fluorine, chlorine and phosphate (Wood et al., 2003 and references therein). Only a small percentage of REE is in solution as free hydrated ions (REE^{3+}), due to the high stability constant of REE with inorganic ligands (Wood, 1990; Millero, 1992; Luo and Byrne, 2004). The REE-complexes and their abundances depend on the stability constant of the complexes and to the relative concentration of anion ligands in solution. The stability constants of the trivalent REE complexes with carbonate, fluoride, phosphate and hydroxide, increase along the REE series, while the stability constants of REE-complexes with chloride decrease along the REE series (Fig. 1.1) (Wood, 1990; Millero, 1992; Luo and Byrne, 2004). In particular the chloride ligand forms weak complexes with REE at temperatures lower than 200°C , whereas the stability of REE-chloride complex increase with the temperature (Wood et al., 2003 and references therein). The constants of REE complexes with SO_4^{2-} ligands do not change in a wide range, showing an almost flat distribution and a slight bulge effect (Millero, 1992; Johannesson et al., 1996). The REE in water with near-neutral pH (including seawater) are mainly dominated by carbonate complexes $[\text{REE}(\text{CO}_3)]^+$ and $[\text{REE}(\text{CO}_3)_2]^-$, while in strong acidic waters the role of carbonates ligands is negligible (Byrne et al., 2002).

Having the same charge and very similar ionic radius (1.019 and 1.015 Å, respectively), Y and Ho behave similarly during primary processes. As a consequence their Y/Ho signature in rocks is close to the chondritic value (52; Jochum et al., 1988). On the contrary, this signature deviates from this value during secondary processes involving aqueous solutions.

During the solidification of pure silicate melt, these elements are CHARGE and RADIUS CONTROLLED (CHARAC) showing smooth normalized patterns mainly due to the lanthanide contraction. Often REE show irregular normalized patterns during the solidification of highly evolved magmas ($>70\%$ SiO_2) and in aqueous solution, indicating that the distribution of REE does not depend only by charge and ionic radius but other processes influence the REE distribution (Bau, 1996).

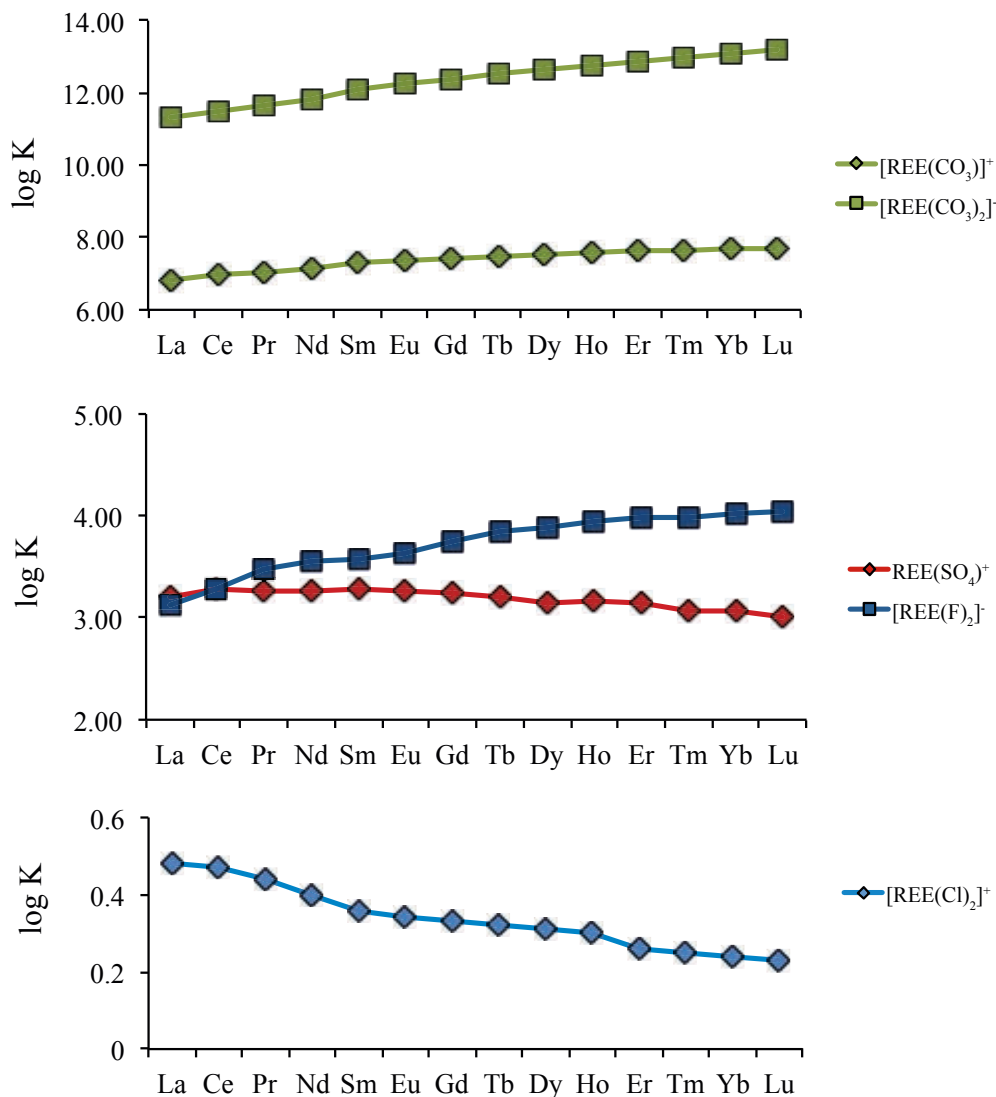


Fig. 1.1 - Stability complexes for the formation of lanthanides complexes (Millero, 1992)

1.3 The normalization of REE

All the elements are characterized by Oddo Harkins effect in which the cosmic abundances of odd atomic numbered elements is lower with respect to the neighbour even elements. The REE are an excellent example of elements affected by the Oddo Harkins effect. If the REE abundance is plotted versus the atomic number, the Oddo Harkins effect is shown. The common way to avoid this effect is to normalize the REE to natural materials. The standard materials most widely used are: Post Archean Australian Shale (PAAS), Upper Continental Crust (UCC) and average chondrite (Piper et al., 2013 and references therein). The UCC and PAAS show a similar distribution of REE

decreasing along the REE series. On the contrary, the distribution of REE in the average chondrite is different with respect to the UCC and PAAS, showing lower REE concentration up to 2 orders of magnitude. Moreover, PAAS and UCC have higher LREE/MREE and LREE/HREE ratios with respect to average chondrite. The normalization of REE is used to compare REE patterns in order to evaluate processes involving different phases generating fractionation of REE. In the last years, the REE dissolved in volcano-hydrothermal fluids began to be normalized to the local rocks in order to evaluate processes of water-rock interactions between fluids and hosting rocks (Varekamp et al., 2015 and references therein).

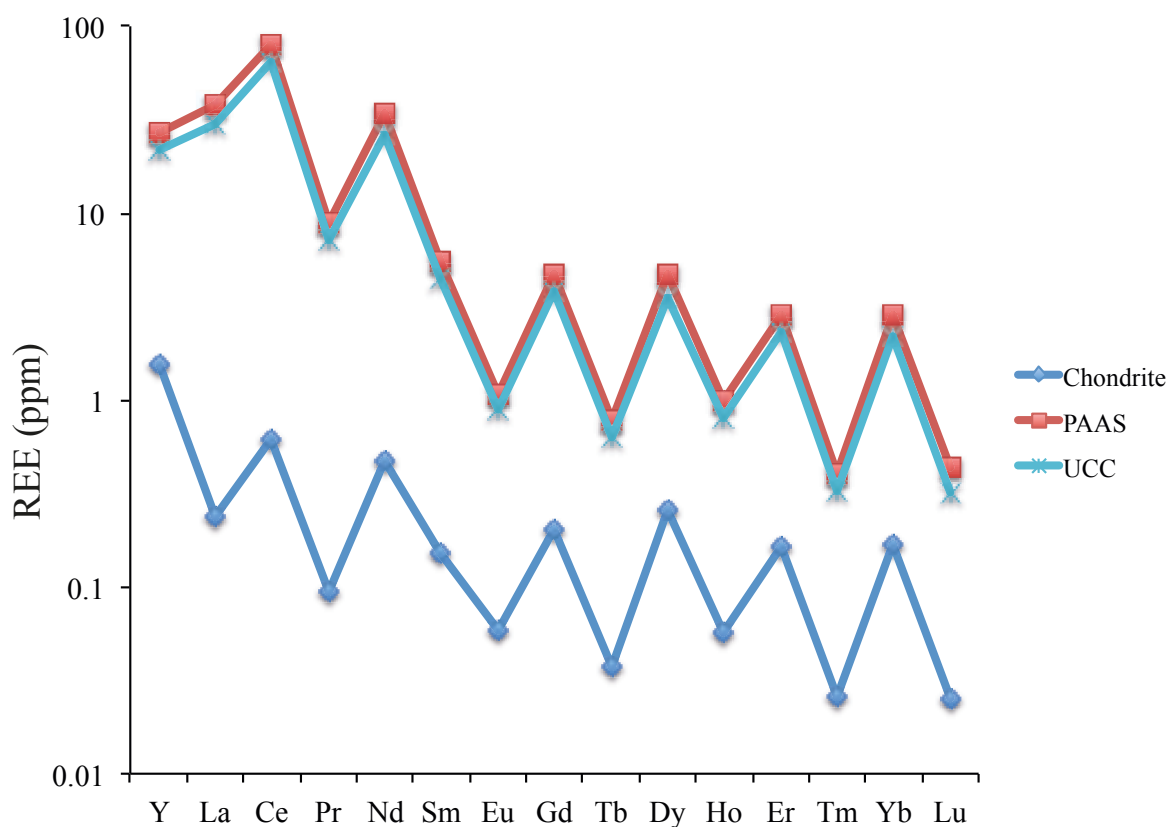


Fig. 1.2 – The distribution of REE (ppm) in Chondrite, PAAS and UCC (Data from: Taylor and McLennan 1985; 1995; McDonough and Sun 1995).

1.4 The aqueous geochemistry of zirconium and hafnium

Zirconium and Hafnium are transition metals belonging to the d-block of the periodic tables. These elements are characterized by the same oxidation state (4+) and similar ionic radius (Zr 0.84

and Hf 0.83 Å). The knowledge of Zr and Hf in solution is poor compared to the REE. In near-neutral waters, the complexation of these elements is dominated by hydroxyl groups $Zr(OH)_4$, $Hf(OH)_4$, $Zr(OH)_5^-$, $Hf(OH)_5^-$ (Byrne, 2002). Moreover, $Zr(OH)_4$ and $Hf(OH)_5^-$ complexes are the species dominated in near-neutral waters (Censi et al., 2014 and references therein), even if Zr-, Hf-complexes with fluoride and chloride ligands (Pershina et al., 2002; Monroy et al., 2010) could be stable in hydrothermal environment. However, there is a paucity of knowledge about Zr and Hf complexes in extreme environments with hyperacid pH where the relative abundance of major anion ligands complexing the metals is completely different with respect to the common natural seawater and continental waters.

During the solidification of pure silicate melt, Zr and Hf are controlled by charge and radius as Y and Ho. Zr/Hf ratios are quite constant in rock with $SiO_2 < 70\%$, with near-chondritic ratio (≈ 73 ; Jochum et al., 1986), while in aqueous solution and their precipitated super-chondritic ratios have been found (Firdaus et al., 2011). In solid-liquid processes, the ionic radius and charge are not the only responsible of Zr-Hf fractionation, showing non-CHARAC behaviour (Bau, 1996) due to the different metal complexation.

CHAPTER 2

INVESTIGATED AREAS AND BACKGROUND INFORMATION

2.1 Nevado del Ruiz

Nevado de Ruiz (NDR) is one of the active volcanoes belonging to the great chain of the Andes (located a few km west of Bogota), connected with the active subduction of Nazca Plate below the South American plate.

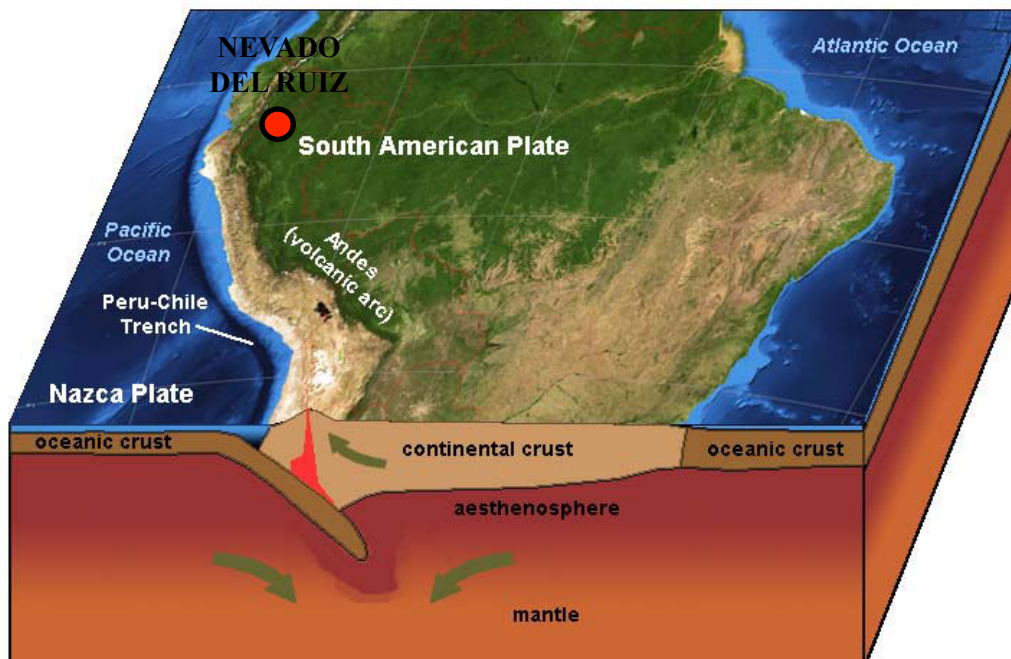


Fig. 2.1 – Location map of Nevado del Ruiz volcano. Active subduction of Nazca Plate below the South American plate, generating the volcanism along the chain of the Andes.

NDR is located at the intersection between the regional fault system with N-S direction and the Palestina fault system oriented NE-SW. The last plinian eruption occurred in 1985, generating a huge lahar that buried Armero town killing approximately 23,000 people. The NDR volcano is a large edifice mainly built up during three major phases over the past 600,000 to 1,200,000 years, with a summit elevation of 5,389 m (Forero et al., 2011 and references therein). The volcanic complex is mainly made of andesitic lava, whereas pyroclastic deposits belonging to the last

eruptive phase overlay the lava flows. This volcanic system is characterized by calc-alkaline rocks ranging from andesitic to dacitic in composition with quite constant distribution of REE, Zr and Hf in different magmatic suites (Borrero et al., 2009). Fig. 1 shows the REE distribution of average local rocks (Borrero et al., 2009 and references therein) normalized to chondrite, displaying a decreasing pattern from La to Lu and the lack of europium anomaly (Borrero et al., 2009 and reference therein). Borrero et alii don't show different trend for different magmatic suites, affirming that the evolution of magma is mainly controlled by the fractional crystallization without recognizing other processes.

The NDR rocks have quite constant Y/Ho and Zr/Hf molar ratios of 58.3 and 66.8 respectively (Borrero et al, 2009 and reference therein), falling in the field of processes controlled mainly by charge and radius (Bau, 1996).

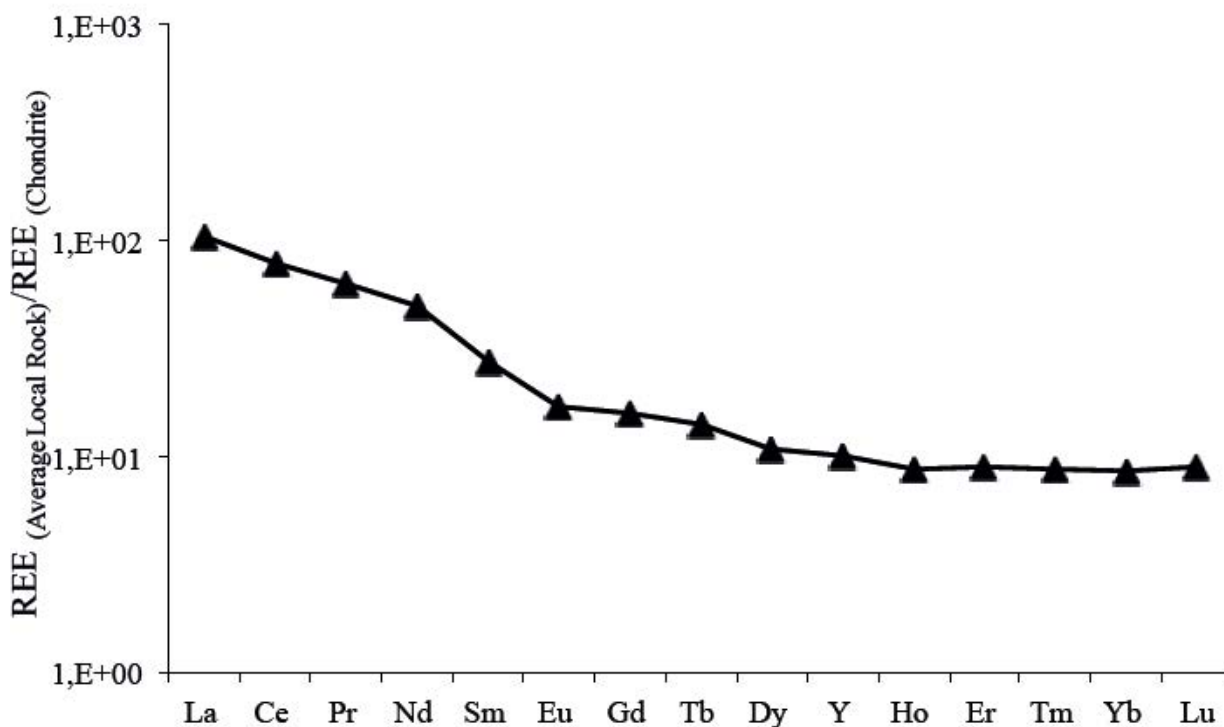


Fig. 2.2 - Chondrite-normalized REE patterns in average local rock (Borrero et al., 2009).

2.2 Pantelleria Island

Pantelleria Island (83 km²) is an active volcano rising 836 m above sea level, located in the Strait of Sicily between Sicily and Africa. The latter is characterized by trans-tensional rift (northwest-southeast) with a thickness of the thinned crust reaching 16 km along the rift axis.

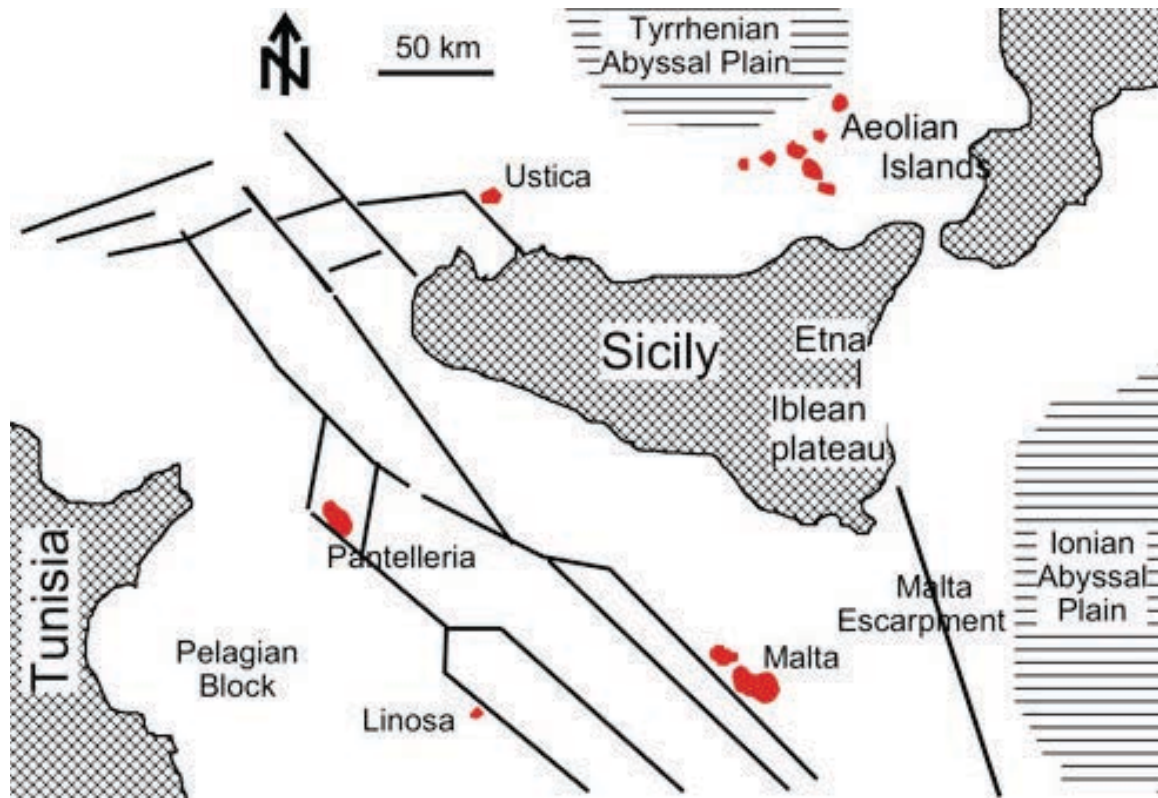


Fig. 2.3 – Location map of Pantelleria volcanic island. Main tectonic features of Strait of Sicily (Esperança e Crisci 1993).

The outcropping rocks in Pantelleria mainly consist of trachyte and pantellerite (peralkaline rhyolites), whereas in the northwest part of the island alkali basalt and hawaiiite occur, representing only the 6% of the total. The local rocks are characterized by a compositional gap of about 13% of SiO₂ between basaltic rocks and trachyte. Moreover, trachyte and pantellerite have a peralkalinity index >1 (White et al., 2009). Basaltic lavas are characterized by 20-30 vol.% of crystals, trachyte lavas have 30-40 vol.% of crystals, while pantellerite consist of 5-25 vol.% of crystals. Forty rock samples were studied by White et alii (2009), showing a decreasing distribution of REE normalized to chondrite from La to Lu. Moreover, the REE concentrations increase with the evolution of the

Currently, the volcanic activity is limited to gas emissions at or below boiling temperature in Favare, Cuddia Di Mida and M. Gibebe area (south-central of island). Thermal waters CO₂-enriched located along the coast in the northwest and southwest areas (Dongarrà et al., 1983) and other thermal springs and anomalous degassing areas situated along the shoreline of the "Specchio di Venere" lake (Favara et al., 2001; Aiuppa et al., 2007). Water temperatures range from 20 to 90°C with pH values from 6.1 to 9.3 (Dongarrà et al., 1983; Parello et al., 2000). The anion chemical composition of the waters is chloride dominated, whereas many thermal waters are rich in carbonatic species due to the interaction with CO₂ discharged from the magmatic system (Parello et al., 2000). The scenario mentioned above suggests that the water circulating in Pantelleria Island represents a mixing between CO₂-rich thermal water, seawater and meteoric water recharge.

"Specchio di Venere" Lake is a saline endorheic basin formed within a calderic depression called "Caldera Cinque Denti", fed by several thermal springs and meteoric water. Aiuppa et alii (2007) excluded any direct implication of seawater in the lake, highlighting intermittent stratification of the lake. Such stratification is unstable and of short duration (generally a few days) and changes of meteorological conditions (rain and/or wind) are able to mix the lake water, which is only 13m deep (Aiuppa et al., 2007). The existence of reducing conditions at the water-sediment interface at the bottom of the lake was recognized (Aiuppa et al., 2007), while isotopic analysis (δD ; $\delta^{18}O$) in "Specchio di Venere" lake evidenced the evaporation of water body (Dongarrà et al., 1983).



Fig. 2.5 - Photo representing an overview of “Specchio di Venere” alkaline lake.

2.3 Dead Sea Fault area

The investigated area of the Dead Sea Transform (DST) is the northern part of the Syrian-Red Sea-East-Africa transform (e.g. Garfunkel, 1981). The transform itself is the boundary between the Arabian plate in the east and the African plate in the west.

Tectonic elements (left) and shaded relief of the topography (right) of the Dead Sea Transform.

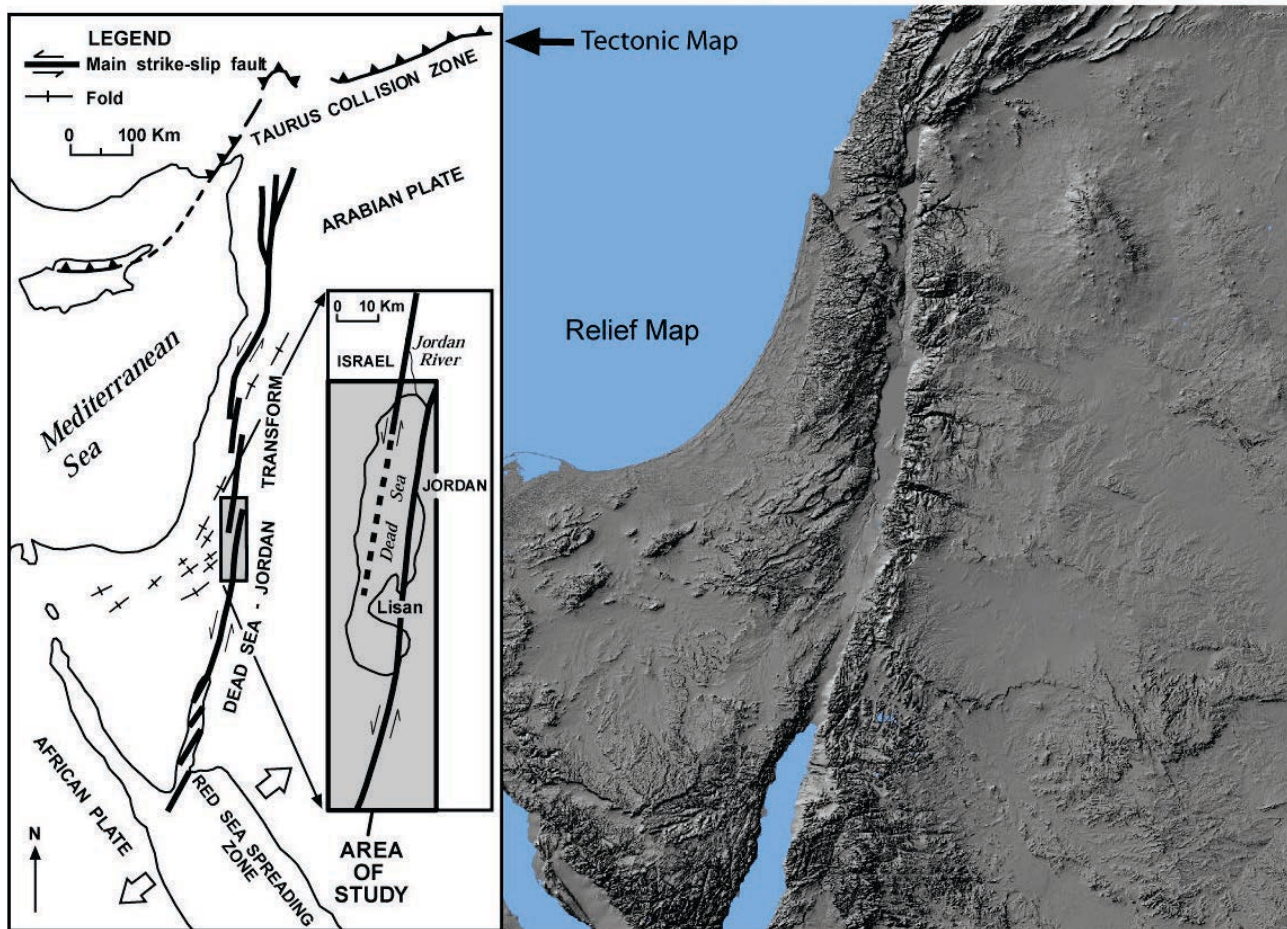


Fig. 2.6 – Tectonic map on the left and relief map on the right concerning Dead Sea Fault system. Map taken from: http://woodshole.er.usgs.gov/project-pages/dead_sea/tectonic.html.

The crustal part consists of an old crystalline basement (more than 580 Ma old) underlying thick sedimentary rock sequences (Garfunkel, 1988; Ginzburg and Gvirtzman, 1979). Only in the southernmost area, close to Eilat, the absence of sedimentary rocks leads to the outcropping of the crystalline basement (Rybakov and Segev, 2004). The sedimentary sequences consist of carbonates, sandstones, clays and evaporates, whereas magmatic rocks occur in the northern part of the investigated area, close to lake Kinneret, (e.g. Weinstein, 2000; Lustrino and Wilson, 2007).

The whole geological structure can be divided into three main areas. The northern area is built of Miocene-Quaternary volcanics and continental sediments belonging to the Tiberias Group in the eastern part of the investigated area (near the Golan Heights) while the western part (adjacent to the

Galilee Mountains) is built mostly of carbonate sequences of Judea, Mt. Scopus and Avdat groups. The central part of the studied area is from the Lake Kinneret to the southern Dead Sea. It is limited in the west by the eastern Judea Mountains whereas the eastern limit is represented by the escarpment formed by the Transform faults. The down most part of this area is composed of evaporitic and alluvium sequences belonging to the Dead Sea Group (Zak, 1967). The third part of the studied area, extending between the Dead Sea and the Gulf of Eilat, is mostly a low area filled by thick alluvium deposits. This southern part is limited between Precambrian crystalline rocks covered by sandstones both forming the Edom mountains at East and the carbonate sequences of the Judea Group outcropping in the Negev area in the west.

Broad changes of the crust-mantle boundary (Moho) were suggested in the studied area with a progressive deepening of the Moho from NW to SE from about 25 to 35 km depth (Segev et al., 2006; Mechie et al., 2013). Along the rift system, geophysical indications provide evidences of a Mantle uprising in northernmost area (about 30 km depth) relative to the Eilat region where it should occur at about 35 km.

The Dead Sea is a terminal lake located in the northern part of the Dead Sea rift valley [Katz and Starinsky, 2009]. Therefore, its water level is influenced by the balance between the evaporation and the input of river and groundwaters from the surroundings area. In 1979, the evolution of the composition of the Dead Sea water attained its current status following the progressive growth of salinity caused by the negative water balance between input and output in the basin (Lensky et al., 2005, and references therein). Since then, halite crystals have been observed in shallow waters (Steinhorn et al., 1983) and widespread halite crystallisation began around 1982 (Herut et al., 1998, and references therein).



Fig. 2.7 – Photo representing an overview of Dead Sea.

CHAPTER 3

MATERIALS AND METHODS

3.1 Sampling and analytical methods

Temperature, pH, Eh and electrical conductivity of waters were measured in the field with an ORION 250+meter. The water samples collected to determine major cations and trace elements were filtered through 0.45µm MILIPORE cellulose acetate filters into 250ml Nalgene bottles and acidified in the field with ultrapure HNO₃. The water samples to determine major anions were filtered with 0.45µm filters in the field into LDPE plastic bottle. The major elements were analysed by Dionex ICS 1100 chromatograph. A Dionex CS-12A column was used for cations (Na, K, Mg and Ca) and a Dionex AS14A column for anions (F, Cl, and SO₄). Alkalinity was determined in the field by titration with HCl 0.1M. Trace elements including also REE, Zr and Hf, were analysed by Q-ICP-MS (Agilent 7500ce) equipped with a Micromist nebulizer, a Scott double pass spray chamber, a three-channel peristaltic pump, an auto sampler (ASX-500, Cetac) and a Octopole Reaction System (ORS) for removing interferences of polyatomic masses and isobaric isotopes. The mass spectrometer was calibrated with a multi-element standard solution, daily prepared and diluted 10 times to obtain a curve with 11 calibration points. The sensitivity variations were monitored using ¹⁰³Rh, ¹¹⁵In, ¹⁸⁵Re at a final concentration of 8 µg/l for each as internal standards added directly online by an appropriate device that mix internal standard solution to the sample just before the nebulizer. Sixty seconds rinse using 0.5% HCl and 2% of HNO₃ solution plus 60-s rinse using 2% of HNO₃ solution reduced memory interferences between samples. The precision of analysis was checked by running 5 replicates of every standard and sample, it was always within ±10%. Data accuracy was evaluated analysing standard reference materials (Spectrapure Standards SW1 and 2, SLRS4, NIST 1643e, Environment Canada TM 24.3 and TM 61.2) for each analytical

session and error for each element was <15%. Fe, Al with high concentrations (> 1mg/l) and Si were analysed by ICP-OES Horiba Ultima 2 at wavelength of 259.940 nm, 396.152 nm and 251.611 nm respectively.

REE, Zr and Hf were analyzed without preconcentration technique in Nevado del Ruiz waters, while 1 liter of sample water for each sampling point was collected along Dead Sea Fault and Pantelleria island, in order to preconcentrate REE, Zr and Hf (see the detailed method in the following section) The sample water was filtered through 0.45µm MILIPORE cellulose acetate filters, stored in Nalgene bottles and acidified with 5ml of ultrapure solution of HNO₃, to attain pH≈ 2.

Scanning Electronic Microscopy (SEM) observations and Energy Dispersive X-RAY Spectra (EDS) were carried out on the suspended particular matter (SPM) collected during the filtration from the investigated waters, in order to get information about the nature of suspended solids. The filters with the SPM were assembled on the aluminium stub and coated with gold. The analysis were performed with LEO 440 SEM equipped with an EDS system OXFORD ISIS Link and Si (Li) PENTAFET.

3.2 Method to determine Zr, Hf and REE in Dead Sea Fault and Pantelleria waters

The samples collected to determine REE, Zr and Hf in Dead Sea Fault and Pantelleria waters were treated in laboratory following the method described by Raso et alii (2013). In each water sample (1 liter) 1 mg of Fe was added and subsequently ammonia ultrapure solution to attain a pH between 8.0 and 8.5, in order to precipitate REE onto solid Fe(OH)₃. The treated solution was agitated for 3 hours and after 48 hours the solution was filtered onto Millipore membranes with 0.45 µm porosity to collect the solid precipitated. The next step was to dissolve the Fe(OH)₃ onto the filter in 5 ml of 6M HCl ultrapure solution. The last step was to dilute the solution 1:5 with ultrapure water to allow the introduction of the sample in ICP-MS. The iron concentration was analysed by ICP-OES for

each solution to check the recovery of the added iron.

3.3 Speciation calculations and saturation indexes

The Saturation Indexes (SI) and the aqueous speciation of elements were calculated using PHREEQC software package (version 3.0.6; Parkhurst and Appelo, 2010). The simulations were carried out using the database LLNL.

3.4 Equation to determine anomalies of REE

Anomalies of Cerium and Europium in waters were calculated with respect to the neighboring elements normalized to the reference material, using the equation proposed by Alibo and Nozaki (1999):

$$\text{REE}_n/\text{REE}_n^* = 2 \times (\text{REE})_n / [(\text{REE})_{n-1} + (\text{REE})_{n+1}]$$

$(\text{REE})_n$ is the concentration of the element chosen to calculate the anomaly, while $(\text{REE})_{n-1}$ and $(\text{REE})_{n+1}$ represent the previous and the subsequent element along the REE series, respectively.

CHAPTER 4

GEOCHEMISTRY OF Zr, HF AND REE IN A WIDE RANGE OF PH AND WATER COMPOSITION: THE NEVADO DEL RUIZ VOLCANO-HYDROTHERMAL SYSTEM (COLOMBIA)

4.1 RESULTS

4.1.1 General aspects

Hot and cold waters were collected in the area close to NDR volcano in November 2013 (Fig. 4.1). NDR waters cover a wide spectrum of pH, ranging from 1 to 8.8. Temperature ranges from 6.8 to 79.5 °C, electrical conductivity values span from 0.2 to 33.5 mS/cm and Eh values range between -31 and +325.4 mV (Tab. 4.1). The acidity recorded in the investigated waters is due to the interaction of magmatic gases, such as HCl, SO₂, and their dissolution and dissociation in groundwater (Giggenbach et al., 1990).

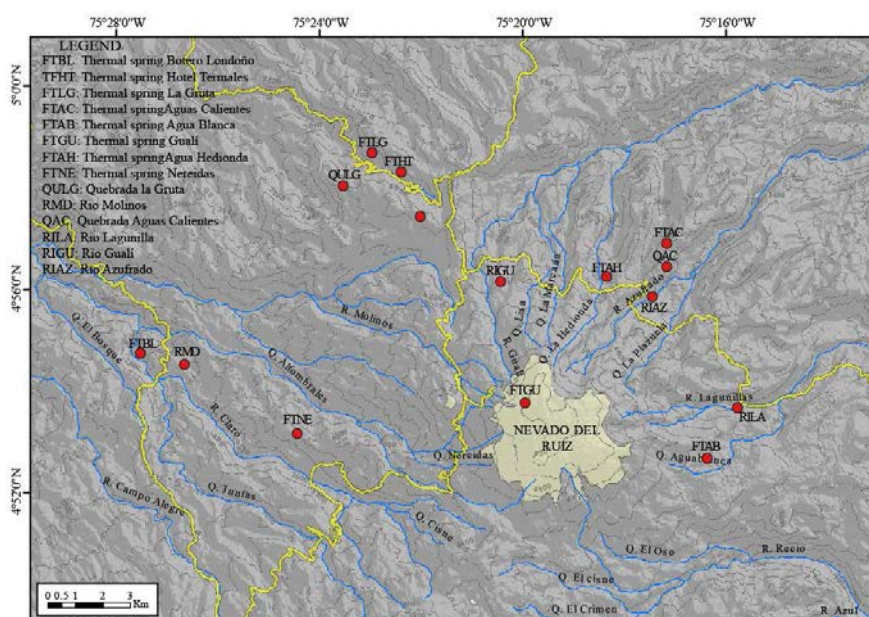


Fig. 4.1 - Location map of sampled waters.

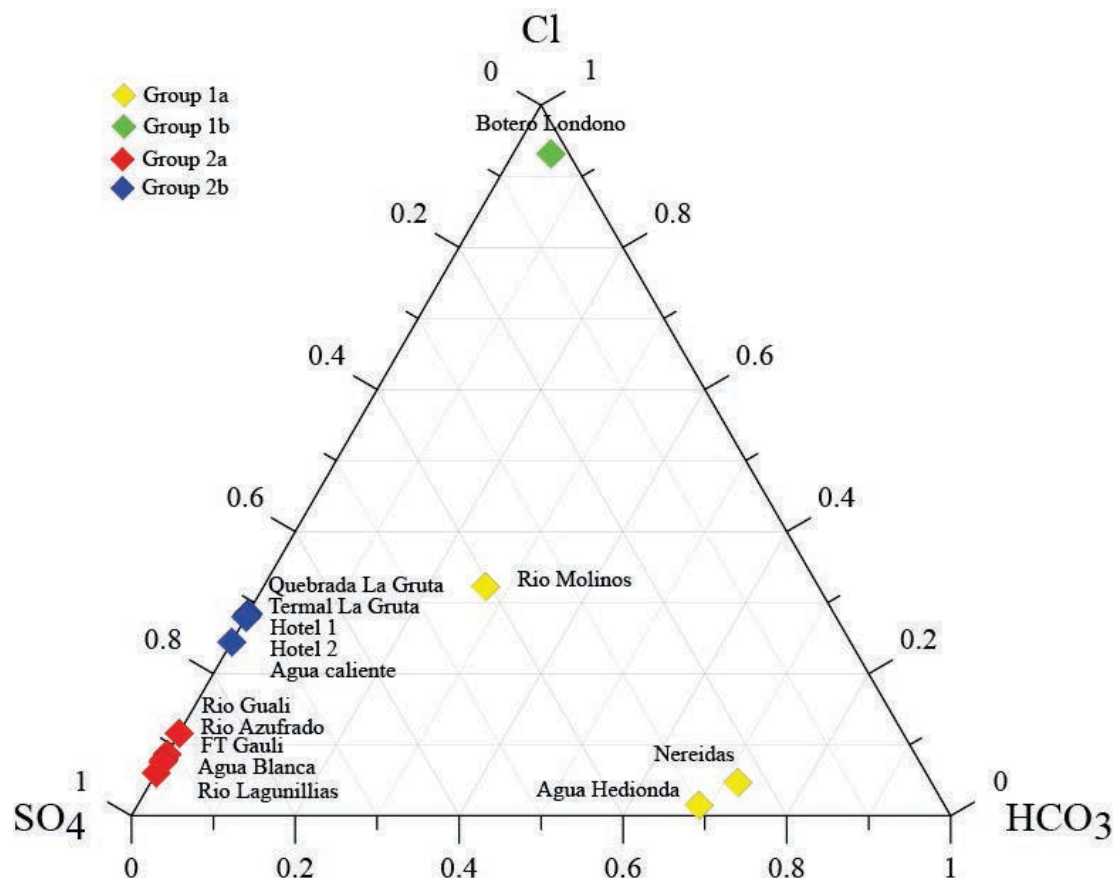


Fig. 4.2 - Triangular plot of major anions dissolved in water.

According to the pH, the waters were classified in two groups: Group 1 (near neutral-to-neutral) is characterized by pH values ranging between 5.9 and 8.8, Group 2 (acidic) has pH values between 1.0 and 3.6. Considering the major anions contents, the groups were further subdivided. Group 1a with the highest amount in HCO₃, Group 1b with chloride dominant composition. The fluids belonging to Group 2 are acid sulphate waters with composition plotting near the SO₄ corner in the ternary anion diagram (Fig. 4.2). The latter group can be subdivided according to the Cl content: Group 2a with lower Cl/SO₄ ratios (< 0.13) and Group 2b with higher Cl/SO₄ ratios (> 0.32).

Fe and Al contents are several orders of magnitude higher (up to 4.14 and 30.23 mmol/l respectively) in Group 2 compared to Group 1 (up to $2.85 \cdot 10^{-4}$ and $5.44 \cdot 10^{-4}$ mmol/l respectively). The water groups have different mineral saturation state (Tab. 4.2). Group 1 waters are

oversaturated with respect to iron and aluminium oxyhydroxides, while the waters of Group 2 are undersaturated with respect to those minerals. SEM-EDS analyses of SPM show amorphous silica in all the investigated waters, sometimes silica sphere probably encrusting organic matter (Fig 4.3b). Moreover, different solid phases were found in the groups of waters classified previously: in Group 1a Fe-, Al-oxyhydroxides encrusting amorphous silica are present (Fig. 4.3a); in Group 2a waters Fe-Al-Ca solid phases (probably sulphates) onto amorphous silica are recognised (Figg. 4.3c; 4.3d).

Group	Sample Name	T (°C)	pH	Cond (mS/cm)	Eh (mV)	Na	K	Mg	Ca	F	Cl	SO ₄	HCO ₃	Al	Fe	Si
Group 1	Agua Hedionda	13.9	5.9	0.4	170	0.48	0.07	1.07	0.76	0.01	0.05	1.01	2.30	0.0007	0.0005	1.64
	Rio Molinos	15.9	8.8	0.5	-	2.04	0.20	0.62	1.43	0.02	1.43	1.80	1.20	0.0005	0.0003	1.15
	Nereidas	50.4	6.1	2.0	96	5.35	0.45	1.95	3.25	0.00	0.62	3.10	9.40	0.0008	0.0004	3.06
	Botero Londono	79.5	7.7	6.8	-31	27.06	2.10	0.26	1.20	0.10	28.4	0.68	1.40	0.0353	0.0098	2.78
Group 2	Termal La Gruta	33.5	1.6	8.7	236	14.06	1.41	5.90	4.42	1.47	14.5	36.9	-	11.09	0.53	2.94
	Hotel 1	59.8	1.4	17.0	271	20.93	1.79	9.23	6.03	2.09	20.8	52.1	-	12.00	1.28	3.67
	Hotel 2	62.6	1.4	10.3	115	21.47	1.93	9.72	6.39	2.07	21.9	56.2	-	12.41	1.30	3.75
	Agua caliente	59.3	1.0	33.3	325	14.99	5.78	7.76	6.15	3.10	35.7	110.2	-	30.23	4.14	2.58
	Quebrada La Gruta	15.3	2.1	3.0	207	4.76	0.86	2.08	1.52	0.55	4.93	12.6	-	3.13	0.28	1.53
	Agua Blanca	29.1	3.3	2.5	205	1.81	0.26	2.16	10.38	0.22	1.39	16.1	-	1.86	0.27	2.03
	Rio Lagunillias	6.8	3.6	0.2	171	0.16	0.03	0.28	0.41	0.01	0.09	1.40	-	0.26	0.07	0.55
	Rio Guali	7.2	3.5	1.2	-	1.06	0.16	1.23	2.68	0.13	0.76	5.77	-	0.83	0.14	1.64
	Rio Azufrado	16.0	3.4	1.8	190	4.59	0.39	4.63	6.62	0.19	1.54	16.1	-	1.50	0.35	2.56
	FT Guali	59.2	2.8	3.5	246	1.81	0.28	2.89	8.67	0.31	1.30	15.7	-	1.78	0.02	3.25

Tab. 4.1 - Chemical composition of the studied waters expressed in mmol/l.

Group	Sample Name	Goethite FeOOH	Hematite Fe ₂ O ₃	Gibbsite Al(OH) ₃	Boehmite AlO(OH)
Group 1	Agua Hedionda	0.02	0.99	0.80	0.92
	Rio Molinos	3.66	8.27	0.48	0.61
	Nereidas	0.14	1.38	1.59	1.91
	Botero Londono	5.90	13.0	0.89	1.32
Group 2	Termal La Gruta	-6.57	-12.2	-3.97	-3.76
	Hotel 1	-7.07	-13.0	-4.62	-4.26
	Hotel 2	-6.22	-11.3	-4.60	-6.22
	Agua caliente	-7.04	-12.9	-5.50	-5.14
	Quebrada La Gruta	-8.25	-15.6	-5.83	-5.70
	Agua Blanca	-6.57	-12.2	-3.97	-3.76
	Rio Lagunillias	-5.08	-9.20	-2.24	-2.18
	Rio Guali	-6.87	-12.8	-4.64	-4.57
	Rio Azufrado	-7.69	-14.4	-5.26	-5.13
	FT Guali	-8.83	-16.5	-4.83	-4.47

Tab. 4.2 - Saturation indexes of studied waters.

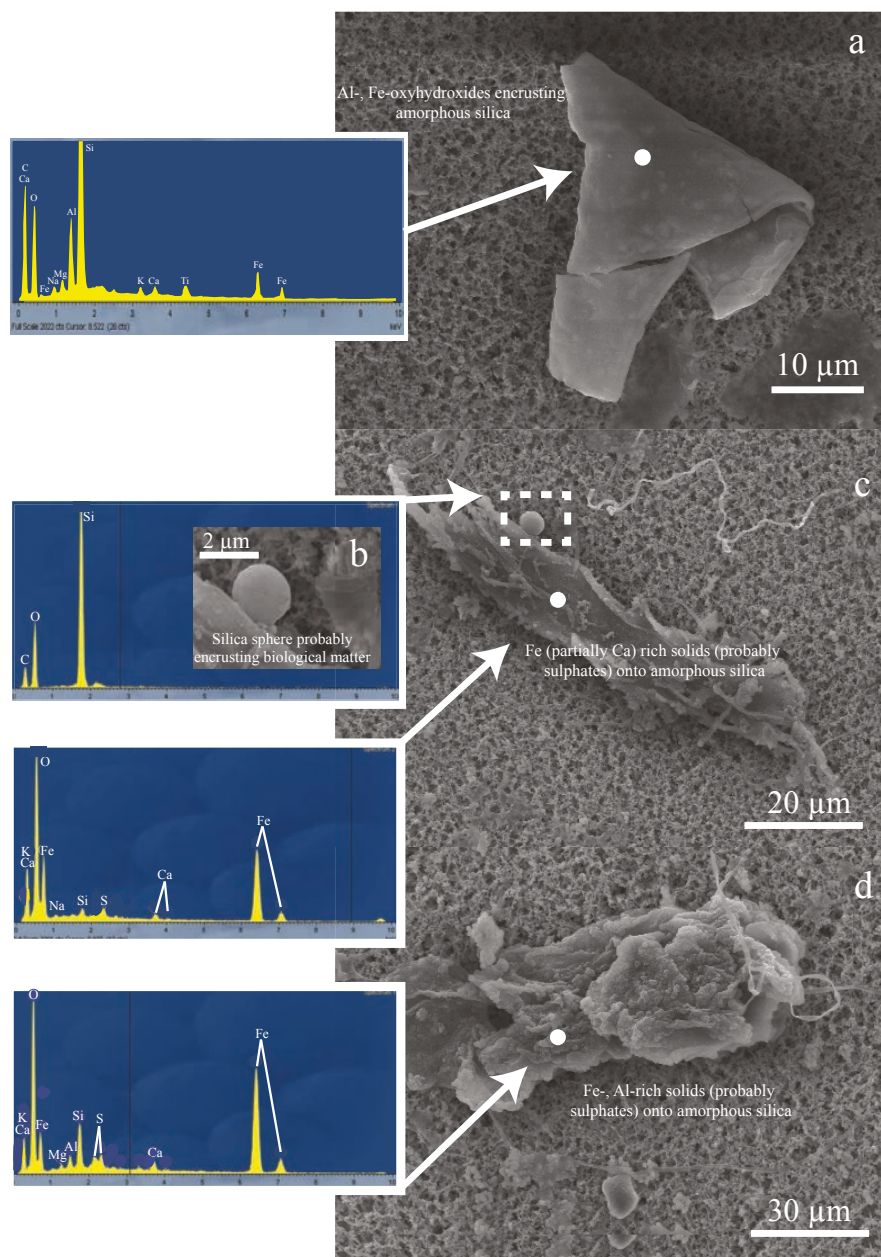


Fig. 4.3 - SEM-EDS observations of SPM showing: in Group 1a Al-, Fe- oxyhydroxides encrusting amorphous silica (a); in Group 2a, silica sphere probably encrusting biological matter (b), Fe (partially Ca) rich solids (probably sulphates) onto amorphous silica (c), Fe-, Al-, rich solids.

The isosal diagram (log-log compositional plot) was used to evaluate the degree of rock dissolution. This diagram allows to evaluate if the chemical composition of waters is a reflection of the rocks (near-congruent dissolution, under hyperacid conditions) and the possible removal of elements by precipitation of secondary minerals (Taran et al., 2008; Colvin et al. 2013; Varekamp

2015 and references therein). The hyperacid waters of Group 2 fall between the isosol lines indicating the dissolution of about 5 to 10 g of rock (Fig. 4.4). The Group 2b waters show to be close to congruent dissolution of the average local rock, for all elements with the exception of Si that is depleted in all samples (Fig. 4.4), probably due to the precipitation of silica minerals. The major elements of Group 2a deviate from the isosol line, with the exception of Mg and Ca that fall close to the 5 - 10 grams of rock dissolution line (Fig. 4.4). Strong depletions of Fe, Al, K and minor depletion of Na (Fig. 4.4) suggest the precipitation of alunite $[(K,Na)Al_3(SO_4)_2(OH)_6]$ and jarosite $[(K, Na)Fe_3(SO_4)_2(OH)_6]$, typical minerals precipitating in hyperacid hydrothermal systems (Taran et al. 2008; Varekamp et al., 2009; Colvin et al., 2013). The waters of Group 1 don't reflect the composition of the average local rock, showing the strong depletions in Fe and Al (Fig. 5), particularly in Group 1a waters, where the near-neutral pH allows the precipitation of iron and aluminium oxyhydroxides.

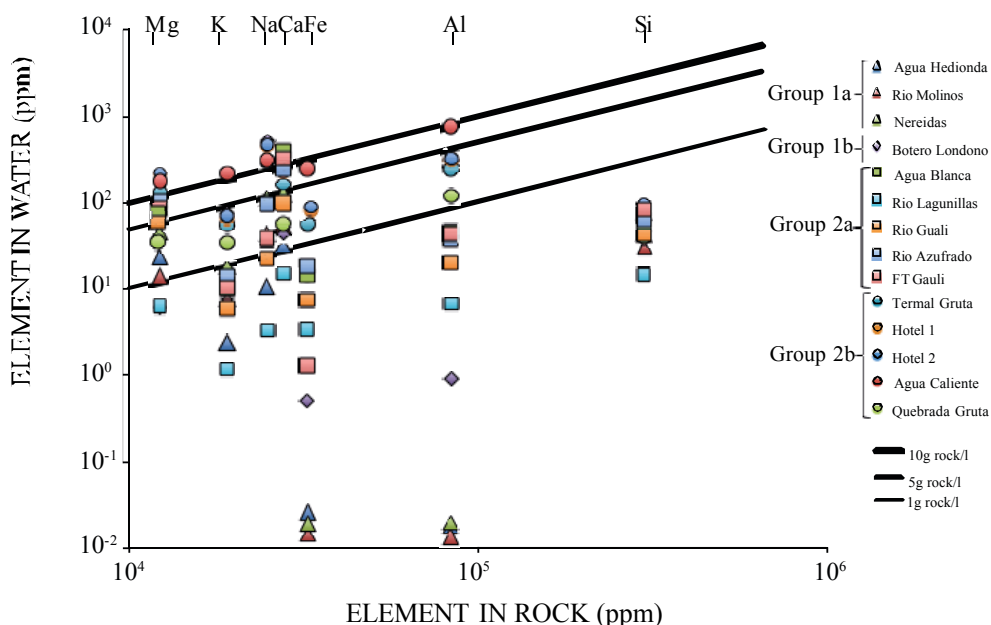


Fig. 4.4 - Isosol diagram is a log-log compositional plot, with the average volcanic rock composition versus the water composition. Isosol lines represent the equal amount of rock dissolved for the element considered. The plot shows the near-congruent dissolution of Group 2b (acid waters) and the depletion in K, Na, Fe, Al, in Group 2a (acid waters). The Group 2 shows a rock dissolution ranging between 5 and 10 g/l. Group 1 (near-neutral pH) is strongly depleted in Fe, Al reflecting the precipitation of Fe, Al- oxyhydroxides. (probably sulphates) onto amorphous silica (d).

4.1.2 REE, Zr and Hf

The total amount of REE in NDR waters ranges between 0.8 and 6722 nmol/l (Tab. 4.3). We found an inverse correlation between the total amount of REE and pH values (Fig. 4.5): higher REE contents are recognised in Group 2 (lower pH values) with respect to Group 1 (higher pH values). Great differences in Σ REE are found between the subgroups 1a and 1b with Botero Londono sample (Group 1b) displaying a higher value with respect to the waters of Group 1a (Fig. 4.5). The correlation between Σ REE and pH values suggests that rock dissolution is occurring more completely under acidic conditions, particularly Group 2b waters showing near-congruent dissolution of up to 10 grams of rock per liter (Fig. 4.5).

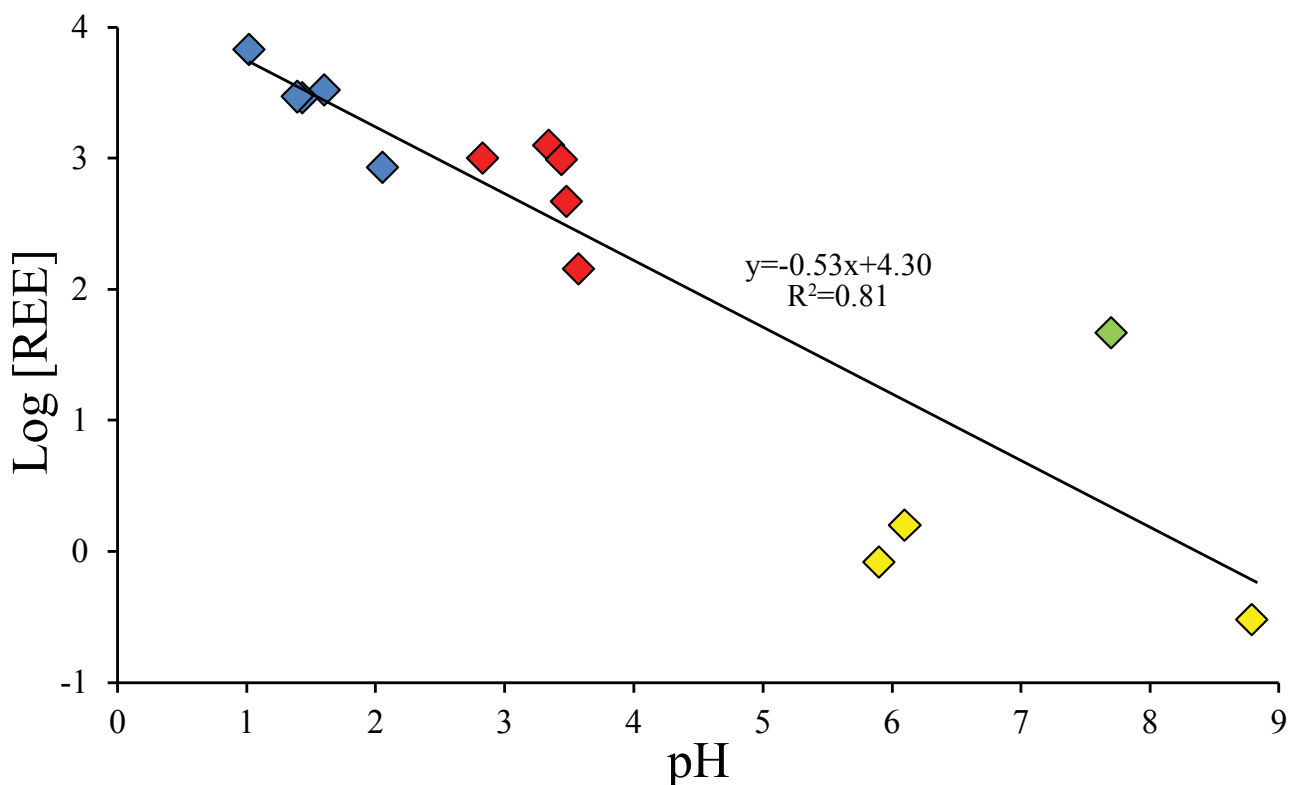


Fig. 4.5 - Variations of total REE dissolved in water as a function of pH. Symbols as in Fig. 4.2.

Considering the constant distribution of REE in the magmatic rocks of NDR, the studied waters were normalised to the average local rock (Borrero et al., 2009 and reference therein) evaluating processes of water-rock interaction in the hydrothermal system. The rock normalized REE patterns

differ among the various water groups (Fig. 4.6). Group 1a show patterns increasing from La to Lu, a positive Eu anomaly and negative Ce anomaly (Fig. 7). The Botero Londono water (Group 1b) shows a slight decrease from La to Lu (Fig. 4.6). The Group 2b waters show a flat pattern, whereas the waters of Group 2a are characterised by anomalous shape of pattern strongly depleted in LREE compared to the Middle Rare Earth Elements (MREE) and Heavy Rare Earth Elements (HREE) (Fig. 4.6).

Group	Sample	Y	La	Ce	Pr	Nd	Sm	Eu	Gd	Tb	Dy	Ho	Er	Tm	Yb	Lu	Zr	Hf
Group 1	Agua Hedionda	0.52	0.04	0.07	0.013	0.051	0.005	0.017	0.020	0.002	0.025	0.007	0.017	0.005	0.034	0.008	1.30	0.013
	Rio Molinos	0.17	0.02	0.008	0.006	0.029	0.007	0.017	0.009	0.002	0.014	0.003	0.01	0.003	0.008	0.003	5.31	0.057
	Nereidas	1.13	0.04	0.07	0.012	0.074	0.015	0.037	0.045	0.005	0.042	0.009	0.03	0.008	0.054	0.012	0.70	0.007
	Botero Londono	5.24	11.1	19.2	1.85	5.95	0.99	0.31	0.89	0.11	0.48	0.09	0.25	0.04	0.21	0.03	2.21	0.03
Group 2	Termal Gruta	642	512	1102	142	545	103	24.5	89.23	11.8	58.8	11.6	32.3	4.36	26.8	3.96	21.7	0.46
	Hotel 1	465	560	1034	119	429	77.9	19.6	71.30	9.07	46.5	9.39	25.8	3.52	21.6	3.16	8.52	0.24
	Hotel 2	483	565	1050	121	439	79.2	20.0	70.37	9.15	47.2	9.57	26.4	3.70	22.3	3.19	14.7	0.33
	Agua Caliente	914	1419	2575	269	944	177	43.8	153	19.1	91.7	17.7	47.6	6.45	38.3	5.62	35.1	0.90
	Quebrada Gruta	147	145	303	35.2	131	24.7	5.89	21.3	2.74	14.3	2.75	8.50	1.04	6.41	0.95	27.7	0.56
	Agua Blanca	629	20.4	108	22.8	177	63.6	19.0	81.6	12.83	64.6	11.7	28.4	3.26	17.5	2.34	3.01	0.28
	Rio Lagunillas	49.7	9.38	28.5	4.81	23.5	6.01	1.17	7.00	1.02	5.04	1.04	2.59	0.35	1.93	0.30	0.48	0.10
	Rio Guali	204	22.2	65.5	12.0	66.2	20.6	4.25	24.9	3.56	19.3	3.90	10.3	1.29	7.53	1.06	2.17	0.10
	Rio Azufrado	565	8.88	42.6	10.1	94.9	49.6	13.4	65.2	9.83	52.1	10.4	27.4	3.52	20.5	2.99	3.65	0.24
FT Guali	599	9.60	47.9	11.0	99.7	39.7	9.61	55.8	9.09	50.6	10.70	28.2	3.72	21.3	3.12	0.74	0.09	

Tab. 4.3 - REE, Zr and Hf dissolved in waters expressed in nmol/l.

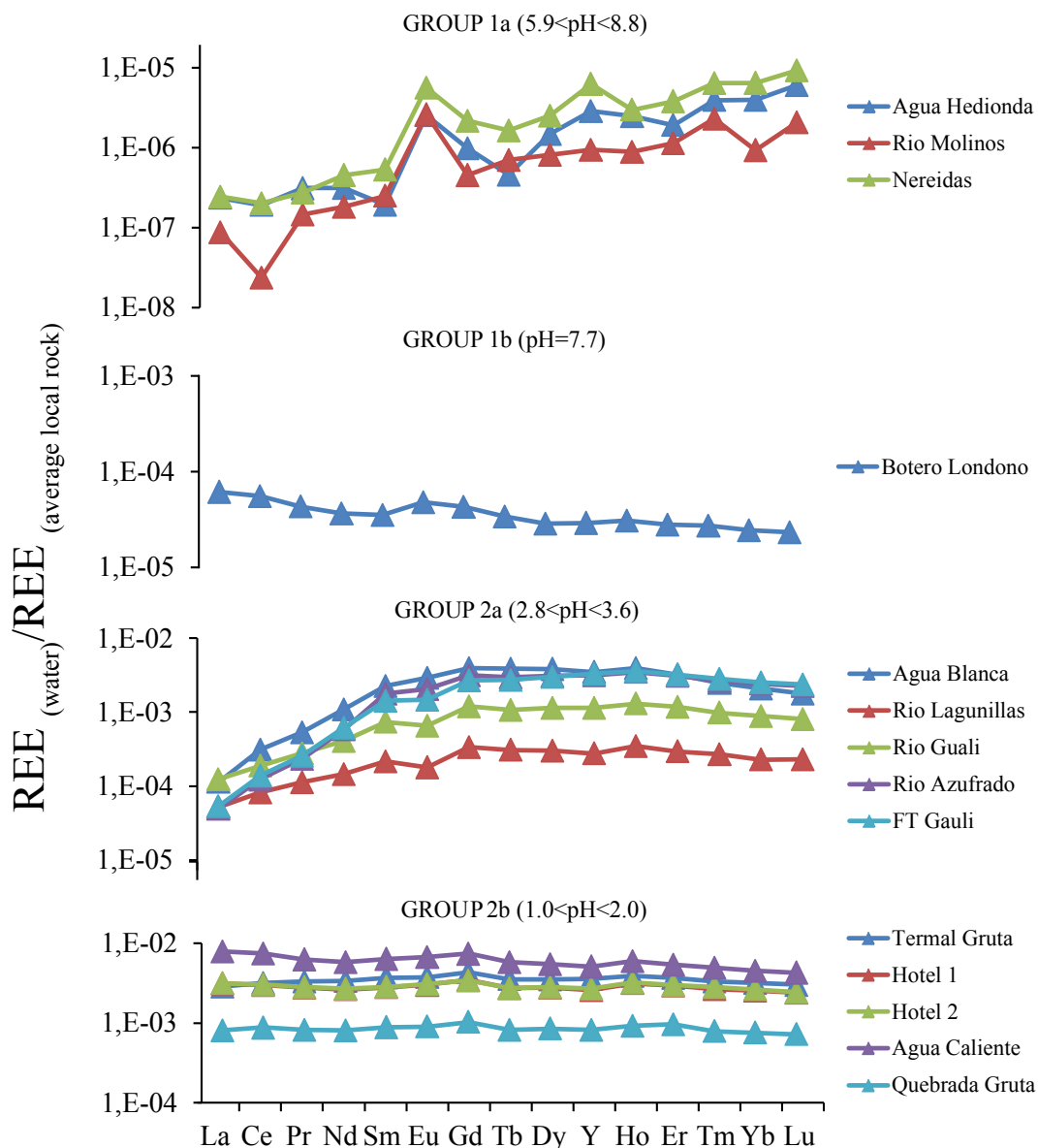


Fig. 4.6 - Average local rock-normalized REE patterns dissolved in water.

The amount of Y and Ho dissolved in waters range from 0.17 to 914 nmol l^{-1} and from 0.003 to 17.7 nmol l^{-1} respectively. Y/Ho molar ratios range between 47.8 and 127, with values changing from chondritic to superchondritic in acidic waters and in near-neutral waters respectively (Fig. 4.7).

The Zr concentration ranges from 0.48 to 35.1 nmol l^{-1} with Hf from 0.007 to 0.90 nmol l^{-1} . Zr/Hf molar ratios are within the range between 4.7 and 104, showing sub-chondritic values in acidic

waters and super-chondritic values in near-neutral waters (Fig. 4.7). Y/Ho and Zr/Hf ratios show simultaneous changes in the waters of Group 1, whereas different behaviour was recognised in acidic waters of Group 2 (Fig. 4.7).

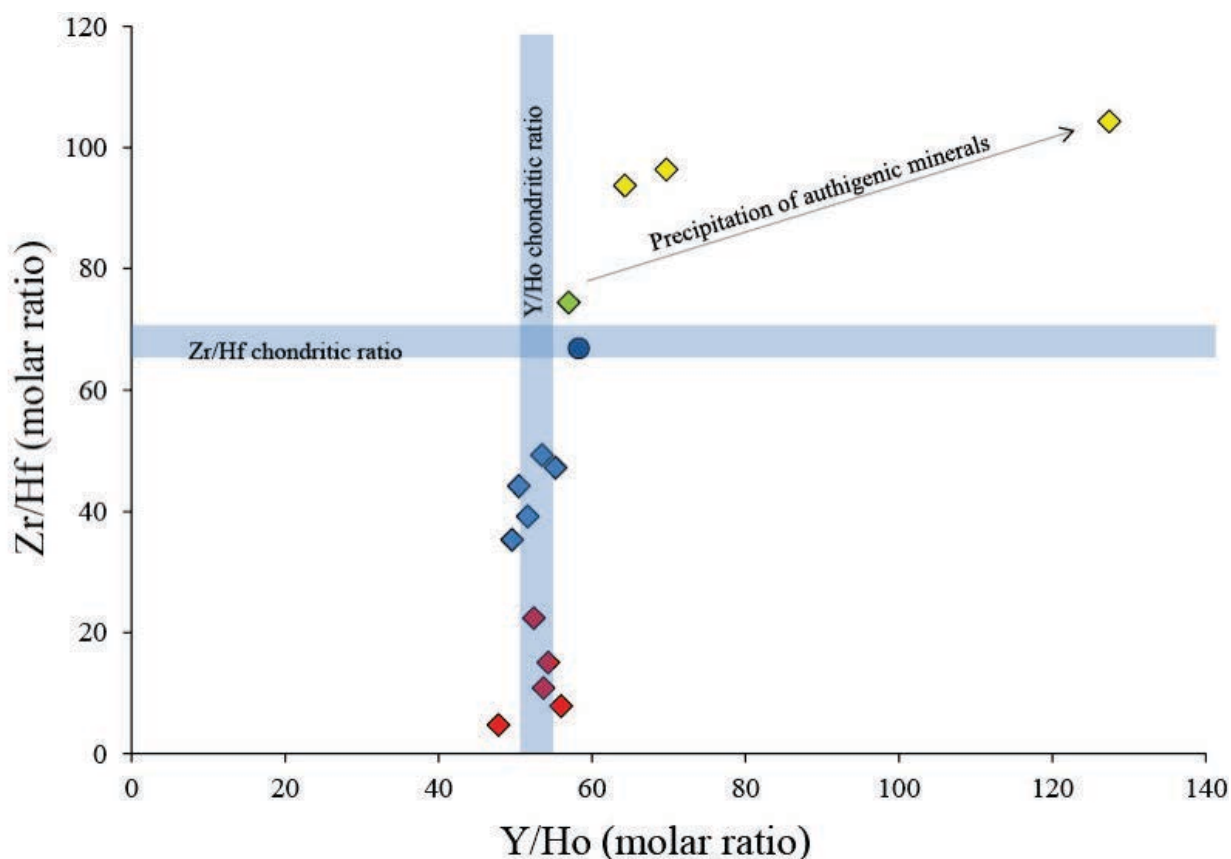


Fig. 4.7 - Zr/Hf and Y/Ho (molar ratios). Symbols as in Fig. 4.2, blue circle represent Y/Ho and Zr/Hf (molar ratios) in average local rock.

4.2 DISCUSSION

4.2.1 REE behaviour

The compositional variation of REE is mainly due to 4 processes: (i) the composition of the rocks interacting with water (dissolution of glass and minerals), (ii) the anionic composition of the waters determining the different complexation of REE, (iii) the incorporation into secondary minerals as function of the chemical-physical property of the waters and (iv) adsorption processes onto newly formed phases at higher pH (oxyhydroxide of Fe, Al, and Mn).

In NDR waters, the REE are strongly released by the rocks into acidic waters (Group 2). The pH controls the precipitation of new solid phases, inducing sorption and desorption of REE. The significant positive correlations between the total amount of REE and Fe or Al dissolved in waters (Fig. 4.8) shows the simultaneous variation of these elements, with the involvement of Fe and Al controlling the abundance of REE dissolved in water. Strong processes of scavenging occur during the co-precipitation and/or adsorption onto the surface of oxide and oxyhydroxide of Fe, Al, and Mn (Censi et al., 2007; Bau and Koschinsky, 2009).

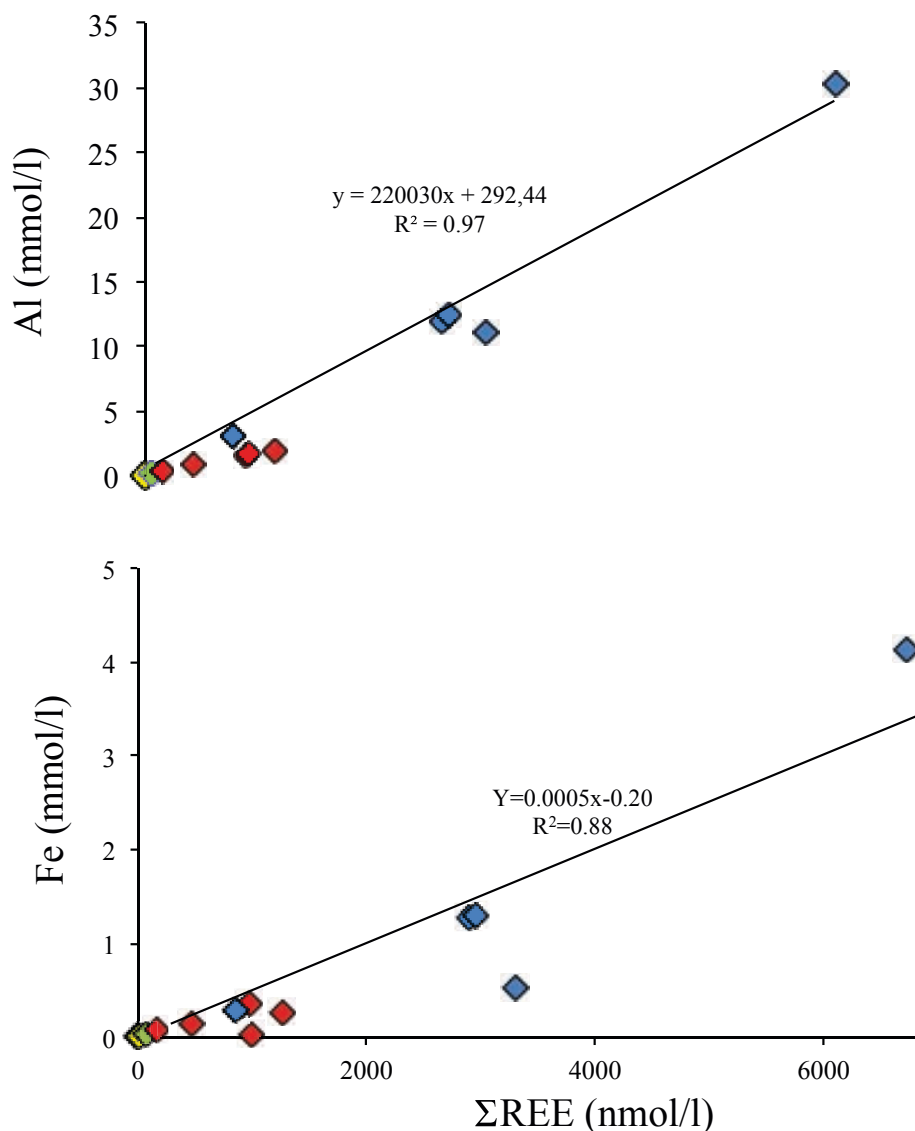


Fig. 4.8 - Total amount of REE versus Fe, Al dissolved in waters. Symbols as in Fig. 4.2

REE-complexes play a role together with other geochemical processes during the fractionation of REE (Lewis et al., 1998). The very low pH of the studied waters (Group 2) suggests that all the inorganic carbon dissolved occurs mainly as dissolved CO₂; consequently, carbonate complexes are negligible in these acidic solutions. However, [REE(CO₃)]⁺ and [REE(CO₃)₂]⁻ play a role in the waters belonging to Group 1, as they are the only ones with higher amount of carbonate species (HCO₃⁻ and/or CO₃²⁻) dissolved in solution.

The assessment of water-rock interaction processes is evaluated by the patterns of REE dissolved in waters normalised to the average local rock (Fig. 4.6). In the acidic solutions of Group 2, the speciation of REE is ruled by complexes with SO₄²⁻, F⁻ and Cl⁻, according to the relative abundance of anions dissolved in waters (Lewis et al., 1998). The Group 2b is the only one with flat patterns suggesting that source rocks mainly control the REE distribution, without processes changing the REE distribution in waters (Fig. 4.6). In Group 2a, the REE-patterns normalised to average local rock (Fig. 4.6) are characterised by strong LREE depletion. A similar shape of pattern with LREE depletion was already observed in other acid-sulphate waters from Waiotapu (New Zealand), Copahue volcano (Argentina), Santa Ana (El Salvador), Kawah Ihen Crater Lake (Indonesia) and Kutomintar and Sinarka volcanoes (Kawah Ijen) (Takano et al., 2004; Wood, 2006; Varekamp et al., 2009; Colvin et al., 2013; Kalacheva et al., 2015). Strong REE fractionation occurs during the hydrothermal alteration in very low pH waters with high SO₄²⁻ contents, showing higher LREE contents in alunitic advanced argillic altered rocks compared to the unaltered volcanic rocks (Hikov, 2011). The alteration minerals play an important role taking up the REE from the aqueous solution and/or releasing the elements, as a function of the chemical physical condition of the system that determines the stability of the solid phases. In particular, the precipitation of alunite-jarosite, was considered responsible of the LREE depletion in the acid-sulphate waters being the solid phases enriched in LREE (Ayers, 2012; Varekamp, 2015 and references therein). In the isosol

diagram, Group 2a waters show depletions in K, Fe, Al, Na pointing to alunite and jarosite precipitation (Fig. 4.4). Moreover, Al-, Fe- sulphates were found by SEM-EDS analysis as SPM (Fig. 4.3c, 4.3d). Coupling these information about the chemical propriety of waters and the nature of SPM, the depletion of LREE Group 2a, can be justified by the precipitation of Al-, Fe- sulphates as alunite and jarosite.

REE-patterns (Group 1a) normalised to average local rocks (Fig. 4.6) show a progressive increase from La to Lu according to the stability constant of $[\text{REE}(\text{CO}_3)]^+$ characterised by a progressive increase along the REE series (Wood et al., 1990; Millero et al. 1992). Botero Londono (Group 1b) is the only water with chloride-dominated composition. Considering the stability constant of $[\text{REECl}]^{2+}$ (Wood et al., 1990), the different pattern (Botero Londono) compared to other groups of samples is due to REE-chloride complexes stability constant, characterised by the same trend recognised for Botero Londono with a slight pattern decreasing along the REE series.

The precipitation of solid phases involving Fe, Al at circum-neutral pH conditions changes the abundance and the distribution of REE in water. Cerium and europium differ from the other REE for being redox sensitive elements. Cerium is removed from waters during neutralisation as CeO_2 and/or from precipitation of Fe, Mn and Al oxyhydroxides in river waters and marine environment (Elderfield et al., 1990; Goldstein and Jacobsten, 1988; Seto et al., 2008). The Ce and Eu anomalies vary with pH (Fig. 4.9). In particular, the waters with $\text{pH} < 3.6$ (Group 2) have no significant Ce and Eu anomalies, whereas the waters with $\text{pH} > 5.9$ (except Botero Londono sample) show strong negative anomalies of Ce and strong positive anomalies of Eu. The Ce anomaly can be explained considering the enhanced removal of Ce with respect to La and Pr, during the processes of co-precipitation and/or adsorption onto the surface of authigenic minerals (Al-, Fe oxyhydroxides).

Ce has a different behaviour in Botero Londono sample compared to the other samples of Group 1, not showing strong Cerium anomaly (Fig. 4.9a). The main differences of Botero Londono water

compared to the other waters belonging of Group 1 are the higher ionic strength and the lower Eh value. These differences could limit the precipitation of Al-, Fe-oxyhydroxide allowing higher amounts of Al and Fe dissolved in water. Moreover, SEM-EDS observations of SPM (Botero Londono) do not show the presence of Al-, Fe-oxyhydroxide solid phases.

Almost all the investigated waters are characterised by a small anomaly of Europium (Fig. 4.9b), except for the waters of Group 1 where a strong positive anomaly (1.22-7.43) occurs, suggesting additional processes that fractionate the REE. The strong positive Eu anomaly found in the water of Group 1a could be justified by the slow interaction of waters with Eu enriched plagioclase, as already recognized in other hydrothermal systems (Wood et al., 2003 and references therein; Varekamp et al., 2009; Peiffer et al., 2011)

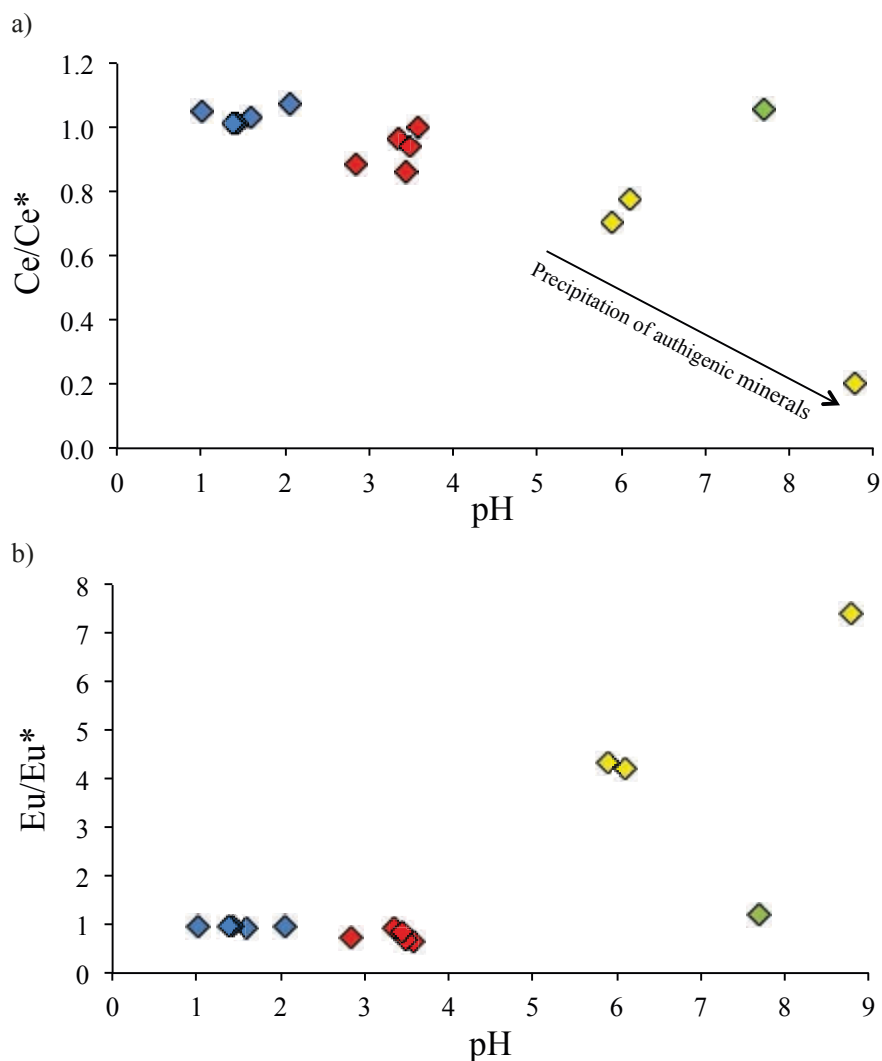


Fig. 4.9 - Variations of total REE dissolved in water as a function of pH. Symbols as in Fig. 4.2.

4.2.2 The behaviour of twin pairs (Y-Ho; Zr-Hf)

The decoupling of Y-Ho and Zr-Hf in seawater indicated that these elements are not controlled only by charge and ionic radius (Bau, 1996; Godfrey et al., 1996). The behaviour of Zr and Hf in natural waters is limited to the neutral-basic environments (mainly sea water), where superchondritic Zr/Hf ratio was recognised (Firdaus et al. 2011; Schmidt et al. 2014). The inorganic speciation of Zr and Hf in water with circum-neutral pH is dominated by hydroxyl groups ($Zr(OH)_5^-$, $Hf(OH)_5^-$, $Zr(OH)_4$, $Hf(OH)_4$), whereas Y and Ho are mainly complexed by carbonate species (Byrne 2002). The different charge of metal complexes determines the adsorption behaviour onto

the solid surfaces (Koscinsky and Hein, 2003). Bau and Kochinsky (2009) show that the Y/Ho ratio in marine Fe-Mn hydroxydes is significantly lower than seawater, suggesting an enhanced scavenging of Ho with respect to Y in the Fe-Mn crusts. Recently, Schmidt et al. (2014) investigating the fractionation of Zr-Hf between seawater and Fe-Mn crusts, showed that Zr/Hf ratio is lower in the Fe-Mn oxyhydroxides compared to seawater. These studies indicate that both Hf and Ho are more easily removed than Zr and Y during the formation of marine Fe-Mn oxyhydroxides and that the geochemical behaviour of these twin pairs is not simply ruled by charge and ionic radius.

The near neutral-to-neutral waters of Group 1 have higher values of Y/Ho and Zr/Hf ratios with respect to the acidic waters and the average local rock (Fig. 4.7). The twin pairs fractionation in Group 1 is due to the formation of the observed authigenic solid phases (Fe-, Al-oxyhydroxides) stable at neutral pH. The preferential removal of Ho and Hf with respect to Y and Zr is attributed to the enhanced scavenging during the co-precipitation onto the surfaces of Fe, Al oxyhydroxides (Bau, 1999; Bau and Dulski, 1999; Bao et al., 2006; Censi et al., 2007; Feng et al., 2010, Schmidt et al. 2014). However, in Botero Londono water (Group 1b), Y-Ho and Zr-Hf do not significantly fractionate and Ce anomaly is negligible (Fig. 4.9a), in agreement with the limited Fe, Al oxyhydroxides formation. Our data show that Y-Ho and Zr-Hf are removed from the hydrothermal system by Fe-, Al-oxyhydroxides precipitating in water with circum-neutral pH.

In Group 2 (acidic waters), Y-Ho and Zr-Hf twin pairs are characterised by a different behaviour. Y/Ho ratios are close to the average local rock, showing the negligible fractionation of these isovalent elements, while Zr/Hf ratios are sub-chondritic. The behaviour of Zr and Hf in extreme acidic environments has not been studied yet. Only few studies were carried out on the speciation of Zr and Hf with fluoride and chloride ligands, but not in water with very high sulphate contents (Perschina et al., 2002; Monroy-Guzman et al., 2010). Molecular dynamic calculation (Perschina et

al., 2002) indicated that in chloride media, chloride complexes are enhanced for Hf with respect to Zr, independently of pH. In Group 2 waters Zr and Hf are decoupled indicating that the geochemical twin is not controlled only by ionic radius and charge. Figure 4.10 shows that Zr/Hf ratio increases as Cl/SO₄ ratio increases highlighting a different behaviour of isovalent elements as a function of anion contents (Cl and SO₄). The Zr-Hf fractionation observed in this acidic environment may result from different stability constants of Zr and Hf complexes with Cl and SO₄ ligands that in turn determine the relative abundance of these metals in hyper-acid waters.

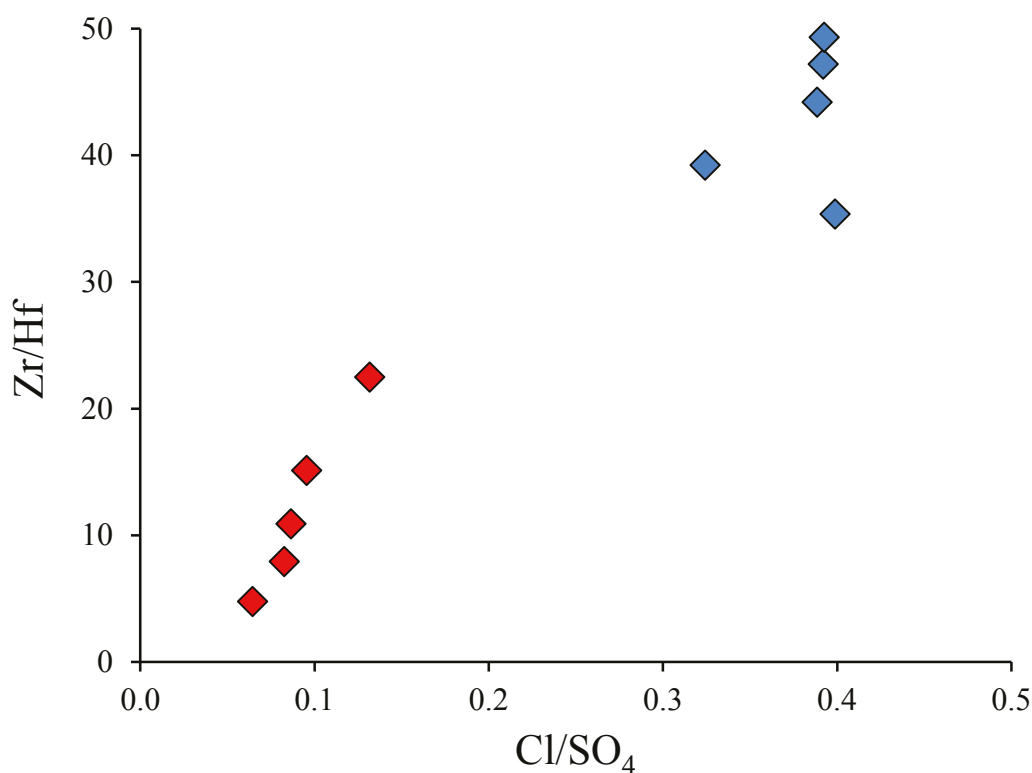


Fig. 4.10 - Zr/Hf versus Cl/SO₄ (molar ratios) in acidic waters (Group 2). Symbols as in Fig. 4.2.

4.3 CONCLUDING REMARKS

The thermal fluids circulating in NDR system have a variety of major chemical composition and cover a wide range of pH values from 1 to 8.8. The concentrations of REE and their patterns normalised to the average local rock change as function of processes occurring in the shallower and/or deep system. The major anions play an important role on the distribution of REE driven by

complexation, whereas the pH values rule the precipitation of solid phases, also fractionating the REE. Negative cerium anomaly in water with near-neutral pH underscores the importance of authigenic minerals (Fe-, Al-oxyhydroxides) on the fractionation of REE, indicating a different behaviour of Ce with respect to the neighbouring elements. Moreover, the precipitation of alunite and jarosite strongly fractionate the REE distribution in Group 2b, depleting the LREE in the aqueous phase.

For the first time, Y-Ho and Zr-Hf behaviour was studied simultaneously in a wide range of pH and chemical composition of major anions. The precipitation of Al-, Fe-oxyhydroxides occurs when pH values are close to neutrality fractionating Y-Ho and Zr-Hf, with a preferential Ho and Hf removal. A different behaviour of Y-Ho and Zr-Hf was identified in acidic sulphate waters with different content of chloride. Y/Ho displays chondritic ratios, showing a negligible fractionation compared to the local rock, whereas Zr/Hf ratios are sub-chondritic, increasing as Cl/SO₄ ratios increase. This evidence suggests a different stability of chemical complexes of Zr and Hf with Cl and SO₄ ligands, leading to sub-chondritic Zr/Hf ratios in strong acid environments.

CHAPTER 5

Zr-Hf AND REE SIGNATURES DISCRIMINATING THE EFFECT OF ATMOSPHERIC FALLOUT FROM THE HYDROTHERMAL INPUT IN VOLCANIC LAKE WATERS

5.1 RESULTS

5.1.1 *General aspects*

The water samples were collected in Pantelleria from springs, wells and lake “Specchio di Venere” (Fig. 5.1). The chemical physical parameters and the major element concentrations of the investigated waters are reported in table 5.1. Temperature ranges between 26.8 and 54.6 °C, Eh values are spanning from -245 to 161 mV, pH values range between 6.0 and 9.1 and electrical conductivity values increase from 2 to 35 mS/cm.

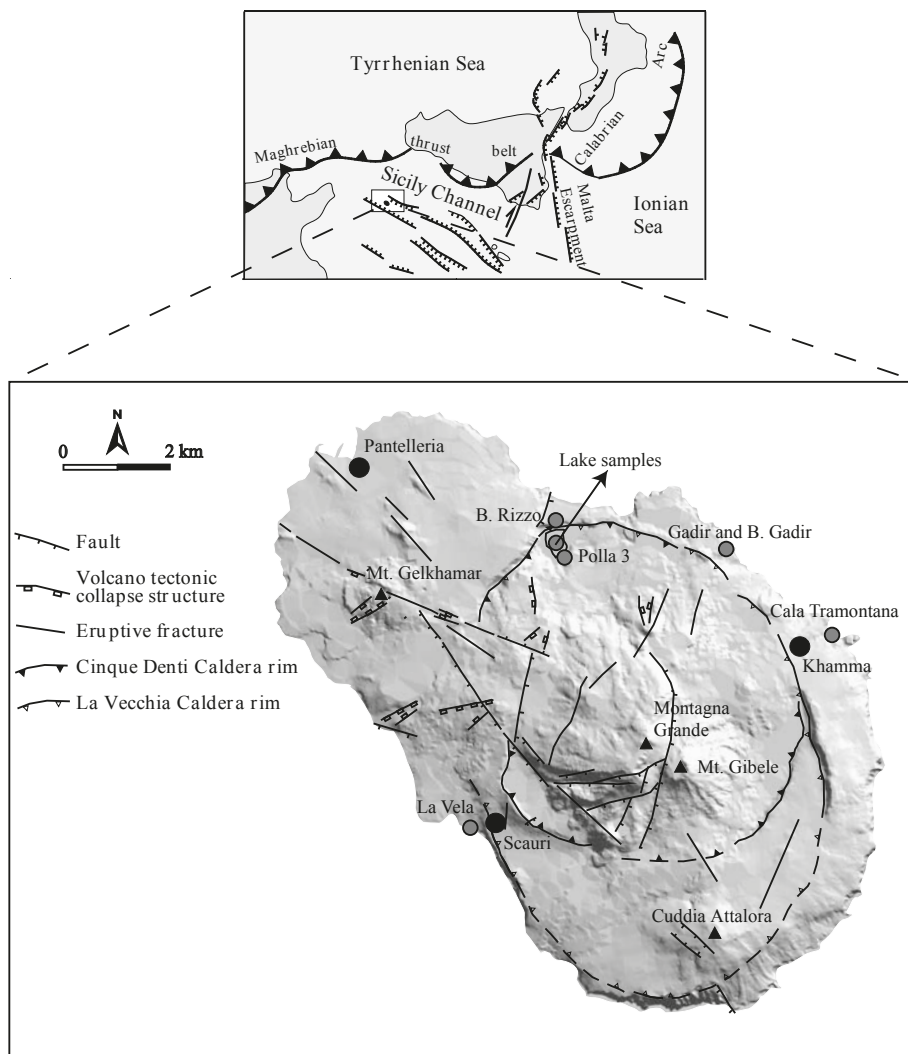


Fig. 5.1 – Location map of sampled waters.

In the anion triangular plot (Fig. 5.2a), waters fall along the line connecting the seawater composition and the alkalinity vertex, suggesting a mixing process between seawater and water enriched with CO_2 . The waters from the top and the bottom of the lake show the same anionic composition. The cation triangular plot displays waters falling close to the Na-K vertex (Na is the dominant cation) with a low dispersion of samples towards the Mg, Ca vertices, whereas waters from the top and the bottom of the lake show quite constant cations composition (Fig. 5.2b).

SAMPLE	DATE	T (°C)	pH	Cond. (mS/cm)	Eh (mV)	Na	K	Mg	Ca	F	Cl	Br	SO ₄	Alkalinity	O ₂	N ₂	CO ₂
Daietti	29/05/13	26.8	6.0	2.02	161.5	13.10	0.68	1.50	0.77	0.06	9.40	0.01	0.78	6.10	1.7	9.6	258.3
Cala tramontana	28/05/13	29.4	8.5	4.26	8.1	34.01	1.02	1.10	0.44	0.42	27.22	0.06	1.32	7.00	3.2	12.6	5.3
Buvira Gadir	28/05/13	34.4	7.8	12.74	6.5	117.77	3.81	4.25	1.78	0.52	103.60	0.19	4.02	18.20	2.5	11.3	16.3
Buvira Rizzo	29/05/13	33.9	7.0	13.95	96.4	127.15	3.82	7.05	1.85	2.01	96.98	0.10	3.72	41.20	1.0	7.6	3.1
Polla 3	29/05/13	54.6	6.4	15.75	-107.6	136.26	4.17	4.31	2.12	0.57	122.73	0.22	4.21	21.35	0.1	4.9	356.8
Gadir	28/05/13	53.8	6.32	16	7	139.38	4.34	6.21	2.06	0.67	125.32	0.18	4.99	19.20	0.9	4.5	309.7
La Vela	29/05/13	48.3	6.5	34	17	326.26	10.51	12.87	4.32	0.23	340.43	0.46	10.02	9.50	1.9	12.2	119.2
Lake (-30 cm)	03/07/14	27.2	8.97	35.1	21.5	351.86	11.56	8.00	0.65	0.64	288.73	0.43	12.61	56.50	4.4	10.4	3.1
Lake (-13 m)	03/07/14	26.8	8.96	35.2	-245	349.80	11.45	7.82	0.40	0.54	284.71	0.39	12.50	56.50	-	-	-

Tab. 5.1 - Chemical composition of cold and thermal waters. The chemical composition of major ions is expressed in mmol l⁻¹, while dissolved gases are expressed in cc l⁻¹ (STP).

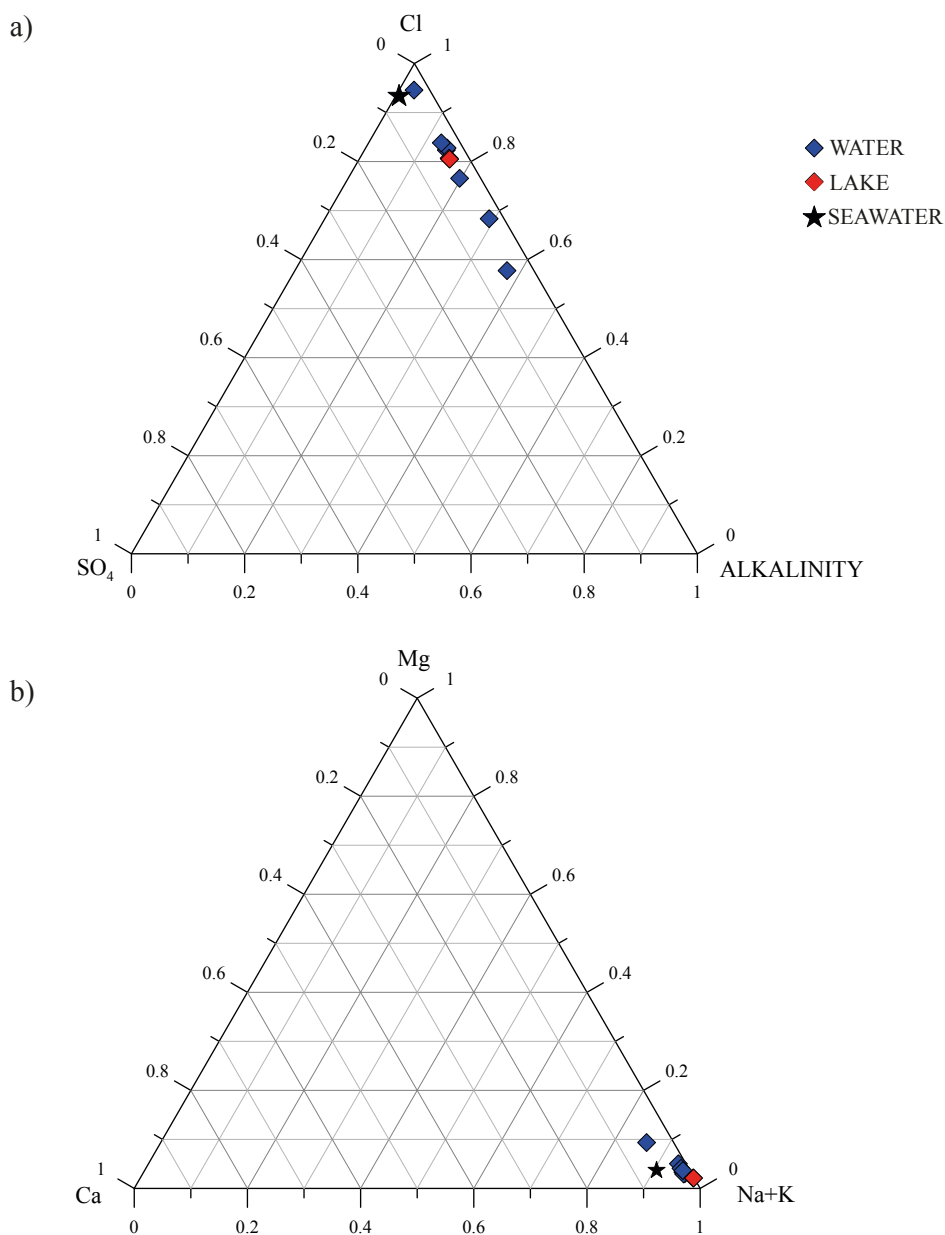


Fig. 5.2 – a) Triangular plot of major anions dissolved in waters. b) Triangular plot of major cations dissolved in waters.

The Na-Cl binary graph (Fig. 5.3) shows that almost all samples are characterized by Na/Cl molar ratios higher compared to the same ratio in seawater. The excess of Na is due to the interaction process of water with the Na-alkaline hosting rocks (Dongarrà et al., 1983).

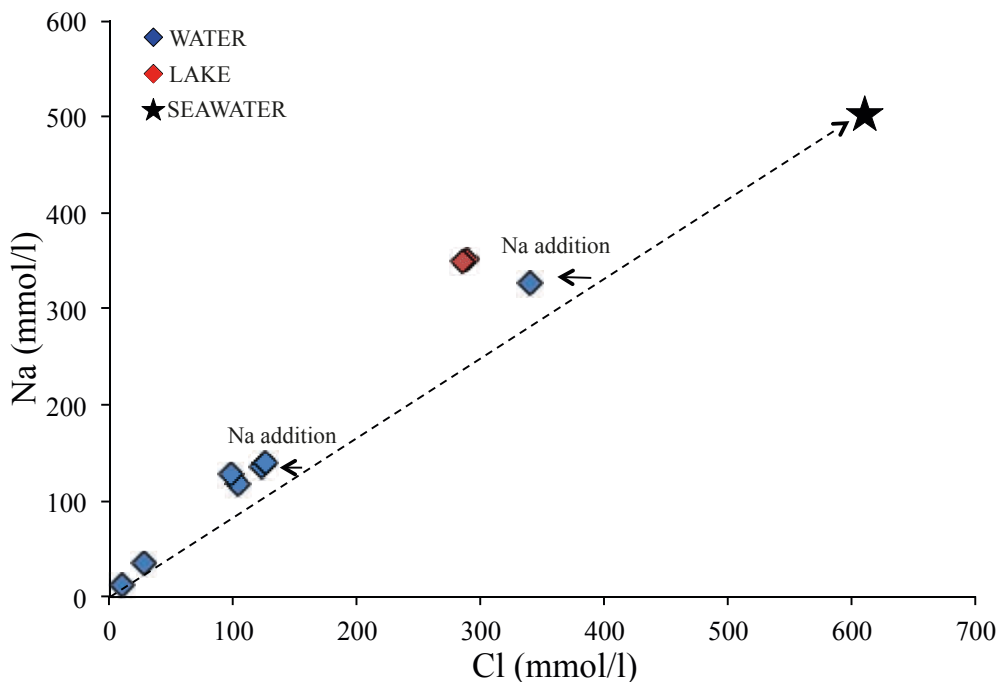


Fig. 5.3 - The binary graph (Na vs. Cl) shows higher Na/Cl molar ratios with respect to the Na/Cl molar ratio in seawater (dashed line). Na enrichments in waters are due to the water-rock interaction with the Na-alkaline hosting rock.

The chemical composition of the elements, pH and electrical conductivity do not show significant difference between the sample water collected in the shallowest part and at the bottom of “Specchio di Venere” lake, whereas Eh values are characterized by a variation from -31.5 (top) to -245 mV (bottom). Moreover, the chemical-physical parameters of the water and the major elements have a quite constant concentration along the water column (Jácome Paz M., personal communication).

CO₂ dissolved in water ranges between 3 and 357 cc l⁻¹ (Tab. 5.1), with values several orders of magnitude higher with respect to the Air Saturated Sea Water (ASSW-0.24 cc l⁻¹ of CO₂). Triangular plot CO₂-N₂-O₂ (Fig. 5.4) displays waters aligned along the line connecting the CO₂

vertex with the ASSW, showing the CO₂-water interaction in different proportion.

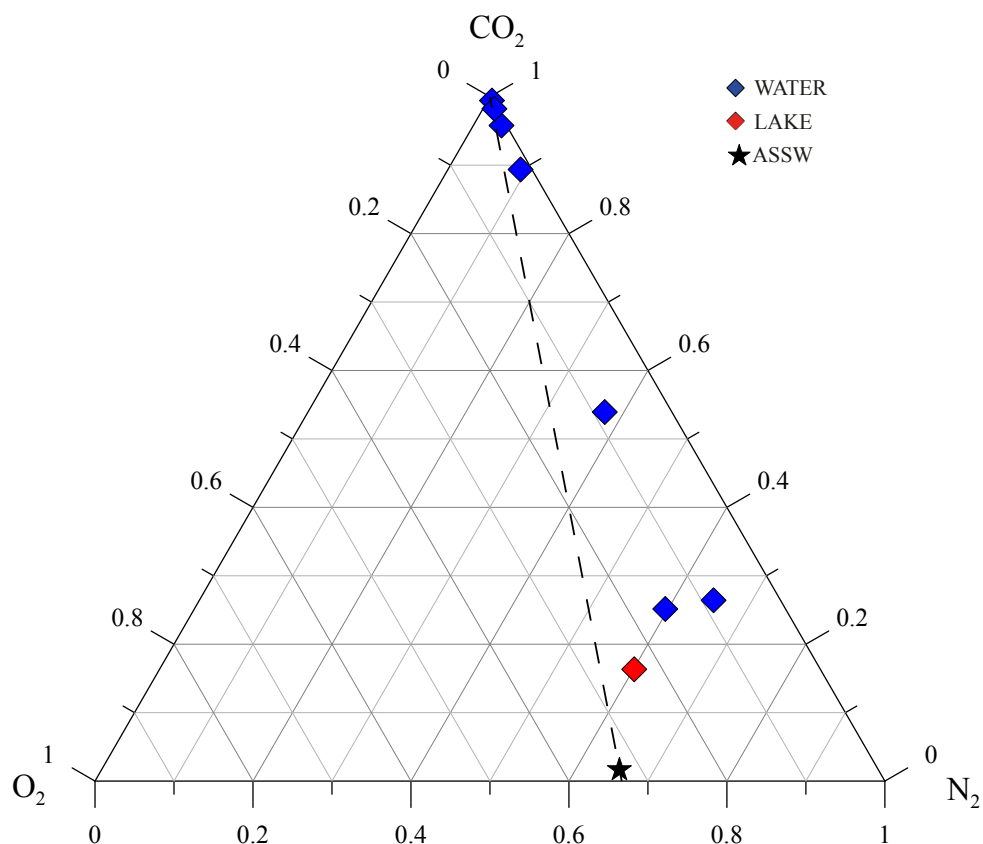


Fig. 5.4 - Triangular plot, relative abundance of CO₂, N₂ and O₂ dissolved in waters. The ASSW (air saturated seawater) values is reported for comparison. The dashed line represents the theoretical mixing between air dominated system and CO₂-rich fluids.

Results of PHREEQC simulation showed waters from wells and springs are oversaturated in comparison with carbonate minerals and Fe oxyhydroxides, except for Daietti well, which is under-saturated in carbonate minerals and Polla 3 that is under-saturated with respect to Fe oxyhydroxides. Furthermore, the investigated waters are constantly saturated in amorphous silica. Further investigations were carried out with SEM-EDS analysis onto the nature of SPM (Fig. 5.5a) from lake water and Polla 3 (thermal-spring feeding the lake). Amorphous silica was recognized in Polla 3 sample (Fig. 5f.5), whereas phyllosilicates (Fig. 5.5c-e) and Fe oxyhydroxides were recognized as SPM (Fig. 5.5b-d) in shallowest water layer of the lake.

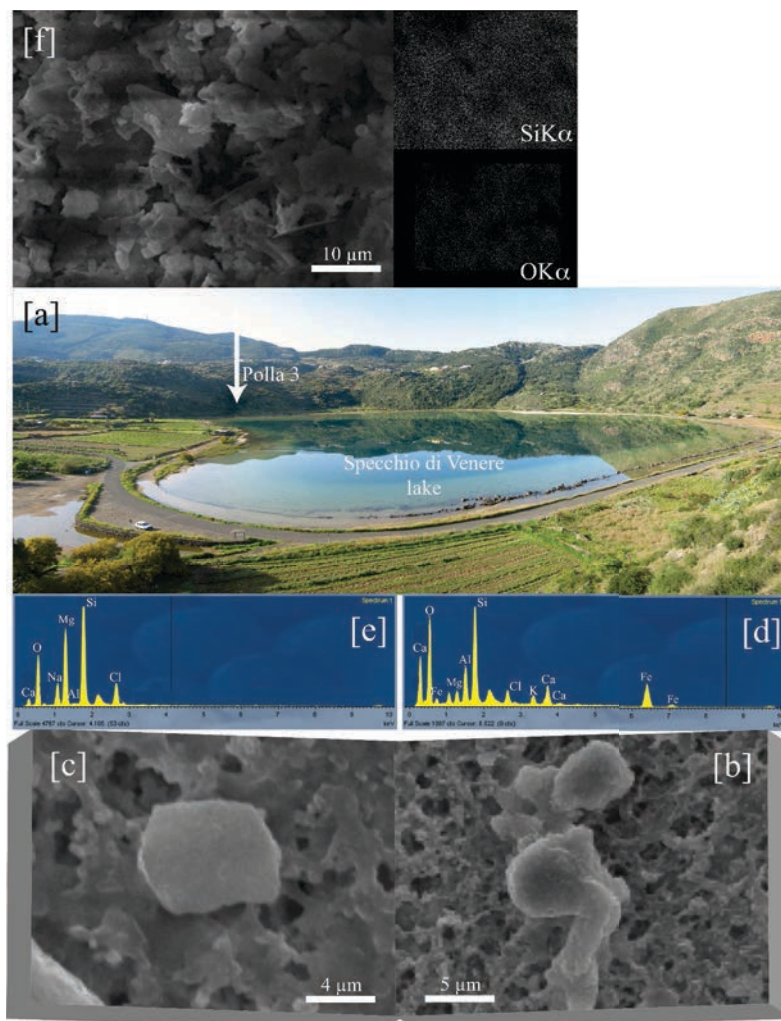


Fig. 5.5 - Nature of suspended particulates in “Specchio di Venere” lake water and Polla 3 thermal-spring feeding the lake [a]. Fe-oxyhydroxides [b] and phyllosilicates [c] from the shallowest water layer, as recognised by X-ray spectra [d] and [e], respectively. On the contrary, suspended particulates from the hydrothermal Polla 3 mainly consist of amorphous silica [f] as indicated by the reported x-ray maps for oxygen and silicon.

5.1.2 REE, Zr and Hf

The total amount of REE ranges between 2.77 and 12.07 nmol l⁻¹, with the highest value found in lake waters (Tab. 5.2). A strong relation between the total REE dissolved in water and the pH values was recognized in several aqueous environments, highlighting the important role of pH for the REE mobility, able to increase the total REE concentration (Lewis et al., 1998; Michard et al., 1989; Inguaggiato et al., 2015). In the investigated waters, the relation between REE and pH values is not well evidenced. The total REE content is not significantly correlated to the TDS, showing that the REE concentration in the investigated waters is not related to the salinity. The lack of a clear

relationship between the concentration of REE and the chemical-physical parameters was already recognized in CO₂-rich waters (pH 6-7) investigated in the Massif Central (France) (Négre et al., 2000).

SAMPLE	Y	La	Ce	Pr	Nd	Sm	Eu	Gd	Tb	Dy	Ho	Er	Tm	Yb	Lu	Zr	Hf
Daietti	2667.31	334.69	179.70	63.52	218.74	58.71	23.99	94.83	19.48	125.44	34.85	116.86	17.98	122.45	19.80	1205.88	7.31
Cala tramontana	1806.65	299.29	474.40	69.39	222.96	53.23	17.68	70.77	14.61	79.52	24.03	79.18	11.99	78.94	12.37	3989.37	33.62
Buvira Gadir	2608.51	521.84	799.41	114.54	392.39	93.06	25.13	132.32	24.35	169.94	42.06	137.19	21.58	149.30	24.75	833.01	4.34
Buvira Rizzo	965.87	278.32	816.68	59.90	202.46	51.14	22.51	81.85	14.61	94.25	21.63	69.11	10.79	69.88	11.88	1205.88	9.24
Polla 3	1999.75	325.46	810.19	73.71	245.24	66.21	24.94	107.72	27.87	168.37	44.88	136.63	23.26	177.37	29.70	2192.50	8.40
Gadir	2375.97	215.22	287.23	48.65	160.88	46.86	18.00	76.77	22.53	129.63	38.74	123.07	19.18	149.06	24.25	2510.41	8.40
La Vela	4556.57	189.82	265.25	35.58	124.59	38.51	14.36	83.40	24.91	186.25	58.48	229.41	33.56	231.13	36.38	619.75	3.17
Lake (-30 cm)	5640.42	454.63	2289.34	157.11	595.07	617.38	186.09	760.43	126.29	614.18	155.04	205.05	30.67	203.73	31.03	23130.31	300.17
Lake (-13 m)	5228.43	421.17	2197.13	149.18	584.75	603.97	183.21	739.58	122.91	594.63	147.82	232.52	29.98	212.81	30.14	22150.34	290.27

Tab. 5.2 REE, Zr and Hf dissolved in waters expressed in pmol l⁻¹.

REE normalized to Post Archean Australian Shale (PAAS) show patterns increasing along the REE series (Fig. 5.6). Ce and Eu anomalies were recognized in the investigated waters with Ce/Ce* values from 0.27 to 1.98 and Eu/Eu* values from 0.95 to 1.53. The water samples collected from the top and the bottom of “Specchio di Venere” lake show REE-patterns with a concave shape facing downward and quite constant REE distribution (Fig. 5.6).

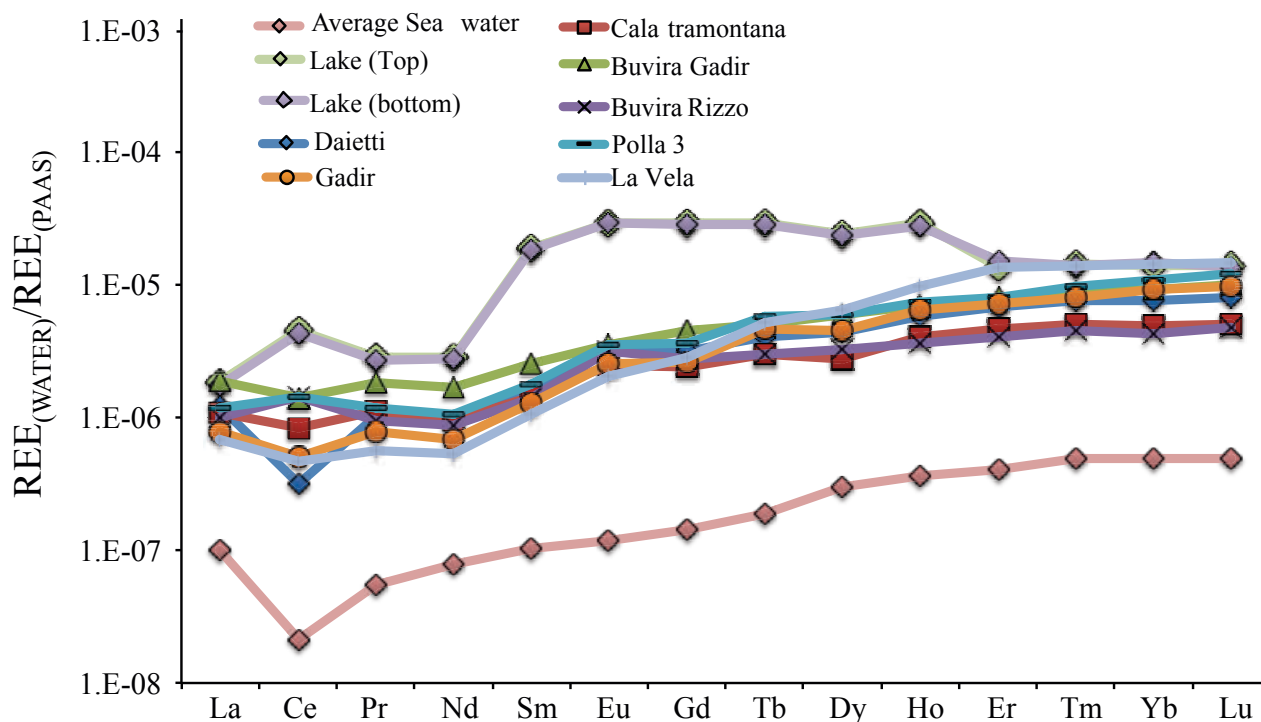


Fig. 5.6 - REE dissolved in waters normalised to the PAAS. The average seawater (Censi et al., 2007) was plotted for comparison.

The REE-patterns display HREE enrichments with $(LREE/HREE)_N$ ratios ranging from 0.05 to 0.36, whereas $(MREE/HREE)_N$ ratios change between 0.22 and 1.53 (Fig. 5.7). MREE enrichments were recognized in water samples from “Specchio di Venere” lake, which are the only samples with $(MREE/HREE)_N$ ratios >1 (Fig. 5.7).

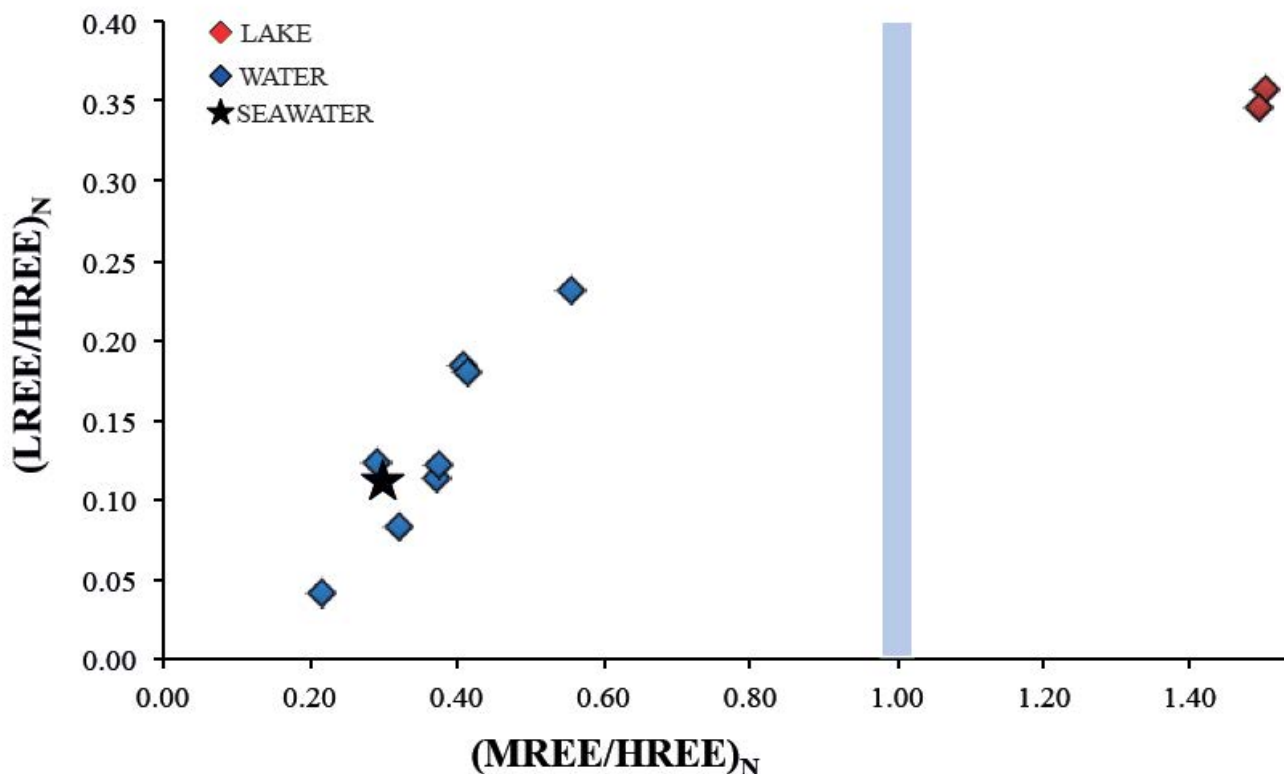


Fig. 5.7 - $(LREE/HREE)_N$ vs. $(MREE/HREE)_N$ showing values <1 , except lake waters characterized by $(MREE/HREE)_N$ ratios >1 . The seawater is reported for comparison.

The amount of Y and Ho dissolved in waters changes from 0.97 and 5.64 nmol l^{-1} and from 0.024 to 0.15 nmol l^{-1} respectively, with Y/Ho molar ratios ranging between 35.37 and 77.91. The amount of Zr and Hf dissolved in waters range from 0.62 to 23.13 nmol l^{-1} and from 0.003 and 0.30 nmol l^{-1} respectively, with Zr/Hf ratios included between 76.30 and 298.72. The highest amounts of Y, Ho, Zr and Hf were found in lake waters without significant differences between shallow and deep samples, characterized respectively by the lower Y/Ho and Zr/Hf ratios of 35.37 and 76.30.

5.2 Discussions

5.2.1 Aqueous speciation

Experimental measurements and theoretical computation were carried out to estimate the complexation constant of REE with inorganic ligands (Millero et al., 1992; Wood et al., 1990). Carbonate ligands with respect to chloride and sulphate show a progressive increase of the REE-complexes stability constant from light to heavy REE. REE complex constants with carbonate ligands are higher respect to the weak chloride complexes (Wood et al., 1990 and references therein). Moreover, Millero (1992) shows that the dominant complexes in seawater are carbonates ligands, with a secondary role for chloride complexes in seawater. Negr el et alii (2010) calculated the dissolved REE speciation in Na-HCO₃ bearing fluids of the Massif Central, recognizing HCO₃⁻ and particularly CO₃⁻² as the main ligands of REE complexes. The REE aqueous speciation calculated by PHREEQC indicates that the free ions (REE⁺³) are always a minority percentage compared to the REE-complexes (Fig. 8). The results show the main role played by carbonate complexes [REE(CO₃)₂]⁻ and [REECO₃]⁺, whereas [REEF]⁺² became significant in water with higher fluorine contents: Gadir, La Vela and Polla 3 (Fig. 5.8). The [REECI]⁺² and [REESO₄]⁺ are negligible with respect to the others complexes. Moreover, the speciation of the lake water from the top and the bottom do not show significant differences and [REE(CO₃)₂]⁻ reaches its almost totality in “Specchio di Venere” lake with pH 9.0 (Fig. 5.8).

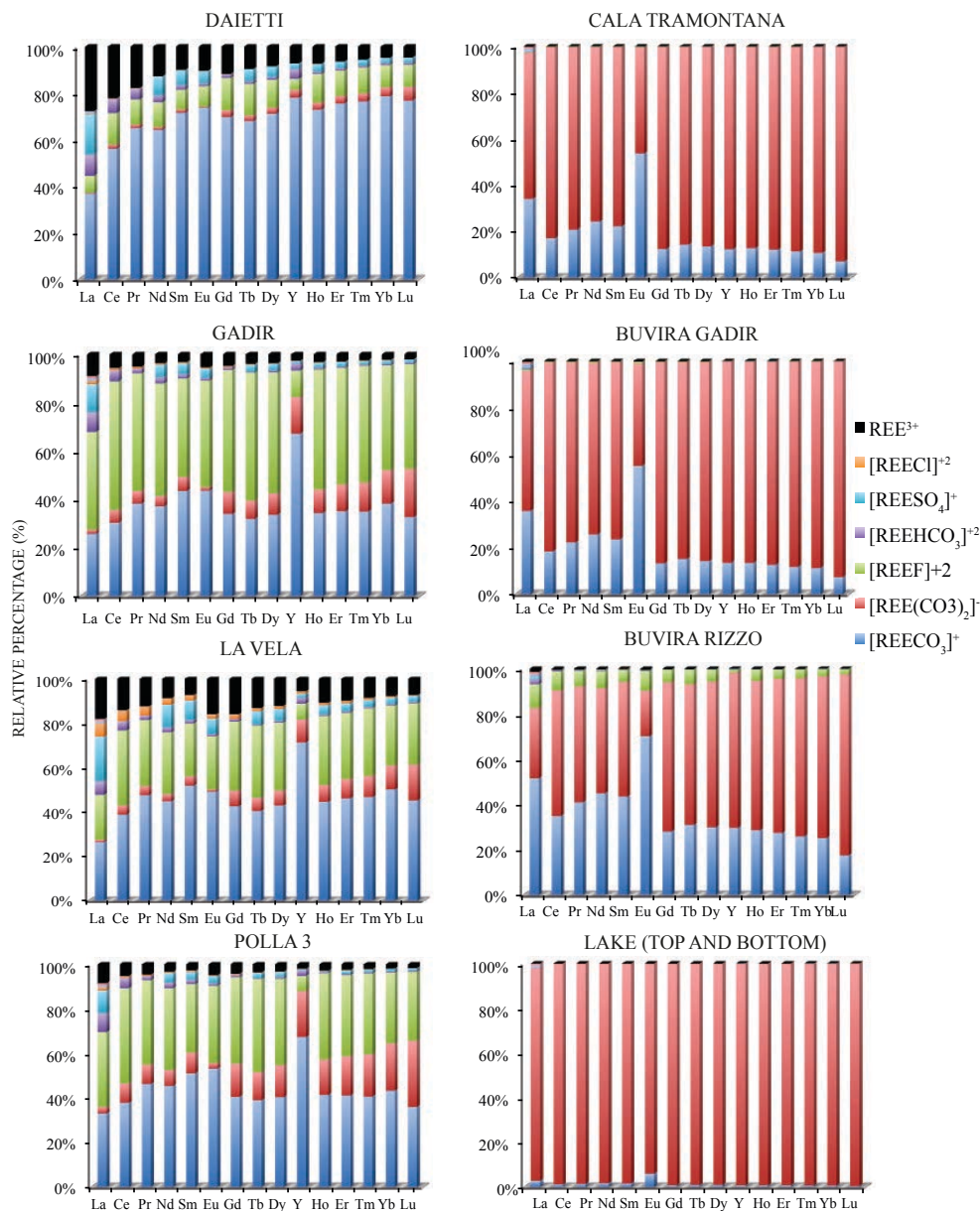


Fig. 5.8 - Relative abundance (percentage) of the REE complexes in the investigated waters. REE aqueous speciation was performed with Phreeqc software (LLNL database).

5.2.2 REE behaviour in springs and wells

The distribution of REE in waters circulating in Pantelleria Island is the result of the mixture in different proportion between a marine component, CO_2 -rich fluids and meteoric water; as already recognized studying the major elements (Dongarrà et al., 1983; Azzaro et al., 1983). The water samples from springs and wells are characterized by similar patterns with the exception of Ce and Eu, suggesting one or more geochemical processes in common. REE dissolved in the seawater of the Strait of Sicily (Censi et al., 2004) were normalized to the PAAS to compare the distribution of

REE with the waters circulating in Pantelleria. The investigated waters display REE-patterns with the same trend of the average Strait of Sicily seawater, whereas the REE amount dissolved in Pantelleria waters is about 1 order of magnitude higher with respect to seawater (Fig. 5.6). This evidence indicates that the marine contamination is not able to change significantly the REE distribution in the studied waters. The main processes responsible of REE distribution in water are therefore: the interaction with the hosting rocks, the precipitation of authigenic minerals and the REE complexation as function of the anionic composition.

In order to compare the waters with the host rocks, REE concentrations of the local magmatic rocks (White et al., 2009) were normalized to the PAAS. The normalized patterns of local rocks are flat in shape, showing positive Eu anomalies in basalts and occasionally in trachytes. In more evolved tuffs and pantellerites, Eu anomalies became negative as the result of fractional crystallization of an alkali feldspar-rich assemblage (White et al., 2009). The positive Eu anomalies observed in the studied waters (Fig. 5.9) are the consequence of the interaction process between the water circulating in the hydrothermal system within the less evolved rocks. Since pantellerite is formed after the fractional crystallization of feldspar-rich assemblages from the trachyte magma, the presence and the amplitude of Eu anomaly can be considered as a geochemical tracer of the water-rock interaction with the less evolved rocks, the only one with positive Eu anomaly.

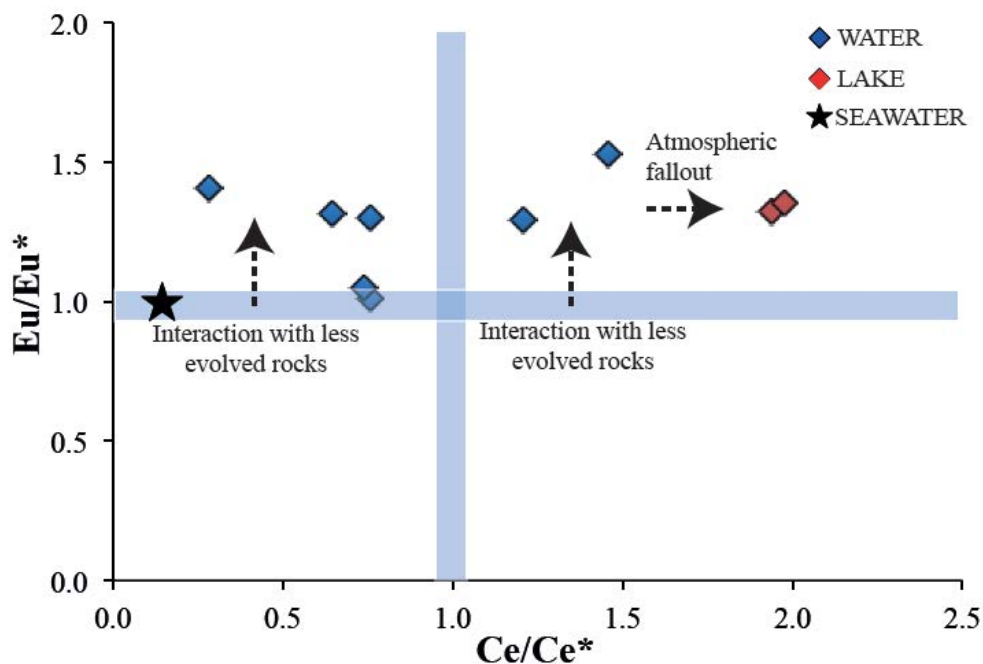


Fig. 5.9 - No correlation was found between Eu and Ce anomalies, showing a different chemical behaviour. Positive Eu anomalies identify the interaction of waters with the less evolved hosting rocks.

Choi and co-workers (2009) investigated the REE in CO₂-rich waters in the Kangwon district (South Korea) showing HREE enrichments respect to LREE in the Na-HCO₃ water type. Moreover, they studied the distribution of REE in carbonate minerals precipitated by the same waters, without finding significant changes in the REE distribution between the residual waters obtained after the filtration of solid phases and the original waters. The precipitation of carbonate solid phases occurs in Pantelleria waters (as suggested by PHREEQC calculation) but it should change only the REE amount dissolved in water and not their distribution. The explanation of the lack of REE fractionation during the precipitation of carbonates has been attributed to the main complexation of REE with carbonate ligands causing the preferential co-precipitation with carbonates, resulting in HREE enrichment compared to LREE, both in water and in the precipitated carbonates (Feng et al., 2014 and references therein; Choi et al., 2009). The distribution of REE in the investigated waters is the result of carbonate-REE complexation driving the REE distribution in CO₂-rich water. This effect is consistent with the progressively increasing shale-normalised REE patterns along the element series.

5.2.3 *Ce anomaly*

Cerium differs from the REE being sensitive to the change of redox conditions. This element in oxidizing environment is easily removed from the solution as CeO_2 and/or by adsorption onto Mn, and Fe oxyhydroxide, as recognized in several environments and laboratory experiment (Bau, 1999; Seto et al., 2008; Bau and Koschinsky, 2009 and references therein). Figure 5.10 shows the inverse trend between Ce anomaly and Eh values. Almost all waters are saturated or oversaturated compared to Fe-oxyhydroxides, except Polla 3, where lower pH (6.4) and Eh (-107 mV) values were measured. Polla 3 shows a positive anomaly of Ce (1.3), in agreement with the lack of Fe minerals stability, as shown by PHREEQC simulation. Buvira Rizzo is the only sample water showing a different behaviour of Ce with respect to water; positive Cerium anomaly and positive Eh value occur (Fig. 5.10). Buvira Rizzo is an unexploited old hand-dug well of 3 meters deep, where a high amount of organic matter was recognized (D'Alessandro personal communication). Cerium concentration in water could be controlled by the amount of Dissolved Organic Carbon (DOC). When DOC was higher than 10 mg l^{-1} , no negative Ce anomaly was recognized (Seto et al., 2008 and references therein). Moreover, higher amount of organic compounds could enhance the stability of Fe in the dissolved phase, increasing the Ce concentration in waters and justifying the positive Ce anomaly in Buvira Rizzo water.

Strong positive Ce anomaly was found in lake water, showing a different behaviour compared to the hydrothermal waters. Considering that Ce is enriched in Desert Varnish, the addition of Ce is justified by the contribution of atmospheric fallout from the nearby Sahara Desert.

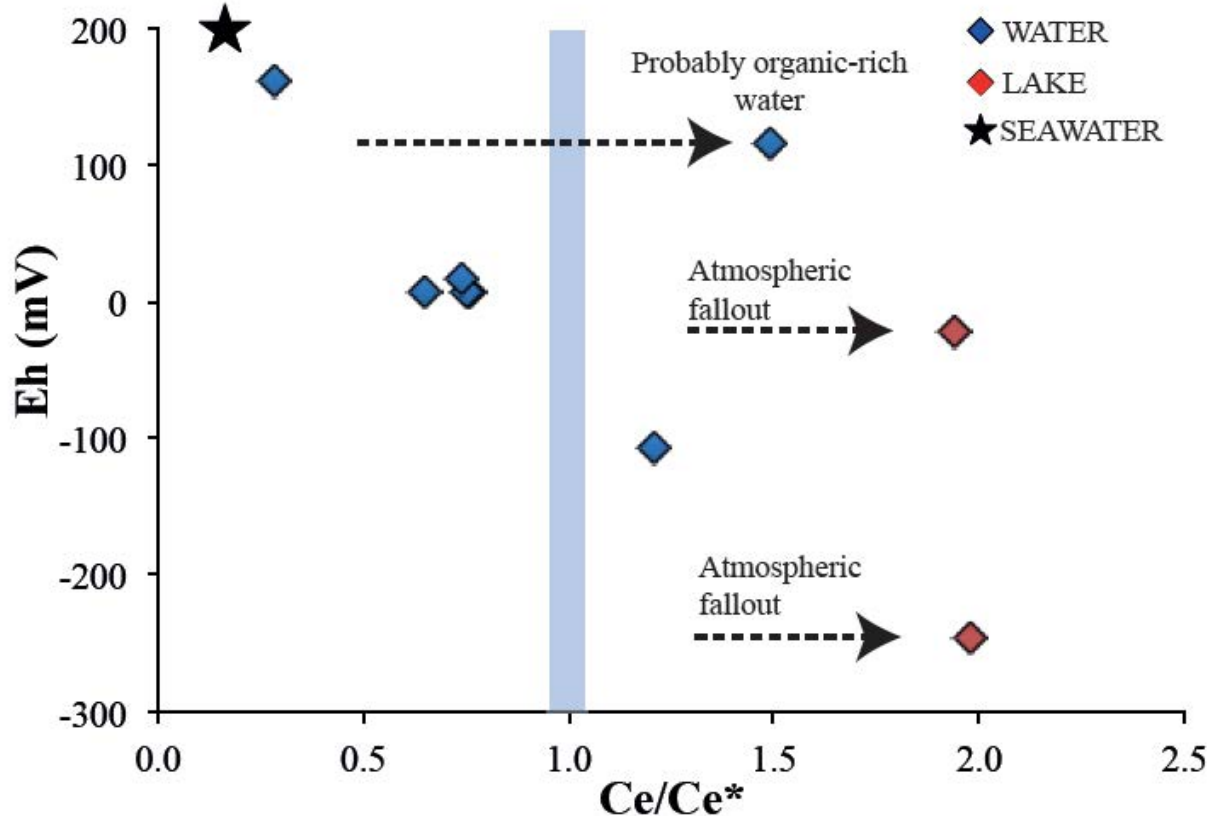


Fig. 5.10 - Ce/Ce* displays to be function of the Eh values, showing negative anomalies increasing the Eh values. Buvira Rizzo sample has an anomalous behaviour, probably due to the higher organic carbon concentration that enhanced the stability of Ce in the dissolved phase. The highest values of Ce anomalies are caused by the interaction of water with the atmospheric fallout enriched in Ce.

5.2.4 Y/Ho and Zr/Hf fractionation in spring and wells

The investigated waters should have Y/Ho and Zr/Hf molar ratios close to the hosting rocks, 49 and 80 respectively (White et al., 2009). The Y/Ho and Zr/Hf ratios found in the investigated springs and wells show values far from the local rock, suggesting the occurrence of processes partitioning these couples of elements (Fig. 5.11). Assuming that these elements are released into waters with Y/Ho and Zr/Hf ratios close to the source rocks, secondary processes (as scavenging into and/or onto the secondary minerals) would explain the fractionation of the twin pairs in the investigated waters. The processes responsible of fractionating Zr-Hf pairs are not well known and up to this day no experiment was carried out in laboratory. On the contrary, when compared to the Y and Ho, Zr and Hf are not complexed by carbonate species. Byrne (2002) shows that Zr and Hf are mainly complexed by hydroxyl groups in the pH range between 6 and 8: Zr, Hf(OH)₄ and Zr,

Hf(OH)₅⁻. Qu and co-authors (2009) have recognized the fractionation of Y and Ho during the precipitation of calcite and aragonite with enhanced removal of Ho respect to Y, due to the different electronic configuration of these elements. Moreover, several studies have shown the ability of Fe-Mn oxyhydroxides precipitation to fractionate Y-Ho and Zr-Hf. Inguaggiato et alii (2015) investigated Y/Ho and Zr/Hf ratios in Nevado del Ruiz volcanic waters (Colombia), showing superchondritic values in waters with pH from 6 to 8.8, where the precipitation of Fe and Al oxyhydroxides occurs. Schmidt and co-authors (2014) investigated Zr/Hf ratios in seawater hydrogenetic ferromanganese crusts, showing strong enrichment compared to the average crust and highlighting an enhanced Hf removal respect to Zr. Moreover, the preferential removal of Hf with respect to Zr in SiO₂ solid phase was found (Firdaus et al., 2011 and references therein). Particularly, Censi and co-authors (2015) investigated a microsystem occurring in the south-western sector of “Specchio di Venere” lake, identifying higher surface-reactivity of Hf than Zr in siliceous stromatolies and microbial mats.

PHREEQC calculations revealed that the investigated waters are oversaturated in Fe-Al oxyhydroxides, carbonate minerals and saturated amorphous SiO₂. Moreover, amorphous SiO₂ was found in Polla 3 thermal spring by SEM-EDS analysis. Considering the geochemical processes above mentioned, the precipitation of authigenic minerals and consequently the interaction between the elements dissolved in waters and the solid phases can be considered the process responsible to decouple Y/Ho and Zr/Hf ratios in spring and wells showing higher values (up to 298) than in the source rocks.

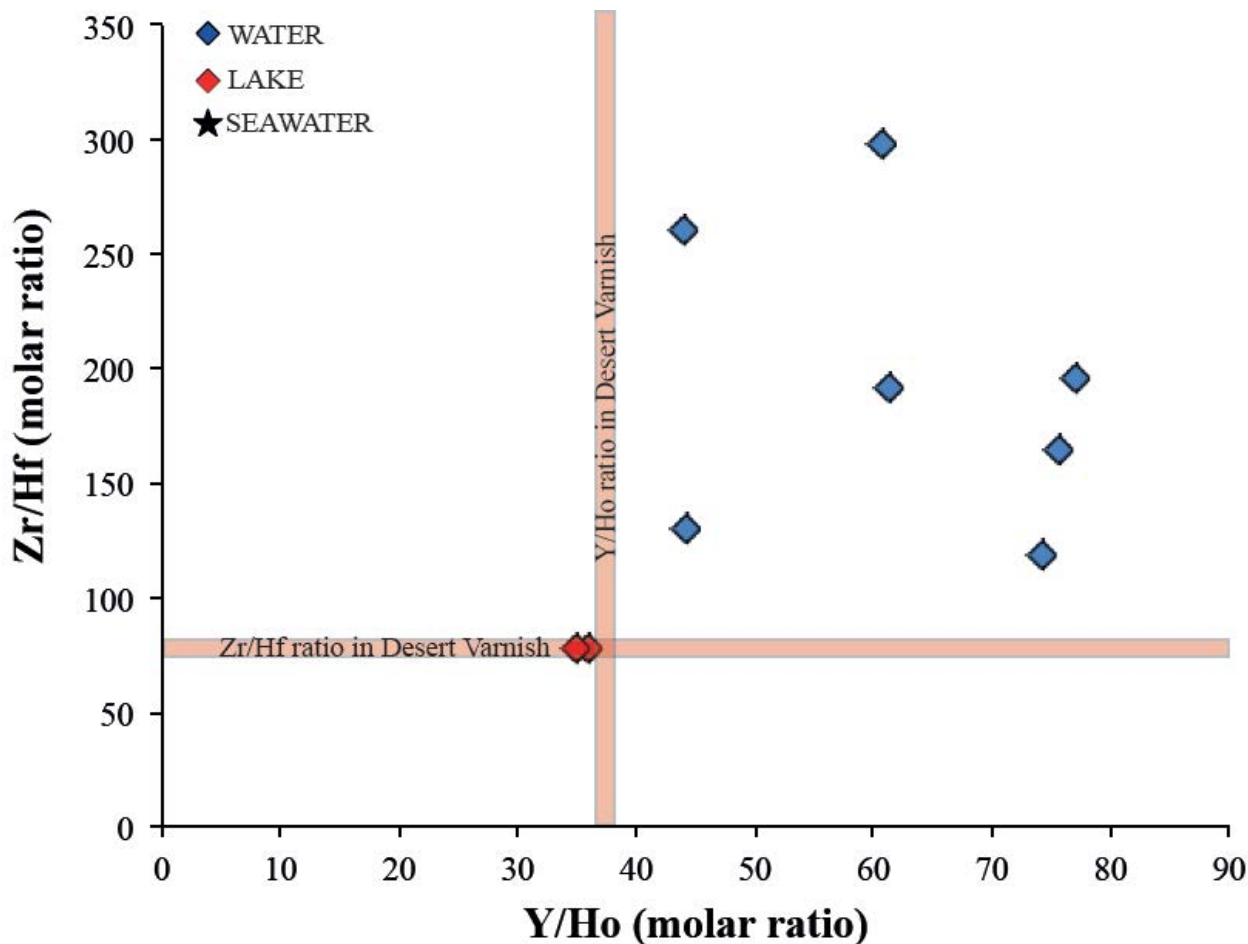


Fig. 5.11 - Changes of Y/Ho and Zr/Hf molar ratios in waters. The coloured band in the graph represents the range of Y/Ho and Zr/Hf ratios in Desert Varnish (Thiagarajan et al., 2004).

5.2.5 The source of REE, Zr and Hf in “Specchio di Venere”

The main problem concerning the anomalous behaviour of REE, Zr and Hf in water lake is to understand which is the main process controlling the geochemistry of REE, Zr and Hf in Specchio di Venere water lake.

The geochemistry of REE, Zr and Hf in alkaline lakes is poorly documented. Johannesson and Lyons (1994) investigated the Mono lake water recognizing a pattern increasing from La to Lu, highlighting the importance of carbonate complexes for the REE distribution.

The atmospheric fallout delivered by Sahara Desert (North Africa) inevitably involves Pantelleria Island, located 70 km at east from the Tunisian coast. The open water body of “Specchio di Venere” lake shows MREE enrichment not recognized in the other waters collected from springs and wells

in Pantelleria Island (Fig. 5.6). In particular, the lake water body has REE amounts higher compared to the other waters, including Polla 3 thermal spring feeding the water lake along the shoreline. This evidence suggests an external process adding REE to the lake water, increasing the relative abundance of MREE with respect to LREE and HREE.

Several studies have been carried out in order to evaluate the role of the atmospheric fallout in REE composition of seawater. Influence of aeolian dust from the Asian continent affects the composition of REE in western Pacific Ocean (Greaves et al., 1999). Greaves and co-authors (1991) showed higher REE concentrations in Mediterranean Seawater with respect to the Atlantic Ocean, suggesting the aeolian dust as REE source (Greaves et al., 1991 and references therein). Moreover, the Mediterranean outflow was recognized to produce anomalies in the Atlantic seawater by mixing of different seawater masses (Greaves et al., 1991).

In arid environments, the formation of the Desert Varnish, mainly composed of clay minerals and Fe–Mn oxyhydroxides coatings, occurs onto the rock surfaces (Thiagarajan and Lee, 2004; Goldshmidt et al. 2014). The Desert Varnish is characterized by a REE-pattern similar to the settling dust proposed as source material (Fig. 5.12) (Goldshmidt et al., 2014 and references therein). Moreover, the solid phases above mentioned are enriched in REE (especially MREE), showing a pattern similar to that recognized in the “Specchio di Venere” lake, characterized by $MREE/HREE > 1$ (Fig. 5.12). Greaves and co-authors (1994) carried out a laboratory experiment evaluating the dissolution effect of marine Aerosol of Saharian origin into shallow seawater collected in the Indian Ocean, showing a higher solubility of MREE into seawater respect to LREE and HREE.

Y/Ho and Zr/Hf ratios in “Specchio di Venere” lake are close to the values recognized in the Desert Varnish (averages Y/Ho and Zr/Hf ratios 38.00 and 73.37, respectively). The reducing condition and the higher pH of lake water compared to seawater, certainly enhances the dissolution of the Fe-oxyhydroxides coating the Saharian fallout. Considering the evidences shown in this

paragraph, coupled with presence of Fe-oxyhydroxide and phyllosilicates as SPM in the shallowest water layer (Fig. 5.5), we propose that the dissolution of the atmospheric fallout from the Saharian Desert surrounding area is responsible for the changing of the chemical composition of water. Such changes are reflected in the increase of Zr, Hf and REE concentrations, in the formation of a Ce anomaly, in the “bulge effect” in the REE-pattern and in Y/Ho and Zr/Hf ratios with a Desert Varnish signature.

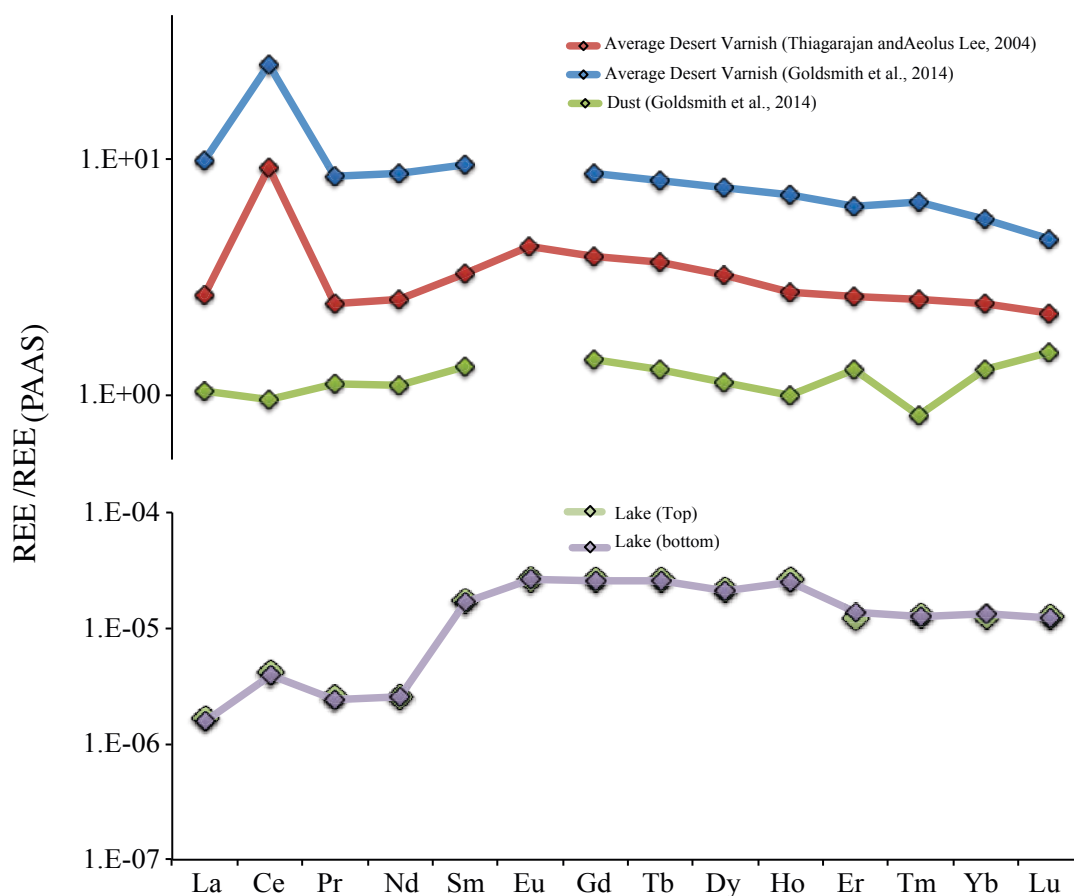


Fig. 5.12 - PAAS-normalised REE in lake waters (from top and bottom), average Desert Varnish and settling dust (values from: Thiagarajan and Aeolus Lee, 2004; Goldsmith et al., 2014).

5.3 Concluding remarks

The CO₂-rich waters in Pantelleria Island have variable REE amounts, whereas similar REE-patterns normalized to PAAS with HREE enriched compared to the LREE are shown in springs and wells. The distribution of REE does not depend only on the source rocks, but mainly reflects the distribution of REE with carbonate complexes, as recognized in others studies carried out in

different regions of the world. The last evidence of the behaviour of REE in CO₂-rich waters allows to give shape to an hypothesis on the REE distribution in natural system in carbon storage reservoirs. Positive and negative Ce anomalies were recognized as a function of the redox conditions. The negative anomalies are due to the co-precipitation onto the surface of the Fe-oxhydroxides in water with positive Eh values. The positive Eu anomaly proved to be a useful tool in the evaluation of the water-rock interaction with less evolved hosting rocks, also characterized by positive Eu anomaly. Y/Ho and Zr/Hf in springs and wells show higher ratios compared to the local rock, evidencing fractionation processes in the aqueous system. The decoupling of these elements is due to the different affinity to the secondary solid phases occurring in waters (carbonate minerals, Fe oxyhydroxides and amorphous Silica).

REE, Zr and Hf in the “Specchio di Venere” lake have the highest concentrations recognized in Pantelleria hydrothermal system. Similar distribution of REE normalized to PAAS were found in both the top and the bottom of the lake, showing a shape of pattern comparable to that identified in the Desert Varnish and the settling dust, with MREE enrichment and positive Ce anomaly. Moreover, Y/Ho and Zr/Hf ratios in lake water show values comparable to those found in the Desert Varnish. REE coupled with the Y/Ho and Zr/Hf ratios showed to be useful geochemical tracers to identify the atmospheric particulate contribution to water body.

CHAPTER 6

GEOCHEMISTRY OF Zr, Hf AND REE IN A WIDE SPECTRUM OF Eh AND WATER COMPOSITION: THE CASE OF THE DEAD SEA FAULT SYSTEM (ISRAEL)

6.1 RESULTS

6.1.1 *General aspects*

Samples of several natural waters were collected along the Lake Kinneret – Jordan Valley – Dead Sea rift area. Sampling sites are located at Baniyas springs, in the Golan Heights, Hamei Teveria spring along the western shores of the lake Kinneret, the shallow water of lake Kinneret, Zukim and Qedem springs and Ein Gedi thermal water collected from the well located in the local spas along the western shore of Dead Sea. Yishai spring water was collected in a little pool close to the Dead Sea shoreline between Ein Gedi and Qedem. Hamei Yoav and Hamei Gaash waters come from the western plan of Israel along the Mediterranean coast. Qetura and Ya'Alon are samples coming from the southern Israel and were collected from wells. Sample collection was carried out during May 2013, March 2014 and May 2015. The location of collection sites is reported in Fig. 6.1.

The chemical-physical parameters and major elements concentrations of the studied waters are reported in Table 6.1. Water temperature ranges between 14.6 and 57.2 °C and pH values range from 5.4 to 8.5. The total dissolved salts (TDS) and the Eh values cover a wide range from 0.3 to 193.5 g l⁻¹ and -400 to 390 mV, respectively. Sample waters are characterized by a wide spectrum of major elements composition due to the mixing between meteoric water and ancient brines interacting with local rocks, as found by previous studies (Moller et al., 2007 and references therein).

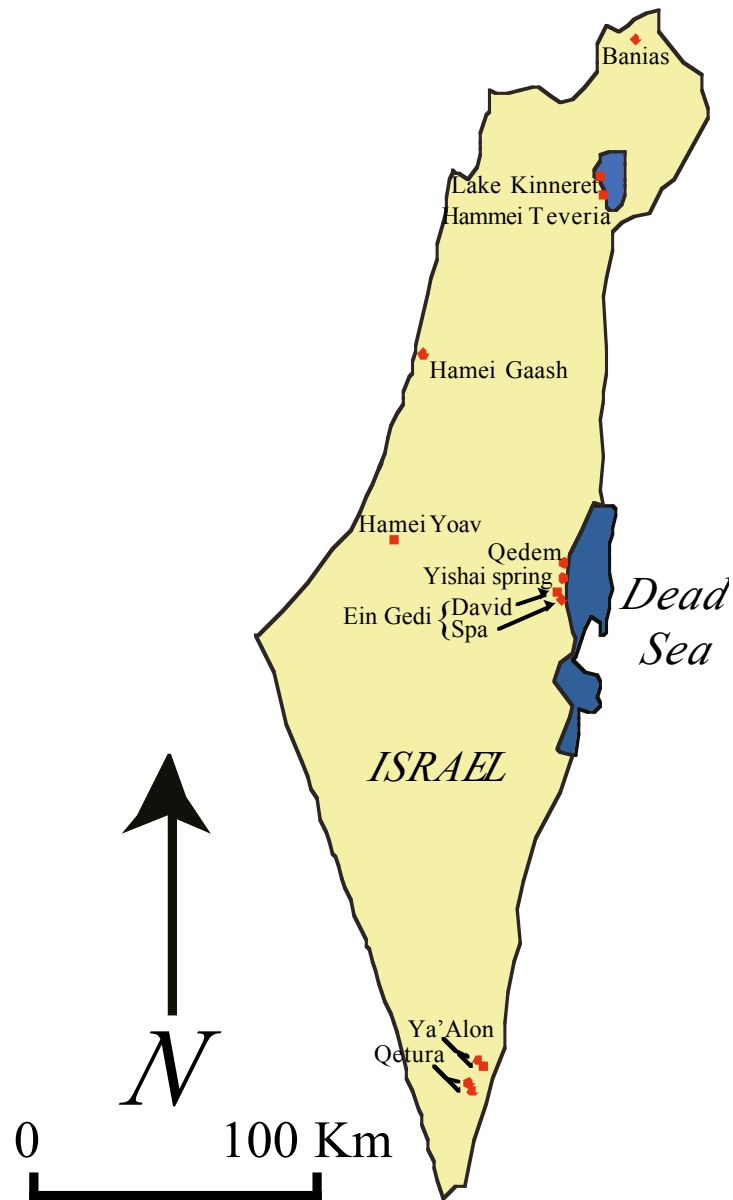


Fig. 6.1 - Location of sampling sites.

Group	Sample Name	T (°C)	pH	TDS (g l ⁻¹)	Eh (mV)	Na	K	Mg	Ca	F	Cl	SO ₄	Alkalinity
Group 1	Banias	14.6	7.6	0.3	256	0.24	0.02	0.22	1.39	0.004	0.26	0.13	3.00
	Kinneret	25.0	8.5	0.7	192	5.28	0.18	1.34	1.19	0.02	6.73	0.53	3.40
	Ein Gedi (David)	27.7	7.5	0.5	185	2.09	0.08	1.20	1.47	0.02	2.43	0.35	4.40
	Ya'alón 6	40.0	6.9	1.4	-100	7.20	0.22	3.33	3.67	0.06	11.57	2.62	5.00
	Qetura 5	33.7	6.9	1.8	-15	10.18	0.35	3.68	5.08	0.05	15.83	4.02	4.40
	Qetura 115	33.2	6.9	2.1	61	10.39	0.33	4.94	5.59	0.12	13.16	7.29	5.00
Group 2	Hammei Teveria	57.2	6.0	29.8	-248	303.44	9.13	26.39	86.69	0.38	483.83	7.84	2.30
	Hamei Gaash	24.5	7.2	25.6	-276	366.37	4.97	20.77	9.36	0.23	435.16	1.47	6.60
	Ya'alón 1A	33.3	6.9	1.9	-323	10.94	0.60	4.00	4.67	0.08	13.74	5.53	5.10
	Hamei Yoav	39.4	7.0	2.9	-380	35.40	0.53	2.60	2.97	0.04	41.39	0.23	6.20
	Qedem	44.3	5.4	178.9	-272	1119.12	97.45	718.63	296.58	1.45	3276.22	8.67	1.50
	Ein Gedi (SPA)	41.4	5.8	138.1	-402	1096.89	59.13	427.25	217.56	-	2492.49	13.70	2.30
	Yishai Spring	35.0	5.6	193.5	-378	2396.57	58.12	384.78	108.30	-	3330.68	29.57	4.60

Tab. 6.1 - Chemical composition of the studied waters expressed in mmol/l.

The anion triangular plot shows water compositions falling along the imaginary line jointing the Cl and HCO₃ vertices, probably representing the mixing between brines and meteoric waters interacting with carbonate rocks (Fig. 6.2a). A group of waters (Ya'alón 1a, Ya'alón 6, Qetura 5 e Qetura 115) is characterized by a relative enrichment in SO₄²⁻ compared to the other waters, showing in the triangular plot a deviation of the samples toward the SO₄ vertex (Fig. 6.2a). The cation triangular plot shows waters falling close to the Na-K corner with a slight dispersion toward both the Ca, Mg corners (Fig. 6.2b). The water with Ca dominated composition is Banias, while the waters with relative high Ca contents are the samples characterized by relative high SO₄ contents. The enrichment of Ca and SO₄ is justified by the dissolution of gypsum, while the waters with high Na-Cl contents are ancient brines or meteoric water dissolving halite (Moller et al., 2007 and references therein).

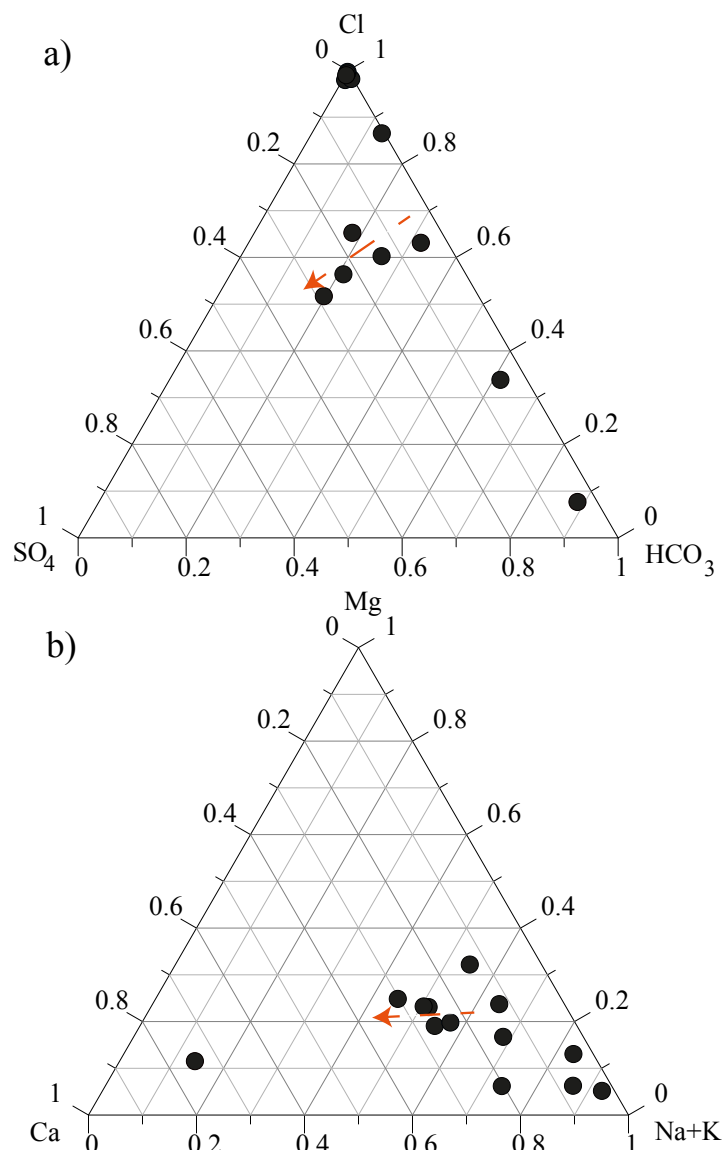


Fig. 6.2 - a) Triangular plot of major anions dissolved in water. The red arrow indicates SO₄ enrichments probably due to the gypsum dissolution. b) Triangular plot of major cation dissolved in water. The red arrow indicates Ca enrichments probably due to the gypsum dissolution.

The saturation indexes of minerals were calculated by PHREEQC software using the LLNL database. The solid phases considered are Fe-oxyhydroxides, carbonate minerals, gypsum, pyrite, halite (Tab. 6.2). The waters were classified according to their saturation indexes with respect to Fe-bearing minerals and to Eh values. According to this approach, two different water groups were identified: Group 1 saturated or oversaturated with respect to Fe-oxyhydroxide with Eh values ranging between -100 and 256 mV; Group 2 oversaturated with respect to pyrite with Eh values lower than -100 mV. Sometimes, both Group 1 and Group 2 are saturated or oversaturated with

respect to dolomite and calcite whereas the studied waters are always undersaturated with respect to gypsum and halite.

Group	Sample Name	Fe-oxyhydroxide	pyrite	dolomite	calcite	gypsum	halite
Group 1	Banias	3.80	-116.60	0.40	0.00	-2.60	-8.80
	Kinneret	0.50	-73.74	-3.20	-1.50	-2.20	-6.10
	Ein Gedi (David)	5.10	-94.66	1.60	0.30	-2.20	-7.00
	Ya'alón 6	-0.40	-19.49	1.50	0.20	-1.20	-5.80
	Qetura 5	-0.10	-37.38	1.20	0.10	-1.00	-5.50
	Qetura 115	1.00	-54.09	1.30	0.10	-0.80	-5.60
Group 2	Hamei Teveria	-4.18	7.20	-0.70	-0.80	-9.00	-1.43
	Hamei Gaash	-4.69	4.80	2.04	0.23	-24.47	-2.72
	Ya'alón 1A	-4.50	7.00	0.80	-0.20	-12.00	-5.50
	Hamei Yoav	-2.95	4.58	1.57	0.18	-21.00	-4.61
	Qedem	-8.05	3.50	-1.80	-1.00	-19.00	-1.40
	Ein Gedi (SPA)	-6.91	5.50	-0.50	-1.00	-16.00	-1.50
	Yishai Spring	-9.03	2.61	-0.09	-0.97	-32.75	-1.03

Tab. 6.2 - Saturation indexes of studied waters.

Scanning electron microscopy (SEM) observations carried out on SPM from the studied waters show lithic fragments, crystals and apparently amorphous or cryptocrystalline materials. SEM-EDS analyses revealed Mn and Fe oxyhydroxides sometimes couple to calcite and/or dolomite in Group 1 and pyrite in Group 2 (Fig. 6.3).

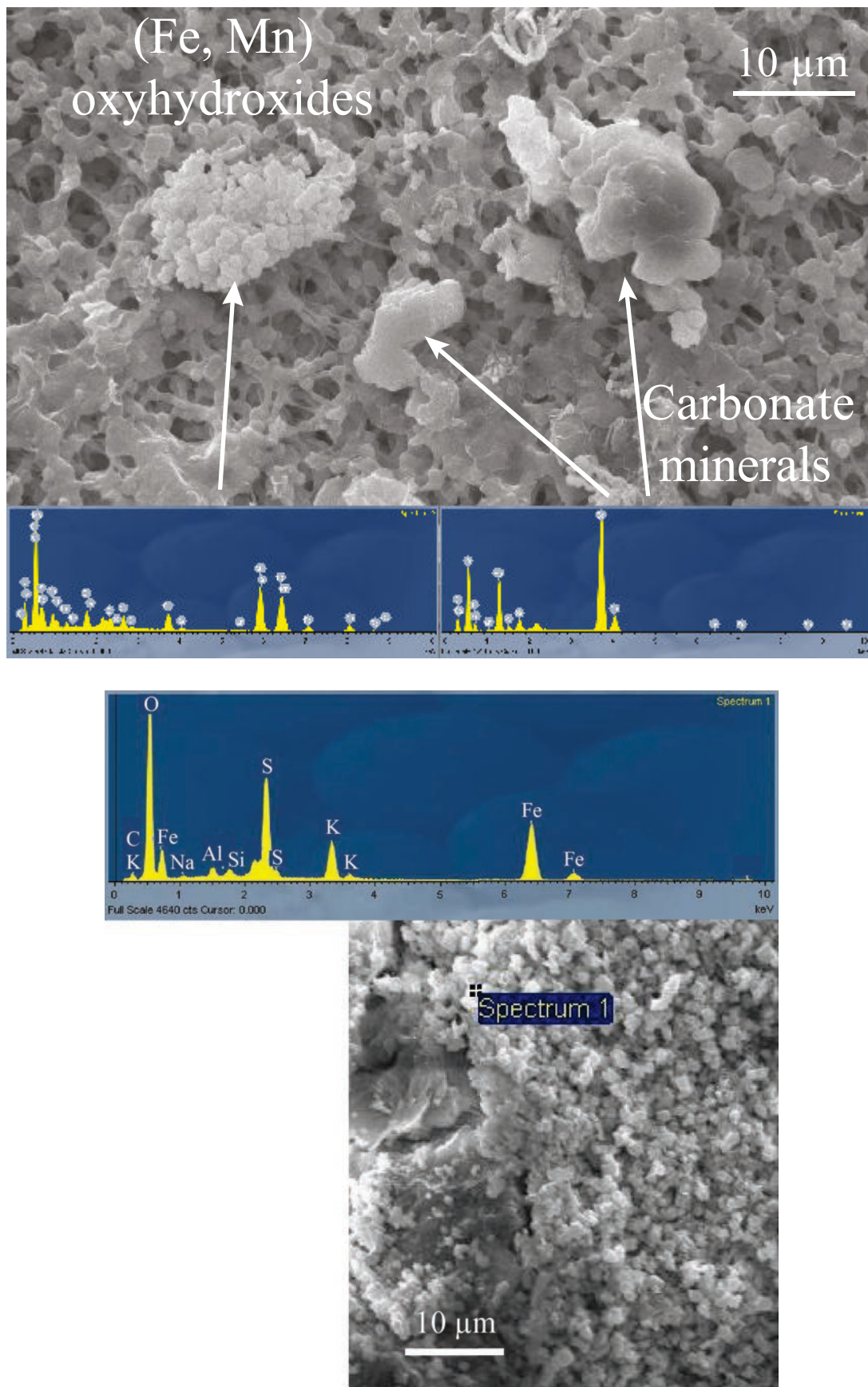


Fig. 6.3 – Carbonate minerals and Fe-, Mn-oxyhydroxides in SPM collected from water of Group 1; Pyrite in SPM collected from water of Group 2.

6.1.2 REE, Zr and Hf

Zr and Hf concentrations cover the 11.3–955.2 $\mu\text{mol l}^{-1}$ and 0.3–10 $\mu\text{mol l}^{-1}$ ranges respectively (Tab. 6.3). The amount of Y and Ho dissolved in waters range from 6.2 to 1066 $\mu\text{mol l}^{-1}$ and from 0.05 to 15.07, respectively. Zr/Hf and Y/Ho molar ratios change between 68.1–156 and 41.8–134.3, respectively, from close to chondritic (70.8 ± 5.6 and 51.2 ± 5 , respectively; Jochum et al., 1986) to super-chondritic values. Fig. 6.4 shows that Y/Ho and Zr/Hf ratios change simultaneously in Group 1 towards super-chondritic values, whereas a different behavior was found in Group 2 with Zr/Hf ratios always close to chondritic values and Y/Ho ratios spanning from chondritic to super-chondritic.

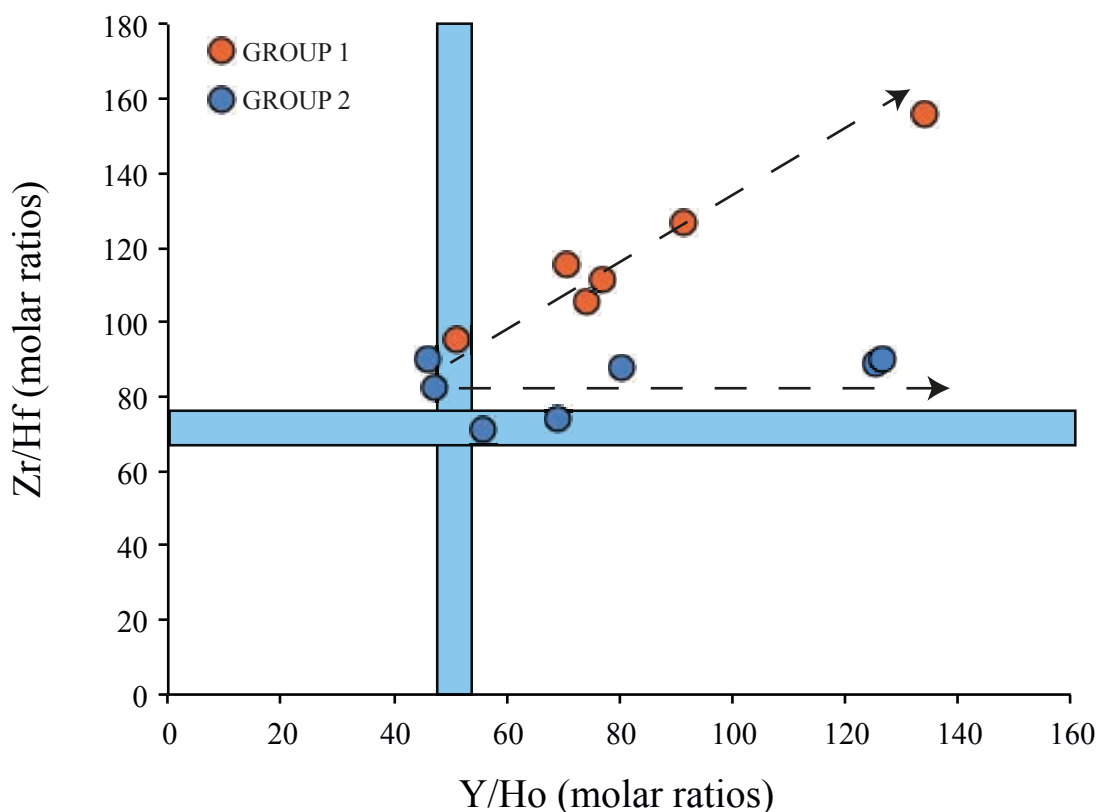


Fig. 6.4 - Zr-Hf and Y-Ho molar ratios. The coloured bands indicate the chondritic Y/Ho and Zr/Hf molar ratios.

REE speciation in Groups 1 and 2 show REE-complexes dominated by carbonate and halide species (Fig. 6.5). On the contrary, Zr and Hf speciation does not change for the range of pH values recognized in waters from Groups 1 and 2 (Byrne, 2002).



Fig. 6.5 - Relative abundances (percentage) of the REE complexes in the investigated waters.

The total REE contents range from 19.1 to 2977.8 pmol l⁻¹ (Tab. 6.3). Fig. 6.6 shows the shale-normalized REE patterns, relative to PAAS (Post Archean Australian Shale; Taylor and McLennan, 1995). Group 1 waters show patterns slightly increasing along the REE series and medium REE

(MREE) enriched at Qetura 5, Qetura 115, Ya'alon 6 and in Lake Kinneret. Moreover, negative Ce anomalies are found in almost all waters belonging to Group 1. Group 2 waters show shale-like patterns with slight MREE enrichments centered on Gd or Eu whereas a strong MREE enrichment and lack of Eu anomalies in Ya'alon 1a water. Moreover, Group 2 is characterized by strong Eu anomalies and no Ce anomalies.

Group	Sample Name	Zr	Hf	Y	La	Ce	Pr	Nd	Sm	Eu	Gd	Tb	Dy	Ho	Er	Tm	Yb	Lu
Group 1	Banias	38.45	0.25	6.19	7.04	2.69	0.38	1.37	0.32	0.10	0.40	0.05	0.21	0.05	0.13	0.02	0.13	0.02
	Kinneret	154.51	1.22	13.35	16.37	20.59	1.53	6.38	1.29	0.33	1.61	-	0.93	0.15	0.55	-	0.50	0.07
	Ein Gedi (David)	11.26	0.11	31.38	43.64	37.31	2.66	5.92	1.99	0.66	2.69	0.44	2.05	0.42	1.49	0.30	2.61	0.46
	Ya'alon 6	955.24	10.03	324.13	294.95	613.71	72.01	271.70	56.61	13.02	55.83	8.18	36.71	6.33	19.15	2.55	16.33	2.23
	Qetura 5	55.80	0.50	1066.06	132.01	116.66	19.43	167.77	75.98	23.16	118.24	16.43	78.22	13.86	30.48	2.66	14.30	2.34
	Qetura 115	33.22	0.29	42.62	57.30	63.50	3.37	7.59	2.08	0.64	3.25	0.57	2.14	0.60	1.88	0.25	1.85	0.23
Group 2	Hamei Teveria	375.26	4.23	24.00	26.11	32.81	1.85	6.08	1.21	1.22	1.82	0.19	1.05	0.19	0.81	0.10	1.03	0.21
	Hamei Gaash	134.05	1.63	176.67	157.80	300.50	33.35	133.76	29.59	22.62	28.66	4.22	19.29	3.74	11.00	2.36	18.89	4.34
	Ya'alon 1A	18.99	0.22	34.00	61.70	77.44	3.74	8.68	1.99	0.64	3.08	0.43	2.02	0.42	1.20	0.17	0.92	0.11
	Hamei Yoav	99.02	1.45	114.09	200.82	243.35	20.80	78.57	16.73	22.76	16.74	2.39	11.83	2.05	6.87	1.72	18.36	3.83
	Qedem	439.58	6.16	545.09	369.68	538.47	58.27	225.88	43.50	11.19	54.14	6.76	37.15	7.91	22.80	2.88	19.18	2.89
	Ein Gedi (SPA)	126.06	1.40	18.61	20.65	27.47	1.75	6.35	1.13	0.55	1.67	0.16	0.85	0.15	0.58	0.07	0.54	0.10
	Yishai Spring	711.52	7.87	694.09	469.34	898.83	105.95	414.48	84.18	33.20	89.91	13.07	69.62	15.07	38.65	5.89	38.86	6.69

Tab. 6.3 - REE, Zr and Hf dissolved in waters expressed in pmol l^{-1} .

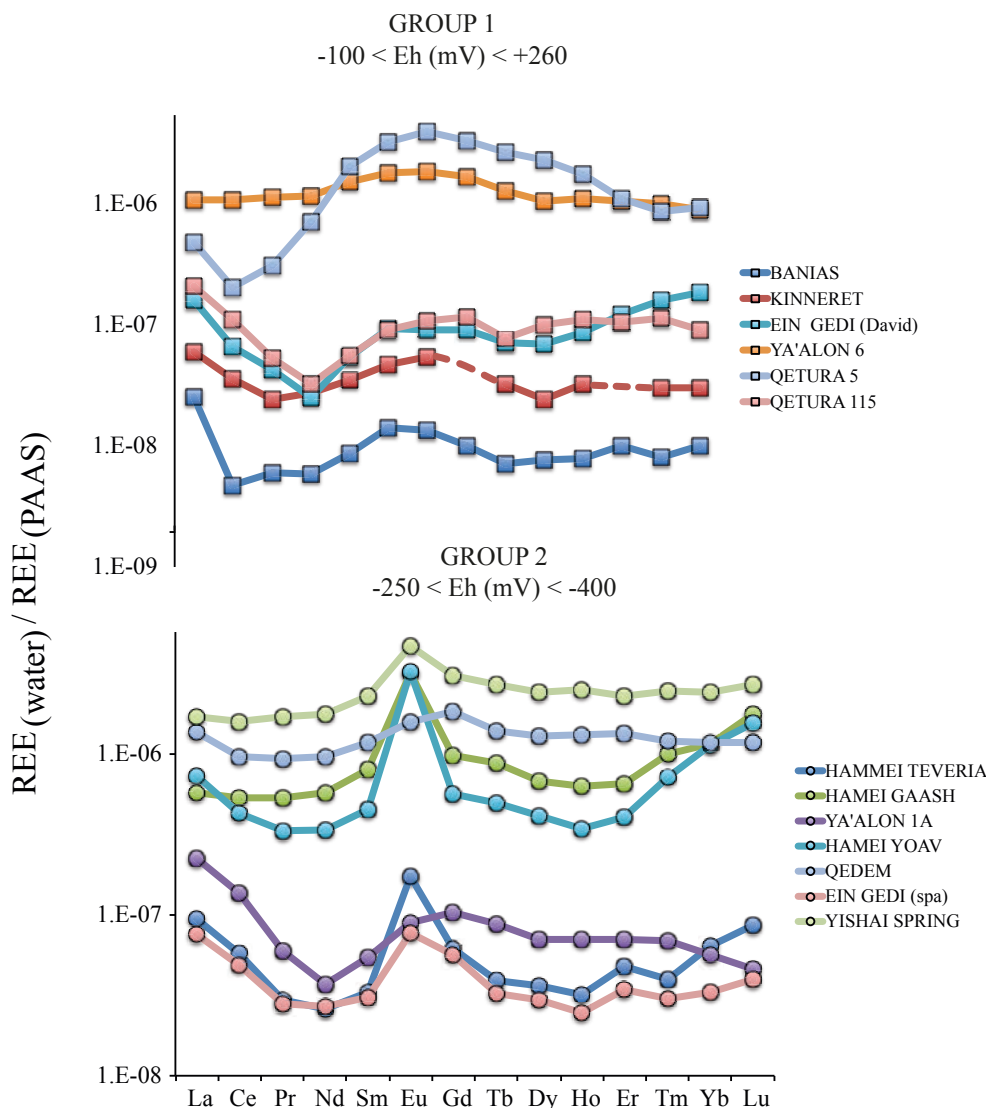


Fig. 6.6 - PAAS-normalized REE patterns dissolved in water.

6.2 DISCUSSION

6.2.1 Zirconium and hafnium

Previous studies carried out on natural waters from the Rift Valley-Dead Sea area (Moller et al., 2003, 2007; Siebert et al., 2012) did not take in account the Zr and Hf behaviour and considered the dissolved REE distribution as mainly related to the effects of water-rock interactions in different aquifers. The latter processes were considered responsible of a wide spectrum of dissolved compositions under the different thermochemical conditions occurring in the natural waters.

Fig. 6.7 shows that Zr/Hf molar ratios increase as Eh values increase. Group 2 waters have Zr/Hf

molar ratios quite constant clustered around chondritic value while Group 1 waters have Zr/Hf ratios directly related to Eh values starting from the chondritic signature. Considering that Zr and Hf are not redox sensitive elements and their dissolved speciation is not influenced by redox conditions (Byrne, 2002), the different Zr/Hf ratios found in Group 1 and 2 can be related to the stability of Fe-bearing minerals (Fig. 6.4).

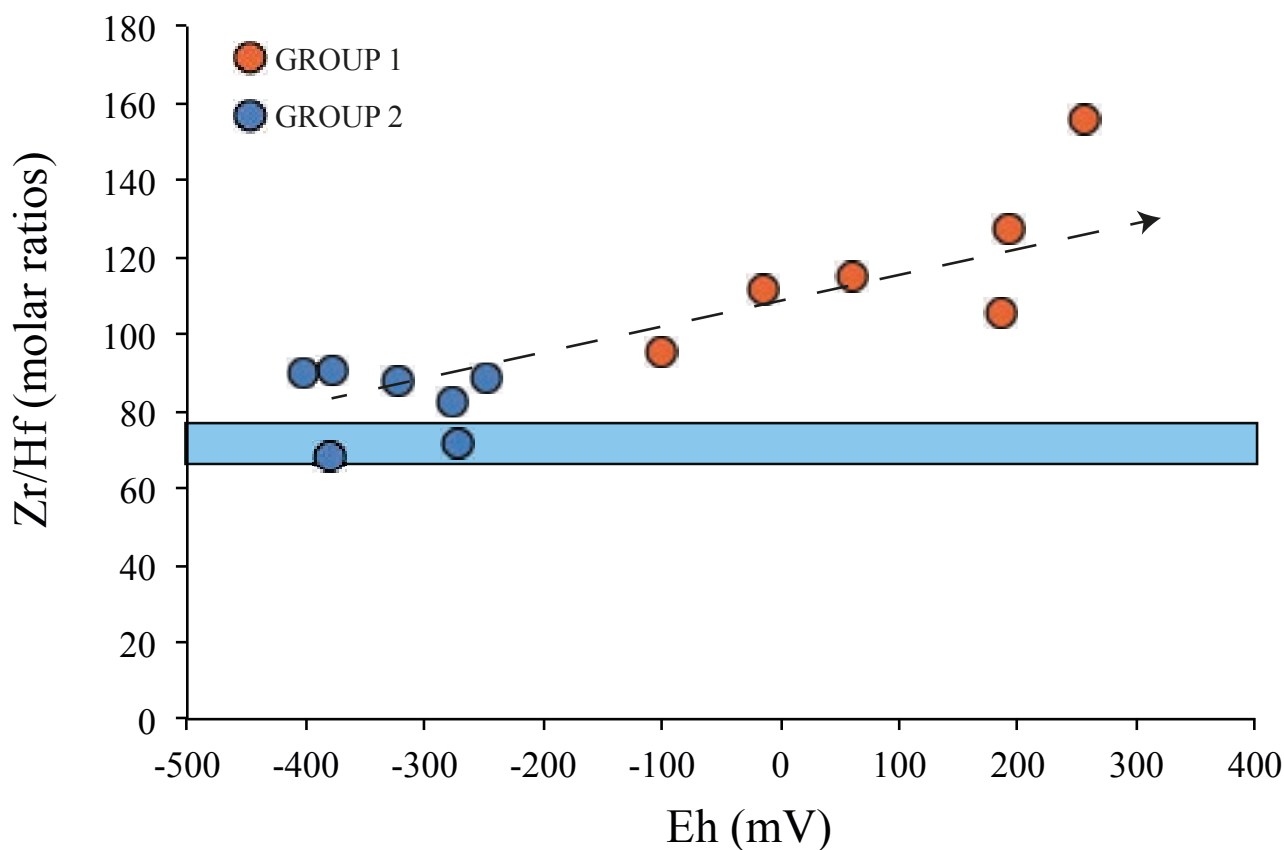


Fig. 6.7 - Zr/Hf molar ratios versus Eh values.

Fig. 6.8a shows that Zr/Hf ratio is almost constant around the chondritic signature in Fe-oxyhydroxide undersaturated Group 1 waters whereas super-chondritic values are observed in oxidizing Fe-oxyhydroxide oversaturated Group 2 waters. Fig. 6.8b shows progressively decreasing Zr/Hf values in oxidizing Group 1 waters undersaturated in pyrite and the chondritic signature is observed in Group 2 waters where the oversaturation in pyrite is attained. These evidences agree with the larger Hf reactivity relative to Zr onto surfaces of Fe-oxyhydroxides reported by Bau and Koschinsky (2009) and with the lesser extent of this process onto sulfide surfaces (Kosmulski, 2012

and cited references). As waters are oversaturated relative to Fe-oxyhydroxides, Hf is preferentially scavenged therein and dissolved Zr/Hf values progressively increase. On the contrary, under reducing conditions allowing the stability of pyrite, the findings from Vergouw et al. (1998) indicate neutral charged pyrite surfaces suggesting a limited interaction with dissolved $[\text{Zr}(\text{OH})_4]^0$ and $[\text{Hf}(\text{OH})_5]^-$ species and therefore a lack of Zr-Hf fractionation induced by the pyrite.

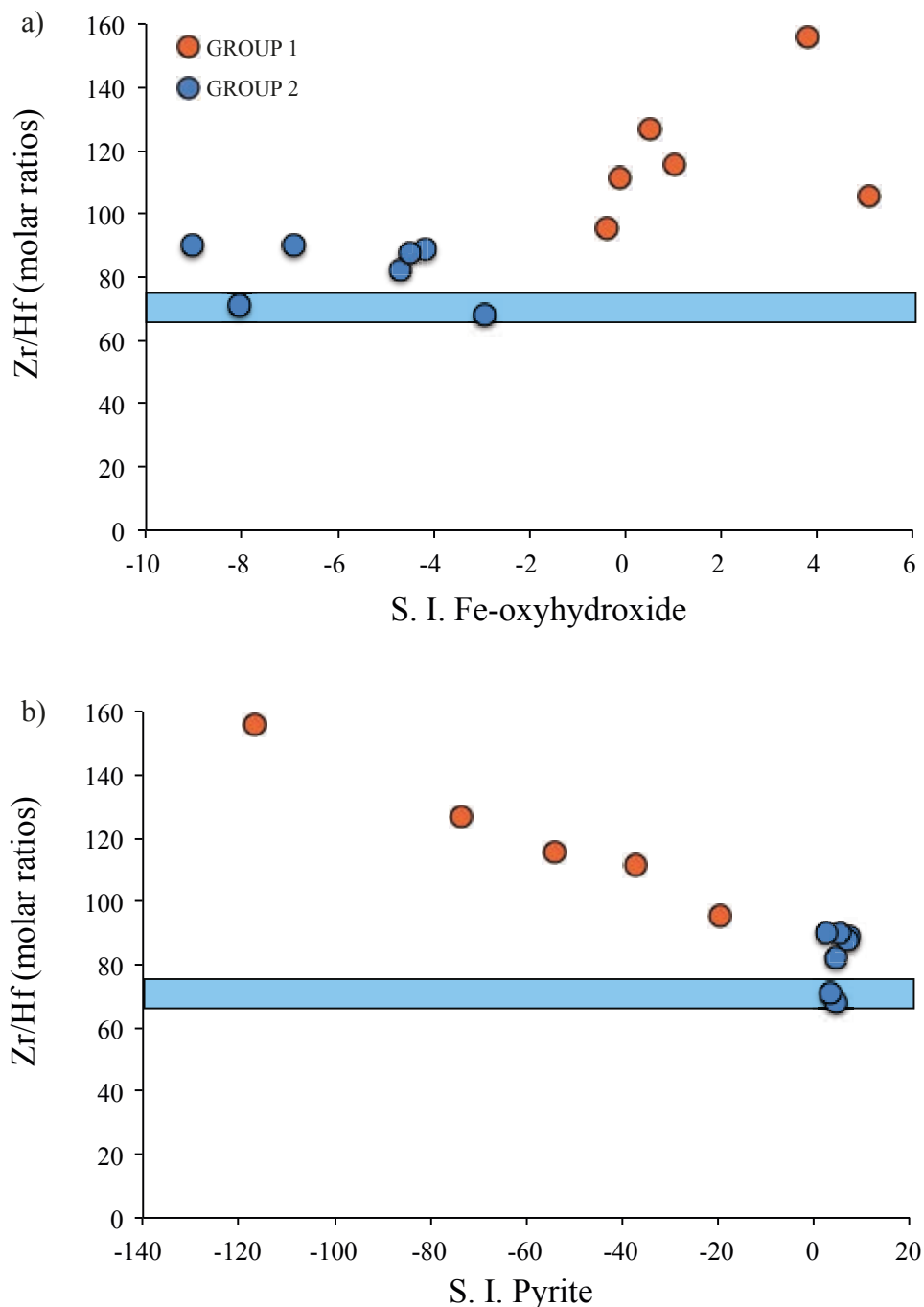


Fig. 6.8 - a) Zr/Hf molar ratios vs. saturation indexes of Fe-oxyhydroxides. b) Zr/Hf molar ratios vs. saturation indexes of pyrite.

6.2.2 *Yttrium and Holmium*

Differently from the Zr and Hf behaviour during dissolved complexation, the Y and Ho dissolved species always show the same ionic charge if formed with the same ligand (i.e. $[(Y, Ho)CO_3]^+$, $[(Y, Ho)(CO_3)_2]^-$, $[(Y, Ho)Cl]^{2+}$, $[(Y, Ho)F]^{2+}$ (Fig. 6.5). Therefore, the Y–Ho decoupling observed in almost all of the Group 1 and 2 waters (Fig. 6.4) cannot be driven by electrostatic considerations, probably depending from the different covalent character of the dissolved Y and Ho complexes (Bau, 1996). This suggestion is confirmed by the preferential Ho scavenging onto Fe oxyhydroxide relative to Y (Bau, 1999). At the same time, laboratory experiments on $CaCO_3$ crystallisation (both calcite and aragonite) indicate the preferential incorporation of Ho into $CaCO_3$ relative to Y (Qu et al., 2009). These results were confirmed by Tanaka et al. (2004, 2008) recognizing a preferential Y enrichment relative to Ho in the dissolved phase during calcite crystallisation that was interpreted as a Ho– CO_3 and Y– CO_3 bonding difference in carbonate minerals.

6.2.3 *REE distribution*

Fig. 5 shows that the most abundant REE species in Group 1 are $[REECO_3]^+$ and $[REE(CO_3)_2]^-$ according with the increasing stability of the REE constant complexes with carbonate ligands (Millero 1992; Luo and Byrne 2004). The patterns increasing from La to Lu show similarity with the REE distribution found in natural waters characterized by the REE-complexation with carbonate ligands (Millero, 1992). MREE enrichments of shale-normalised patterns in Qetura 5, Qetura 115, Ya'alon 1a and Ya'alon 6 waters (Fig. 6.6) agree with the dissolution of MREE-enriched minerals as gypsum (Toulkeridis et al., 1998 and references therein) as confirmed by the distribution of these waters in Fig. 2. The water of lake Kinneret is also characterized by MREE enrichments, whereas the lack of relative high Ca and SO_4 contents does not allow explaining the MREE enrichments with the dissolution of gypsum. On the other hand, the MREE enrichment in the Lake Kinneret can be induced by the MREE release from Fe-oxyhydroxides (Bau, 1999). The latter represent the coating of atmospheric fallout particles from desert environments (Thiagarajan and Aeolus-Lee,

2004; Goldsmith et al., 2014) and are delivered to the shallowest water layer of the lake Kinneret with an annual flux close to 70 g m^{-2} (Ganor et al., 2003). As a consequence, we propose that the MREE delivery to the water lake is due to the leaching of atmospheric particles.

The slight MREE enrichments showed in shale-normalised REE patterns of Group-2 waters is consistent with their interactions with evaporates minerals occurring in aquifers. This hypothesis is corroborated by the distribution of these samples that are clustered close to alkali and chloride ion corners. Moreover, the limited studies focused on the REE distribution in salt minerals concur to indicate that these minerals are enriched in MREE (Yui et al., 1998; Theofilos et al., 1998).

Ce and Eu are redox sensitive elements, with multiple oxidation states. Ce has 3+ and 4+ oxidation states and Eu has 2+ and 3+ oxidation states. In studied samples, Ce and Eu anomalies cover a wide range of values from 0.3 to 0.97 and from 1.09 to 6.29, respectively. Fig. 6.9 shows different distribution of Eu and Ce anomalies in Group 1 and 2 according to their different redox conditions. Group 1 waters with higher Eh values show negligible Ce ($\text{Ce}/\text{Ce}^* \approx 1$) and positive Eu anomalies up to 6.29. Group 2 waters with low Eh values show negative Ce anomalies and negligible Eu anomalies close to 1 ($\text{Eu}/\text{Eu}^* \approx 1$). $\text{Eu}/\text{Eu}^* > 1$ values in Group 2 waters agree with the Eu speciation as Eu^{2+} suggested by PHREEQC model calculations and is consistent with the larger Eu^{2+} stability in aqueous phase relative to its neighbours Sm^{3+} and Gd^{3+} (Bau, 1991; Bau and Moller, 1993). In Group 1, the negative Ce anomalies are in agreement with the Ce scavenging as CeO_2 under oxidizing conditions and/or the Ce(IV) removal onto Fe-oxyhydroxides (Koschinsky and Hein, 2003, Seto et al., 2008). On the other hand, waters characterized by strong negative Eh values (Group 2) do not show significant Ce anomalies being this element retained in dissolved phase as Ce^{3+} coherently with the other REE.

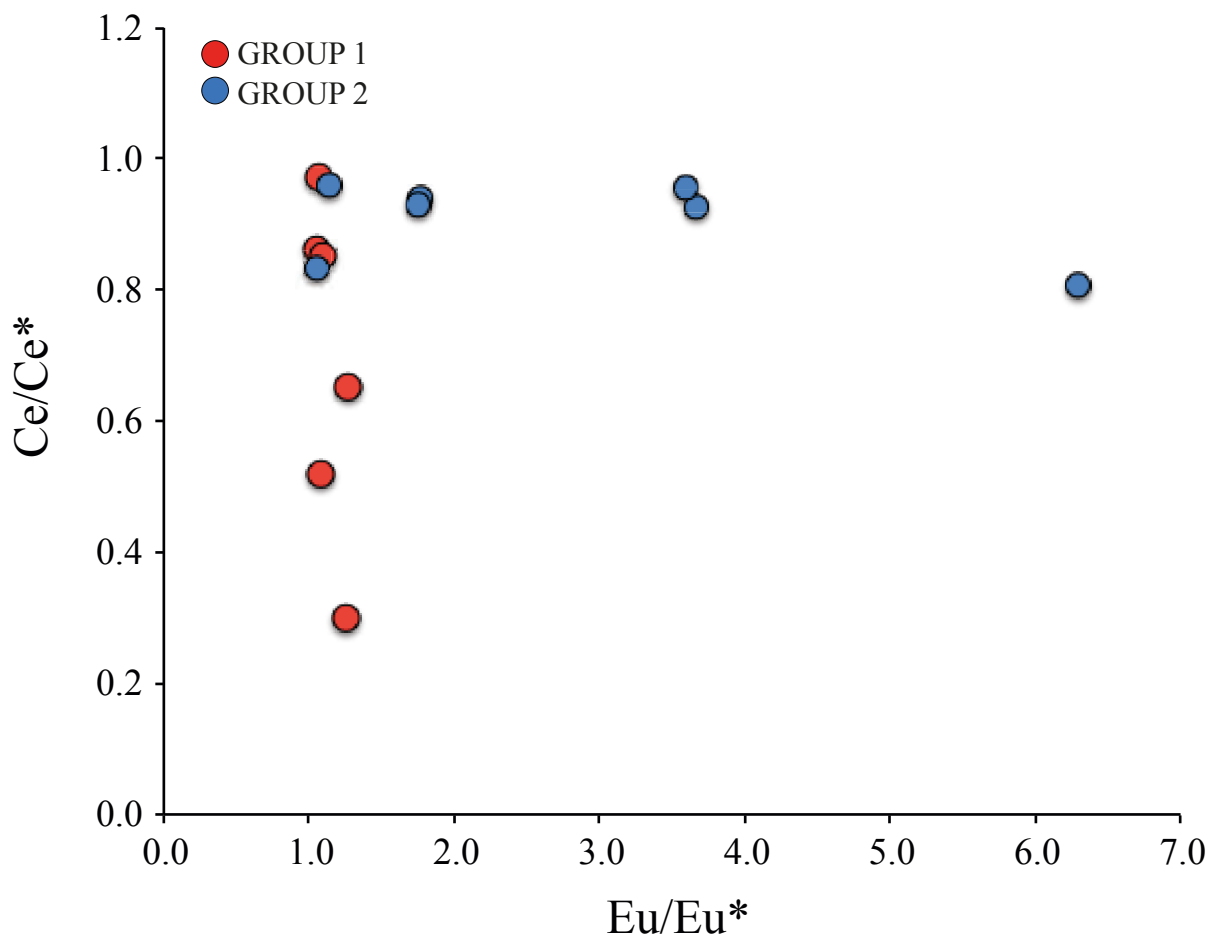


Fig. 6.9 - Relationship between Eu anomalies and Ce anomalies.

6.3 CONCLUDING REMARKS

The study of Zr, Hf and REE distributions in thermal and natural waters spanning a wide range of physical-chemical and salt content conditions show a strong dependence of Zr/Hf, Eu/Eu* and Ce/Ce* from Eh values. The latter parameter allows to group the studied waters according to their oversaturation relative to Fe-oxyhydroxides ($Eh > -100$ mV) and pyrite ($Eh < -100$ mV), respectively. The deposition of Fe-oxyhydroxides suggested by geochemical modelling involves Hf fractionation relative to Zr onto solid surfaces influencing the dissolved Zr/Hf signature. At the same time, the redox conditions are responsible of the aqueous Eu speciation as Eu^{2+} according to $Eh < -100$ mV. The latter process enhances the dissolved Eu stability relative to their neighbours along the REE series and the presence of positive Eu anomalies in these waters. Analogously, the oxidative Ce scavenging as CeO_2 onto surfaces of Fe-oxyhydroxides allows negative Ce anomaly

values in oxidizing waters. A very interesting point of this study is that the dissolved REE speciation cannot simply explain the observed distribution in natural waters and the solid-liquid processes play a key role on the geochemical behaviour of these elements.

CHAPTER 7

GENERAL CONCLUSIONS

The findings of the present study represent the most comprehensive recognition of the Zr and Hf geochemistry in natural non-marine waters. This thesis added new knowledge about the mobility of REE and the less known Zr and Hf, implementing the state of the art about the processes involving these elements in the geochemical spheres. Specifically, the behaviour of Zr, Hf and REE was studied in hyperacid, hypersaline, CO₂-rich waters and the alkaline lake “Specchio di Venere” in hydrothermal systems. This study permitted to know the behaviour of these elements under different chemical-physical conditions (pH, Eh and TDS) and various water compositions determining different ion speciation and minerals stability.

A very interesting point is that the ion speciation of Zr, Hf and REE in solution is not always sufficient to explain the distribution of these elements. The precipitation and the dissolution of solid phases are responsible of changing the distribution of these elements, even if most of the near-neutral waters investigated in this thesis are characterized by REE patterns increasing from La to Lu in according to the distribution of REE-complexes with carbonate ligands (as recognized in previous studies). The acidic sulphates waters characterized by the precipitation of Alunite and Jarosite show a strong LREE depletion. When the precipitation of these minerals does not occur, the acidic sulphate waters show the same REE-pattern found in the average local rock. Alunite and Jarosite rule the distribution of REE in deep and/or shallow hydrothermal system changing the distribution of REE in water. The REE in waters along Dead Sea Fault show MREE enrichments mostly in waters with relative high Ca and SO₄ concentrations. The interactions between waters and MREE-enriched salt minerals (mainly gypsum) are responsible of MREE enrichments in dissolved phase. In the natural waters, changing of pH and Eh conditions induce variations of Ce and Eu anomalies, due to the different behaviour of these elements with respect to the neighbour elements

along the REE series.

The geochemistry of Zr and Hf is poorly known, except in seawater where the major parts of the studies were carried out. The paucity of experiments in laboratory and the lack of a complete set of Zr, Hf constant complexes have made the study of Zr-Hf behaviour in natural environments difficult. The behaviour of Zr and Hf was studied simultaneously with the better known Y and Ho. In sulphate acidic waters, Zr/Hf ratios are very low down to 4.7, while quite constant Y/Ho ratio (close to the local rock value) indicates the lack of decoupling. Zr/Hf ratio increases as Cl/SO₄ ratio increases. The formation of Zr-, Hf-complexes characterized by different affinity with Cl and SO₄ ligands could justify the low Zr/Hf values found in acidic waters ($1 < \text{pH} < 3.6$), where the role of the Zr-, Hf-complexes with hydroxyl groups is negligible. Further investigations in laboratory could confirm this different behaviour of Zr and Hf with Cl and SO₄ ligands under acidic conditions.

Zr/Hf and Y/Ho ratios in near-neutral pH waters change from near-chondritic to super-chondritic. Generally, the precipitation of authigenic solid phases fractionates Y-Ho and Zr-Hf pairs, with a preferential Ho and Hf removal. Zr/Hf ratios show a strong dependence with respect to the Eh values, due to the different stability of Fe-bearing minerals sensitive to the redox condition of the system. Particularly, the precipitation of Fe-oxyhydroxides removes preferentially Hf with respect to Zr due to the adsorption onto the solid surfaces, influencing the dissolved Zr/Hf signature. On the contrary, Zr/Hf ratios are near-chondritic for very low Eh values when pyrite is oversaturated, suggesting limited Zr-Hf decoupling

One important finding of this thesis is the capability of Zr, Hf and REE as potential tracers of the interaction process between open water bodies and atmospheric fallout. The interaction of atmospheric fallout from the nearby Sahara Desert with the water of the lake “Specchio di Venere” is able to change the distribution of Zr, Hf and REE compared to the hydrothermal water feeding the lake.

Increasing the knowledge of Zr, Hf and REE geochemistry, these elements can be further

exploited in the near future as tracers of the solid-liquid processes occurring in deep and/or shallow natural systems.

CHAPTER 8

GEOCHEMICAL CHARACTERISATION OF GASES ALONG THE DEAD SEA RIFT: EVIDENCES OF MANTLE-CO₂ DEGASSING

ABSTRACT

The Dead Sea fault where a lateral displacement between the African and Arabian plates occurs is characterized by anomalous heat flux in the Israeli area close to the border with Syria and Jordan. The concentration of He and CO₂, and isotopic composition of He and total dissolved inorganic carbon were studied in cold and thermal waters collected along the Dead Sea Transform, in order to investigate the source of volatiles and their relationship with the tectonic framework of the Dead Sea Fault. The waters with higher temperature (up to 57.2 °C) are characterized by higher amounts of CO₂ and helium (up to 55.72 and 1.91*10⁻² cc l⁻¹, respectively). Helium isotopic data (R/Ra from 0.11 to 2.14) and ⁴He/²⁰Ne ratios (0.41-106.86) show the presence of deep-deriving fluids consisting of a variable mixture of mantle and crust end-members, with the former reaching up to 35%. Carbon isotope signature of total dissolved carbon from hot waters falls within the range of magmatic values, suggesting the delivery of deep-seated CO₂. The geographical distribution of helium isotopic data and isotopic carbon (CO₂) values coupled with (CO₂/³He ratios) indicate a larger contribution of mantle-derived fluids affecting the northern part of the investigated area, where the waters reach the highest temperature.

These evidences suggest the occurrence of a favourable tectonic framework, including a Moho discontinuity up-rise and/or the presence of a deep fault system coupled with the recent magmatic activity recognised in the northern part of Israel.

8.1 INTRODUCTION

The Lake Kinneret-Jordan Valley-Dead Sea area is a complex geodynamic system where a lateral left motion of up to 105 km along the contact between the Arabian and African tectonic plates generated the Dead Sea Transform (DST) fault system (Garfunkel et al., 1981). This fault has been defined as a branch of the Red Sea Rift. The Red Sea area is divided in 3 Zones: the northern part representing the late stage of the continental rift, the central part considered a transitional zone and the southern rift area where active seafloor spreading occurs (Lazar et al., 2012 and references therein).

The DST, whose activity started during early Neogene (≈ 20 Ma), consists of a series of faults going from the northern part of the Red Sea to the East Anatolian fault (EAF). The EAF runs from the end of DST until it reaches the North Anatolian Fault (NAF). Several depression zones (pull apart basins) filled by thick sedimentary sequences (Garfunkel et al., 1981) occur along the whole DST. Among them, the Dead Sea and the Sea of Galilee are included in the investigated area.

The topography of the Moho below the DST is asymmetric, its depth increasing from ≈ 26 to ≈ 39 km moving from west (Mediterranean Sea) to east (Desert Group et al., 2004). Moreover, a 3D model of the DST zone shows that the depth of the Moho also decreases from ≈ 35 to ≈ 25 km going from South to North, reaching the shallowest point in the northern part of Israel (Segev et al., 2006). Simultaneously with the formation of the rift, the investigated area experienced volcanic activity (Weinberger et al., 2003). In the northeastern part of Israel near the Sea of Galilee, there is evidence of volcanism, which produced several volcanic products like lava flows and dykes. The dating of the rocks testifies the presence of magmatic activity in this area from middle Miocene up to at least 0.1 Ma (Mor, 1993; Weinstein, 2000).

Several authors carried out studies to evaluate the geothermal heat flux in Israel, estimating an average value around 40-45 mW/m². Two anomalous heat flux zones have been identified close to the Sea of Galilee and in the Gulf of Elat characterized respectively by 70 and 65 mW/m² (Shalev et

al., 2008; Shalev et al., 2013). The anomalous heat flux zones are characterized by a shallower tectonic zones. The large heat flux anomaly makes Northern Israel a promising area for geothermal energy exploitation (Roded et al., 2013).

The chemical and isotopic compositions of dissolved gases (CO₂ and He) are excellent tools to study and evaluate interaction processes between deep fluids and hydrothermal waters. In fact, in geothermal areas deep gases rising towards the surface intercept the shallow aquifers changing their chemical and physical conditions, i.e.: dissolved gases contents, temperatures and pH values (Inguaggiato et al., 2011 and references therein). The amount of dissolved gases in the aquifers is related to the ratio gas-flux/water-flow determining the degree of gas-water interaction processes (Inguaggiato et al., 2010).

Helium is a chemically inert gas, characterized by negligible isotopic fractionation during gas-water interaction processes. Therefore the isotopic composition of dissolved helium provides useful information about its origin and is used as a geochemical tool to investigate the geodynamic context and evaluate origin and mixing processes of different sources (Sano and Marty, 1985; Hilton et al., 1993; Shaw et al., 2003; Inguaggiato et al., 2005; Pik and Marty, 2009; Inguaggiato et al., 2010; D'Alessandro et al., 2014). Considering that the helium can be produced by alpha-decays (⁴He) or trapped during the formation of the earth (³He), its isotope composition is a tool that provides clear information about the source of ascending fluids. The helium can be used, together with other geochemical data, to identify areas that may be of interest for geothermal power generation (Du et al., 2006).

In this work we have investigated the chemical and isotopic compositions of carbon dioxide and helium in cold and hot waters sampled in the hydrothermal systems along the DST, with the aim to evaluate the origin of deep and hot fluids reaching the shallow aquifers and the involved geochemical processes. Furthermore, this study specifically confirms the uprise of mantle helium through the DST recognized by Torfstein et al. (2013) and displays also a contribution of mantle

CO₂ through the same pathway, which, on the contrary, was excluded by previous studies (Torfstein et al., 2013; Avrahamov et al., 2015).

8.2 MATERIALS AND METHODS

The sampling of discharged fluids was carried-out in April 2013, in March 2014 and in May 2015. Cold and hot waters (springs, wells and lakes) were collected (Fig. 8.1) in the area to the north of the DST, specifically: near the Sea of Galilee (Banias, Tabgha, Hamme Teveria, Hamat Gader), in the west side of the Dead Sea (Qedem, Polla Dead Sea, Zukym, En Gedi, Dead Sea, Eg Doc, En Gedi Spring, Hammei Yoav, Hammei Gaash) and in the area to the south of Dead Sea (Ya'alon 1a, Ya'alon 6, Qtura 5, Qtura 115, Timna Mine, Ein Netafim). No fumarolic manifestations were recognised in these area, while the presence of hydrothermal systems is evidenced by several thermal waters reaching temperatures up to 57.2°C.

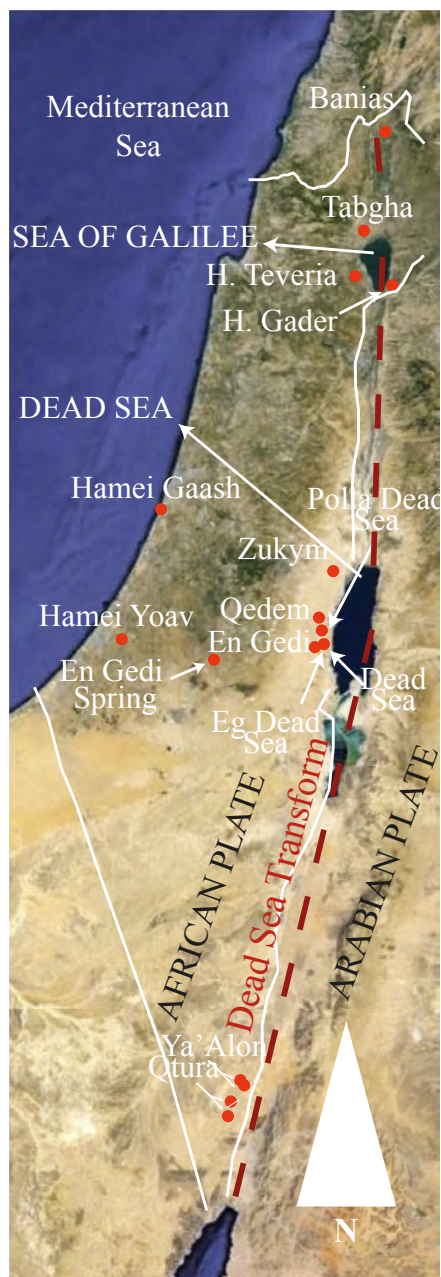


Fig. 8.1 - Location map of sampled waters along Dead Sea Fault area.

Physical-chemical parameters (temperature, pH, Eh and electrical conductivity) of collected fluids were measured in the field using portable instruments. Alkalinity was measured in situ by titration with HCl 0.1N. Dissolved gases were sampled and analysed following the method described by Capasso and Inguaggiato (1998), based on the equilibrium partition of gas species between a liquid and a host gas phase (Ar) that is introduced into the sampling vial. One bubbling gas was sampled using an upside-down funnel submerged in the water connected to a syringe via a teflon tube, and

stored in glass flasks with two vacuum stopcocks. Gas species (He, O₂, N₂, CH₄ and CO₂) were analysed by gas chromatograph (Clarus 500, Perkin Elmer) using Carboxen 1000 columns, two detectors (HWD and FID) and argon as the carrier gas. Typical uncertainties were within $\pm 5\%$.

The isotopic composition of helium was analysed using the method proposed by Inguaggiato and Rizzo (2004). The abundance and isotope composition of helium, as well as the ⁴He/²⁰Ne ratios, were determined by separately admitting He and Ne into a split flight tube mass spectrometer (Helix SFT). Helium isotope compositions are given as R/R_A, where R is the (³He/⁴He) ratio of the sample and R_A is the atmospheric (³He/⁴He) ratio (R_A=1.386*10⁻⁶). Measured values were corrected for the atmospheric contamination of the sample (R_C/R_A) on the basis of its ⁴He/²⁰Ne ratio (Sano and Wakita, 1985). The $\delta^{13}\text{C}$ of Total Dissolved Inorganic Carbon (TDIC) of waters expressed in $\delta\%$ vs V-PDB standard ($\pm 0.2\%$) and was analysed by Analytical Precision 2003 (AP2003) mass spectrometer following the methodology of Capasso et al. (2005).

8.3 RESULTS AND DISCUSSION

8.3.1 General aspect and dissolved gases

Table 8.1 displays the analytical results of the sampled water. The temperature in Hamat Gader, Hamme Teveria, Qedem, Polla Dead Sea, En Gedi, Hammei Yoav, Ya'alón 1a, Ya'alón6, Qtura 5 and Qtura 115 waters was higher ($33.2 < T^{\circ}\text{C} < 57.2$) compared to Baniyas, Tabgha, Zukym, Dead Sea, Eg Doc (Dead Sea), En Gedi Spring, Hammei Gaash, Timna mine and Ein Netafim ($14.6 < T^{\circ}\text{C} < 30$).

Our fluids have pH ranging from 5.4 to 7.6 and dissolved CO₂ contents spanning from 0.28 to 55.75 cc l⁻¹. We found that the waters characterised by higher amounts of dissolved CO₂ have lower pH values (Tab. 8.1), suggesting that CO₂ is the main specie responsible of water acidity. The total salinity (TDS) of the studied waters ranges from 0.27 to 373.30 g/l. The remnants of hypersaline brines (Klein-Bendavid et al., 2004) and possibly old evaporitic terrains embedded in the sequences of the investigated aquifers (Moller et al., 2007), are the source of the occasionally very high

salinity of the sampled waters. The amount of dissolved CO₂, CH₄, O₂, N₂, and He is between 0.28 – 55.75 cc l⁻¹, 3.47*10⁻⁴ – 3.45*10¹ cc l⁻¹, 0.01 – 6.70 cc l⁻¹, 0.27 - 18.71 cc l⁻¹ and, 9.18*10⁻⁶ - 1.9*10⁻² cc l⁻¹ respectively. The triangular plots (Fig. 8.2a, b) show a mixture of water interacting with atmospheric gases and other gases that can be derived from crust, mantle and/or associated to hydrocarbon reservoir. The CO₂-N₂-O₂ triangular plot (Fig. 8.2a) shows that the investigated waters lie in the area defined by the CO₂ and N₂ vertices and the representative point of Air Saturated Sea Water (ASSW). Such pattern can be considered representative of a mixing process between a CO₂-rich end-member and a shallow air-dominated system. The samples plotting closest to ASSW display N₂/O₂ ratios similar to the atmospheric value while the samples increasingly enriched in CO₂ reveal much higher N₂/O₂ ratios. This indicates that the atmospheric component, derived from meteoric recharge, was modified by organic and inorganic redox reactions in the subsurface losing O₂. Based on the dissolved gas composition (CO₂-N₂-O₂) three water groups were identified (Fig. 8.2a). The first group closer to the CO₂ end-member characterized by higher gas-water interaction (Hammei Teveria, Hamat Gader, En Gedi, Qedem), the second group with moderate gas-water interaction (Polla Dead Sea, Hammei Gaash, Hammei Yoav, Ya'alon 6, Ya'alon 1a, Qtura 5 and Qtura 115 and Tabgha) and finally the third group which is close to the ASSW composition representing the waters almost in equilibrium with atmospheric-air (Banias, Zukym, Dead Sea, Eg Doc, En Gedi David and Timna Mine). Triangular plot CO₂-CH₄-N₂ (Fig. 8.2b) shows the same distribution of samples identified with the triangular plot previous mentioned, except two samples (Hammei Gaash and Hammei Yoav) belonging to the Group 2, with higher CH₄ contents compared to CO₂.

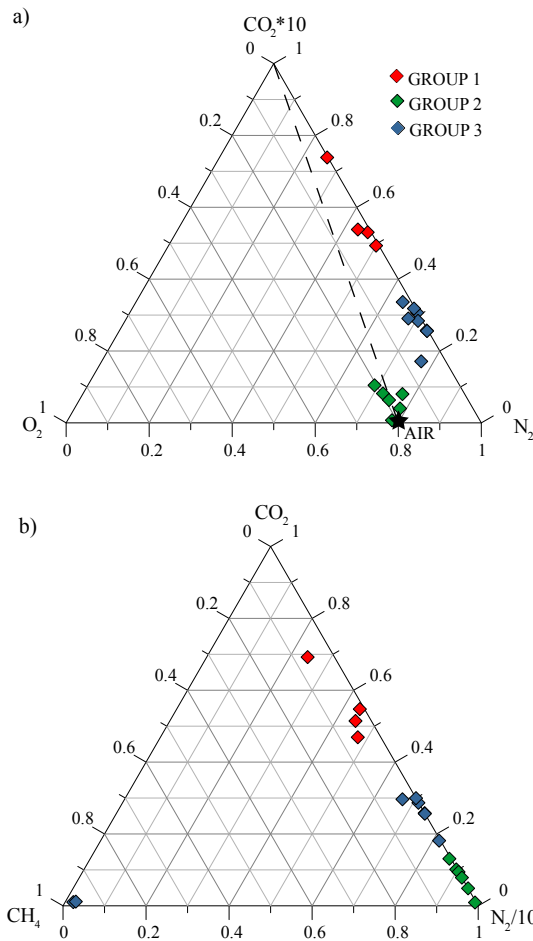


Fig. 8.2 - a) Triangular plot, relative pressure of CO₂, N₂ and O₂. The air values are also reported for comparison; the straight line represents the theoretical mixing between air dominated system and CO₂-rich fluids. b) Triangular plot, relative pressure of CO₂, N₂ and CH₄.

GROUP	SAMPLE	DATE	pH	T (°C)	TDS	R/Ra	⁴ He/ ²⁰ Ne	R/Rac	A%	R%	M%	He	H ₂	O ₂	N ₂	CO	CH ₄	CO ₂	CO ₂ ^δ C	TDIC	δ ¹³ C (TDIC)	L%	S%	M%
GROUP 1	H. Gader (S)	28/04/13	6.7	49.0	1.4	2.14	43.66	2.15	1	64	35	8.72E-03	-	0.41	17.21	6.26E-04	2.03E-01	55.75	2.15E+09	7.38	-9	4	26	70
	H. Teveria (S)	28/04/13	5.9	57.2	29.76	1.10	106.86	1.10	0	82	18	1.91E-03	3.00E-04	1.02	8.88	1.45E-03	4.50E-02	41.12	1.41E+09	3.98	-5.9	0	2	97
	Qedem (S)	29/04/13	5.4	44.3	178.88	0.63	83.13	0.60	0	91	9	9.15E-03	1.69E-02	0.03	2.10	9.02E-04	1.62E-01	31.77	4.16E+09	2.80	-6.69	41	23	36
	En Gedi (W)	29/04/13	5.8	41.4	138.14	0.47	7.13	0.40	4	89	7	9.68E-04	5.52E-03	0.15	6.44	6.70E-04	1.85E-01	30.36	4.90E+10	3.54	-8.12	59	38	3
GROUP 2	Polla Dead Sea (S)	15/05/15	5.6	35.0	193.5	0.58	1.09	0.46	26	69	5	8.87E-05	2.90E-03	0.01	3.32	1.87E-05	5.17E-02	8.70	1.22E+11	4.96	-22.12	4	94	2
	Hamei Gaash (W)	16/05/15	7.2	24.5	25.6	0.34	1.01	0.13	28	72	0	8.28E-05	1.28E-03	0.17	2.64	-	2.98E+01	7.40	1.89E+11	6.90	-5.88	54	45	1
	Hamei Yoav (W)	16/05/15	7.0	39.4	2.9	0.54	1.83	0.47	16	79	5	4.43E-04	4.28E-04	0.04	4.39	-	3.45E+01	9.10	2.75E+10	6.57	-5.99	56	38	6
	Ya'alon 1a (W)	10/03/14	6.9	33.3	1.89	0.11	27.14	0.11	1	99	0	8.15E-03	-	0.11	18.71	-	-	23.12	1.80E+10	6.05	-5.11	57	34	9
	Ya'alon 6 (W)	10/03/14	6.9	40.0	1.37	0.26	21.49	0.26	1	96	3	4.85E-03	-	0.40	15.88	-	2.58E-03	24.99	1.40E+10	6.02	-7.89	49	40	11
	Qtura 5 (W)	10/03/14	6.9	33.7	1.76	0.28	4.52	0.24	6	91	2	1.21E-03	-	0.11	18.70	1.79E-04	1.60E-03	23.11	4.92E+10	5.34	-7.69	53	43	3
	Qtura 115 (W)	10/03/14	6.9	33.2	2.07	0.14	6.72	0.11	4	95	0	1.63E-03	-	1.19	13.90	2.38E-05	-	28.04	8.56E+10	6.15	-6.79	58	40	2
Tabgha (S)	17/05/15	7.0	27.5	2.5	1.26	1.89	1.30	15	67	18	4.31E-04	-	1.85	12.49	3.12E-05	1.11E-02	13.95	1.85E+10	5.67	-18.99	8	84	9	
GROUP 3	Timna Mine (L)	14/05/15	7.4	27.0	44.0	0.63	0.78	0.47	37	60	4	3.50E-05	1.65E-02	4.11	7.89	3.07E-05	5.65E-03	0.39	1.20E+10	1.22	-3.71	52	35	13
	Dead Sea (L)	29/04/13	6.0	30.0	373.30	0.94	0.47	-	57	38	5	9.54E-06	1.72E-02	0.16	0.31	2.15E-04	3.47E-04	0.28	2.37E+10	4.31	-	-	-	-
	Eg Doc (Dead Sea) (L)	12/03/14	6.0	30.0	347.04	0.73	0.43	-	66	33	1	9.18E-06	8.97E-04	0.15	0.27	4.08E-05	5.55E-04	0.33	3.48E+10	6.86	-	-	-	-
	Zukym (S)	29/04/13	7.6	26.6	2.66	0.99	0.41	-	71	24	5	6.41E-05	-	5.68	18.41	2.40E-05	8.28E-04	7.95	9.00E+10	5.53	-10.82	38	60	2
	En Gedi Spring (S)	12/03/14	7.5	27.7	0.53	0.47	0.95	-	30	68	2	1.54E-04	-	5.62	11.41	2.39E-05	-	4.86	4.78E+10	4.60	-11.08	36	60	4
	Banias (S)	28/04/13	7.6	14.6	0.27	1.64	1.03	1.79	28	49	22	1.65E-04	1.08E-02	6.70	15.58	7.36E-05	-	4.53	1.21E+10	3.19	-12.02	22	66	13
	Ein Netafim (S)	14/05/15	7.5	21.0	2.4	0.16	1.35	-	20	80	0	1.40E-04	-	-	-	-	-	-	-	-	-	-	-	-
	H. Gader (B)	28/04/13	-	-	-	2.12	66.18	2.13	-	-	-	927.62	5	5.62	78.44	10	4934	6.96	2.55E+07	-	-	-	-	-

Tab. 8.1 - Total Dissolved Salts (TDS) is expressed in g l⁻¹. Chemical composition of dissolved gases (values expressed in cc l⁻¹ STP), bubbling gases (values of O₂, N₂ and CO₂ are expressed in % vol, while the values of He, H₂, CO, CH₄ are expressed in p.p.m vol). The isotopic composition of C gas (δ¹³C_{TDIC}) is expressed in ‰ PDB standard. Isotopic composition of Helium is expressed as R/Ra, ³He/⁴He ratios normalized to the atmospheric ratio (Ra=1.39×10⁻⁶). While, R/Rac represent R/Ra corrected for the atmospheric contamination. Percentage of Radiogenic (R), Magmatic (M) and Atmospheric (A) represent the contribution of different He source calculated following the description of Sano et al. (1985) Percentage of Mantle carbon (M), Marine limestone (L) and organic Sediment (S) fields represent the CO₂ contribution from different sources calculated following the description of Sano and Marty (1995). The kinds of samples are: Spring (S), Well (W), Lake (L) and Bubbling gas (B).

The concentrations of He and CO₂ dissolved in waters increase simultaneously, due to the interaction with non-atmospheric gases (Fig. 8.3), suggesting a possible common provenance of He and CO₂. With the exception of Dead Sea waters and Timna mine, He and CO₂ contents are higher compared to ASSW (He=4.13*10⁻⁵ cc l⁻¹ CO₂=0.032 l⁻¹ - Capasso and Inguaggiato (1998)) highlighting the input of the before mentioned gases, changing the equilibrium with atmospheric-air, characteristic of most of the natural waters (Fig. 8.3). The lower amount of He in Dead Sea samples and Timna mine is due to the high salinity values changing the solubility of gases (salting out effect) and to the low interaction with non-atmospheric He. In particular, the water belonging to Group 1, which have the highest CO₂ contents, are also strongly enriched in He.

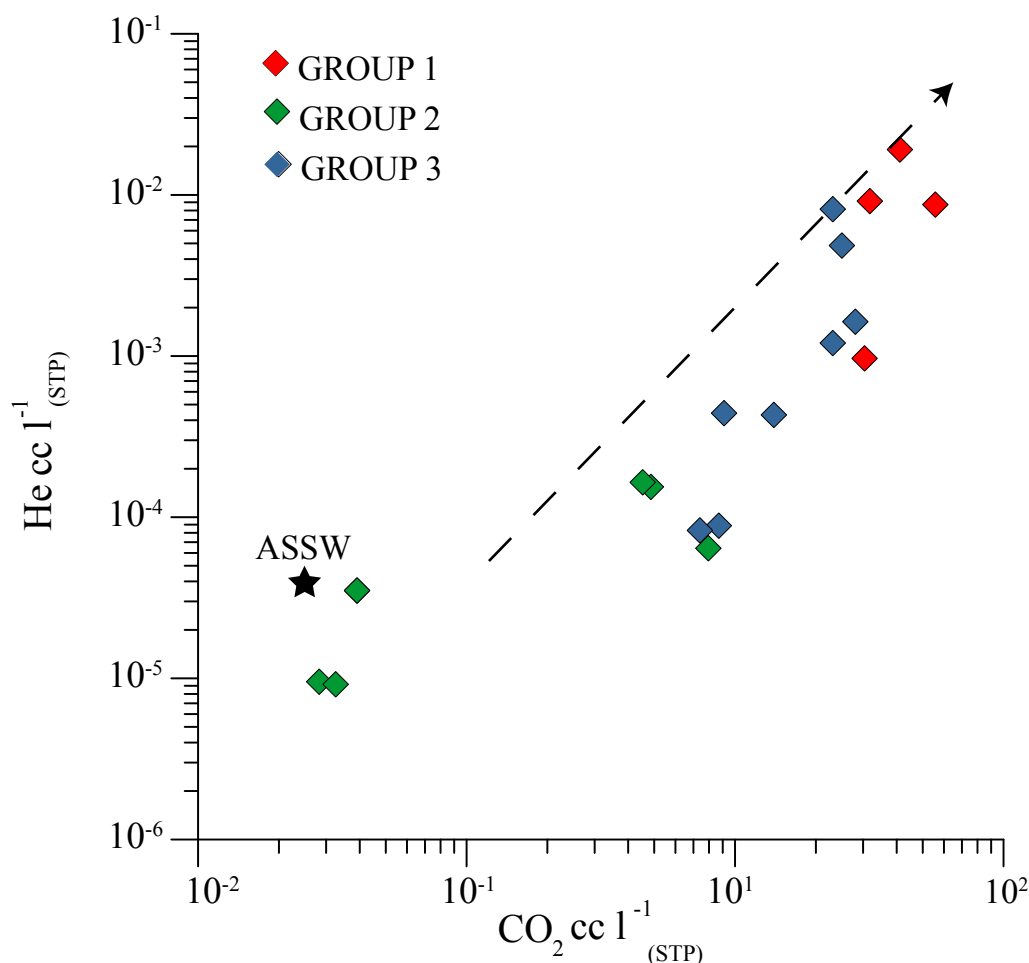


Fig. 8.3 - He vs. CO₂ contents (cc l⁻¹ STP) of dissolved gases in the sampled waters. The ASSW values are also reported for comparison.

Figure 8.4 shows the increase of water temperature respectively with CO₂ and helium amounts

dissolved in water, suggesting input of hot fluids enriched in CO₂ and helium or deeper and longer circulation as responsible of higher water temperature. The samples belonging to the Group 1 with the highest gas content have also the highest measured temperatures. In particular Hammei Teveria and Hammat Gader, respectively with temperature of 49.0 and 57.2 °C, are located in the northern part of DST, close to the Sea of Galilee.

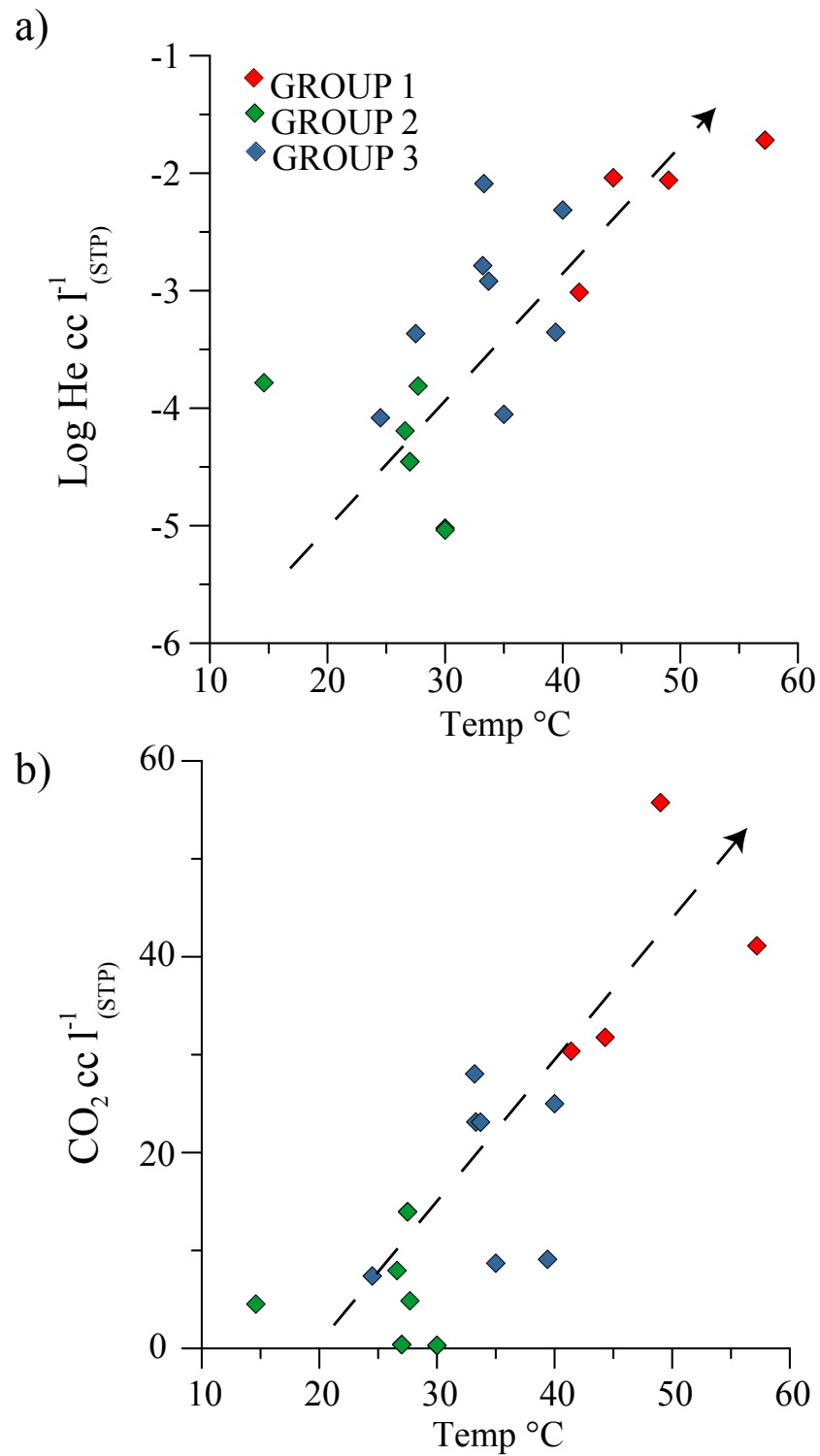


Fig. 8.4 - Changes in ⁴He and CO₂ dissolved in waters (cc l⁻¹ STP) with respect to the temperature values of the waters
 4b) Changes in CO₂ dissolved in waters (cc l⁻¹ STP) with respect to the temperature values of the waters.

8.3.1 Mantle derived helium along Dead Sea Fault

The isotopic ratio of helium is an excellent geochemical tool to trace the helium origin, thanks to the negligible fractionation during gas-water interaction processes. The isotopic compositions of the helium sources, atmospheric-air, MORB and crust are well known.

The measured R/Ra values span between 0.11 and 2.14 while the $^4\text{He}/^{20}\text{Ne}$ ratio changes by nearly 3 orders of magnitude (0.41-107). Figure 8.5 shows that our dissolved gases result from a mixing in different proportions between the radiogenic contribution of the crust, ASW and a MORB-type mantle end-member. Moreover, the samples belonging to Group 1 have the highest $^4\text{He}/^{20}\text{Ne}$ confirming the strong deep gas contribution, whereas the samples with R/Ra values higher than 1 are the only ones located in the northern part of investigated area.

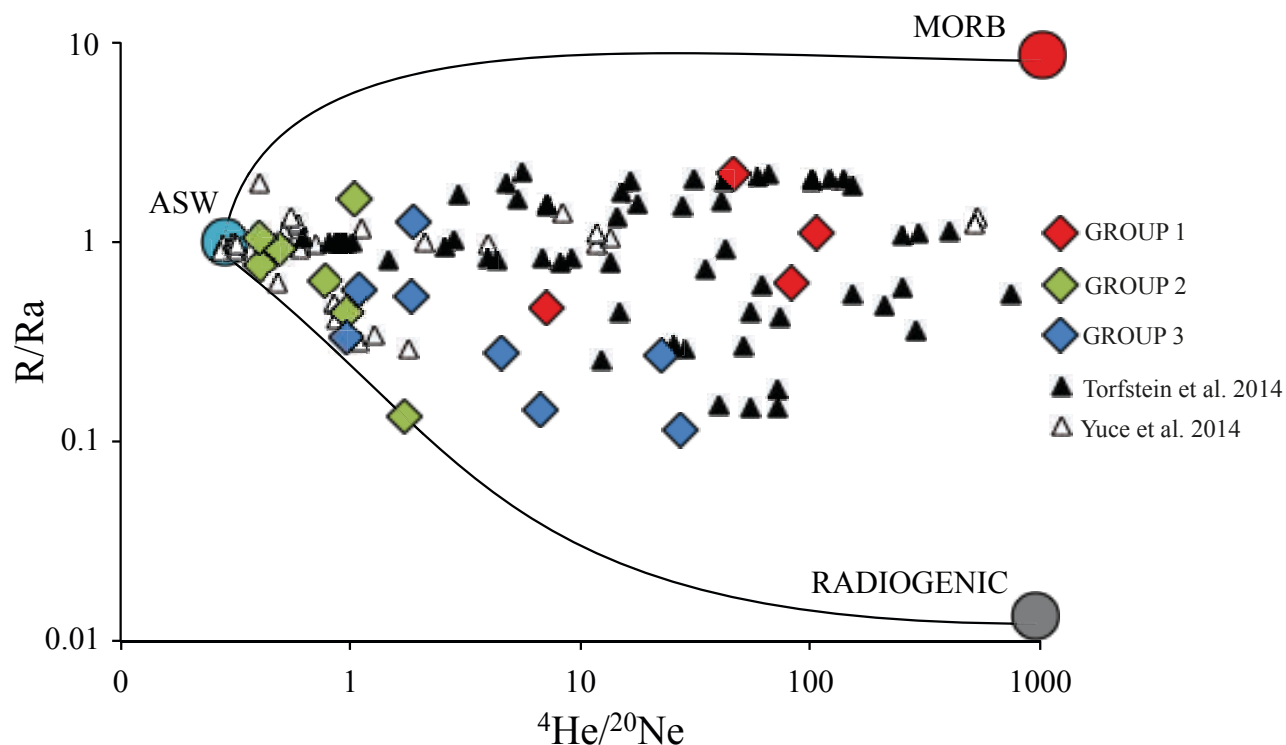


Fig. 8.5 - R/Ra values vs. $^4\text{He}/^{20}\text{Ne}$ ratios diagram. Air Saturated Water (ASW), Mid-Ocean Ridge Basalts (MORB) and Radiogenic fields are reported as reference.

Assuming R/Ra and $^4\text{He}/^{20}\text{Ne}$ ratios of 0.02 and 1000, 1 and 0.285, 8 and 1000 for Crust, ASW and MORB-type mantle respectively, we estimated the mixing proportion using the Sano and Wakita (1985) equation's system. The radiogenic crustal source is dominant in most of the

investigated fluids ranging from about 24 to 99% while the mantle contribution varies from 0 to 35% (Fig. 8.6). Only Dead Sea, Eg Doc (Dead Sea), Zukym, Timna mine display a significant ASW contribution (57-71%). The possibility of mantle fluids injection in the crust through deep-rooted tectonic structures has been highlighted by many studies worldwide. Important examples can be found along the NAF in Turkey (Gülec et al., 2002), the San Andreas Fault in California (Kulongoski et al., 2013) and the Karakoram Fault (Klemperer et al., 2013). Previous studies have still shown that also the DST allows the uprise of mantle He both along the same sector considered in the present study (Torfstein et al., 2013) and in its northern part along the Turkish-Syrian border (Yuce et al., 2014). The data of these two studies have been also plotted in Fig. 8.5 evidencing similar mixing pattern between the three end-members along a great part of the DST.

Figure 8.6 shows that higher mantle contribution (18-35%) is mainly found in the northern part of the DST sector presently studied (Hamat Gader, Hamme Teveria, Baniyas and Tabgha), while significantly lower values (0-9%) are found in the central part (Qedem, En Gedi, Dead Sea, Eg Doc (Dead Sea), Zukym, Polla Dead Sea, Hammei Yoav and Hammei Gaash). In the southern part of DST investigated area (Ya'alon 1a, Ya'alon 6, Qtura 5, Qtura 115, Timna Mine, Ein Netafim) the lowest percentage values of mantle contribution (0-4%) were recognized. The results of our study confirm the geographical distribution of mantle component, with a decrease of mantle-helium towards the southern part of the study area, which was previously recognised by Torfstein et al. (2013). The area with the highest mantle contribution (up to 1/3 of the isotopic budget of dissolved He) corresponds to the anomalous heat flux area close to the Sea of Galilee.

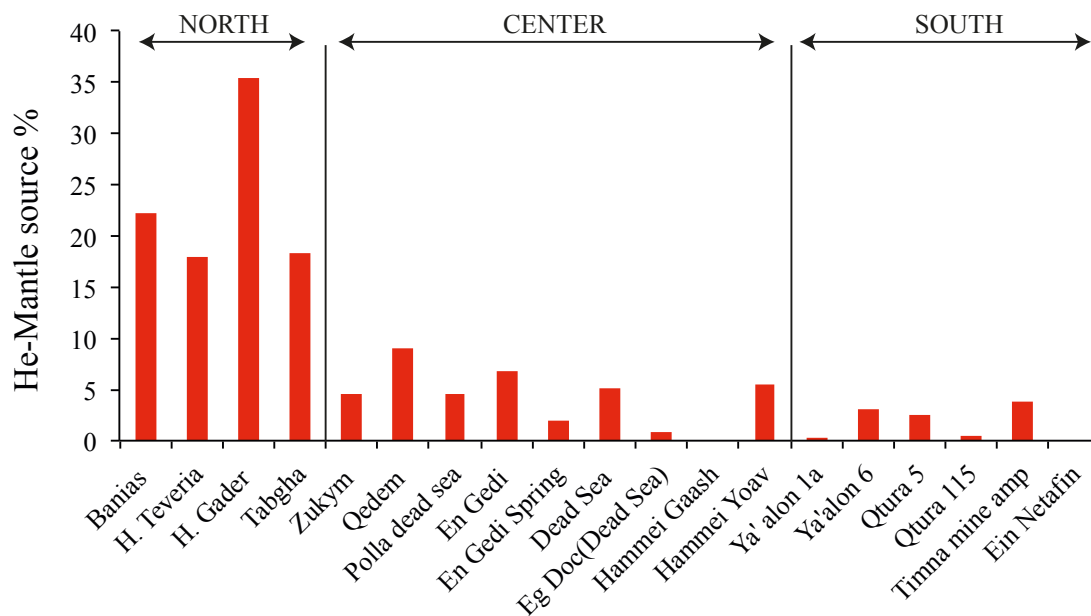


Fig. 8.6 - Geographical distribution of mantle source. The percentage of mantle source was calculated using the equation of Sano and Waikita (1985).

To better constrain the origin of the gases interacting with the water, the CO₂/³He ratios was calculated (Sano and Marty, 1995; Rouwet et al., 2008; Kulongoski et al., 2013). Marty and Jambon (1987) suggest a CO₂/³He ratio of about 2*10⁹ for fluids discharged from the mantle. On the contrary, CO₂/³He ratios ranging between 10¹² and 10¹⁴ occur in crustal fluids (O'Nions and Oxburg, 1988). The CO₂/³He values of investigated fluids span between 1.41*10⁹ and 1.89*10¹¹ (Fig. 8.7), between the values characteristic of the Mantle and Crust end-members. The R/Ra and CO₂/³He ratios are plotted in the binary graph in order to discern the mantle and crust contribution of the investigated fluids (Fig. 8.7). The dissolved fluids in the studied waters fall along a hyperbolic mixing trajectories (Fig. 8.7) between the two end-members, contrarily to Torfstein et al. (2013) who did not observe the above-mentioned mixing using CO₂/³He ratios. In particular, Hammat Gader and Hammei Teveria (belonging to Group 1) have CO₂/³He ratios typical of fluids with mantle signature.

Thermal waters in the investigated area do not show bubbling gases, except Hamat Gader, which is characterized by a very low gas flux, strongly suggesting that the aquifer is able to dissolve

almost totally of deep gases. The CO₂/³He ratio of Hamat Gader bubbling gas shows a much lower value ($2.55 \cdot 10^7$) with respect to the dissolved gases ($2.11 \cdot 10^9$), evidencing a strong chemical fractionation process due to the CO₂ removal due to dissolution in the water and the virtual enrichment of helium in the bubbling gases due to the much lower solubility of helium respect to CO₂ (Capasso et al., 1997; Giammanco et al., 1998; D'Alessandro et al., 2014). Features of CO₂/³He ratio in Fig. 8.7 are consistent with geographic sample grouping with a larger contribution of mantle fluids occurring in waters collected in the Northern area, whereas larger crustal contribution occurs in the sample collected in the central-southern area.

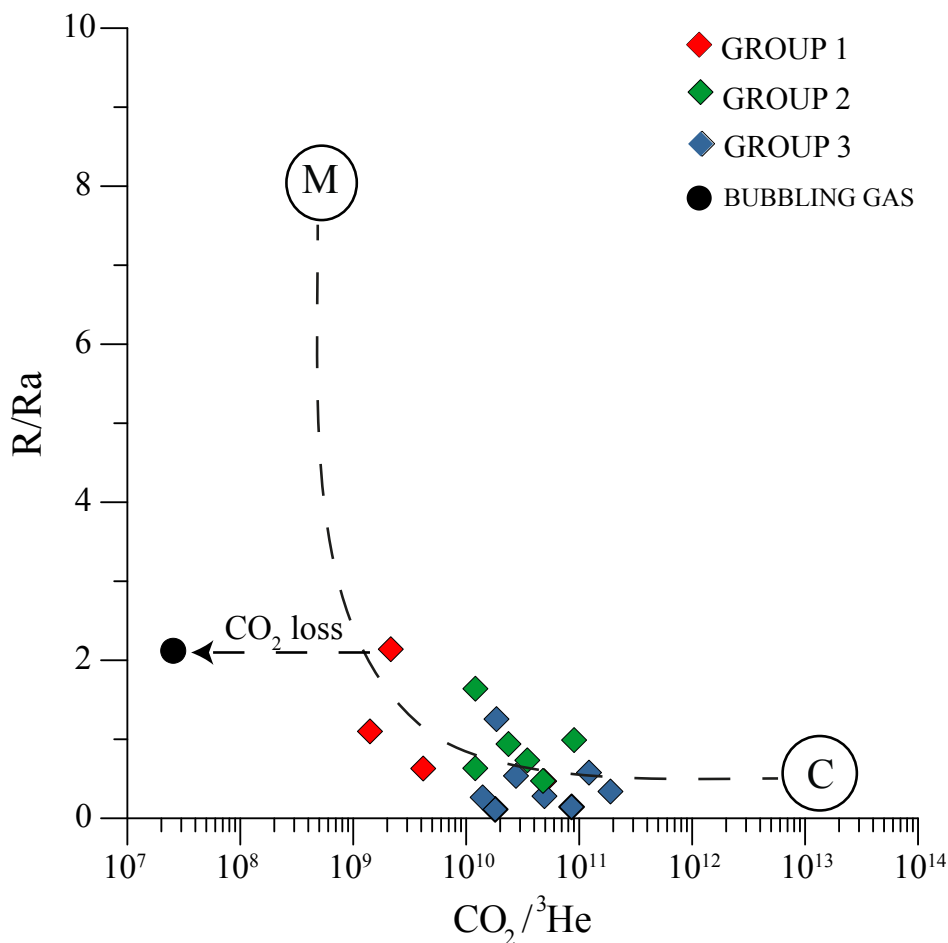


Fig. 8.7 - CO₂/³He plotted vs. R/Ra shows a different proportion of mixing between fluids of crust and mantle origins. Mid-Ocean Ridge Basalts (MORB) and crust fields are reported as reference. The black circle represents the bubbling gas collected to H. Gader, showing a fractionation process of CO₂ and He with respect to the dissolved gases.

8.3.2 *Origin of CO₂*

The determination of the CO₂ origin through its C-isotopic composition is not so straightforward as for helium because of the wide range of sources, sometimes with overlapping isotopic composition, and to the fact that CO₂ is more reactive than helium and consequently involved in many chemical-physical processes that may change its isotopic composition. Nevertheless also the C-isotopic composition of CO₂ or total dissolved inorganic carbon ($\delta^{13}\text{C}_{\text{T DIC}}$) gives important information (Deines et al., 1974; Sano and Marty, 1995; Kulongoski et al., 2013). Marine limestones, the oxidation of organic carbon from soils and sedimentary rocks and the upper-mantle degassing are among the main sources of carbon. These carbon sources have distinct $\delta^{13}\text{C}$ end-members, whereby marine limestone has $\delta^{13}\text{C}$ close to 0‰, sedimentary organic matter less than -20‰ and upper-mantle degassing ranges between -4 and -9‰ (Javoy et al., 1986; Sano and Marty, 1995; Hoefs, 2009 and references therein).

The $\delta^{13}\text{C}_{\text{T DIC}}$ values in our samples display a wide range (between -22.1 and -3.7‰), but while samples with less than 20 cc/l of dissolved CO₂ cover the whole range of measured $\delta^{13}\text{C}$ values, waters with higher CO₂ contents display lower variability ($\delta^{13}\text{C}_{\text{T DIC}}$ from -9.0 to -5.1 ‰ - Fig. 8.8). The samples of Group 3, except Timna Mine, show $\delta^{13}\text{C}_{\text{T DIC}}$ values typical of aquifers in which organic soil CO₂ equilibrates with marine carbonates (Chiodini et al., 2000). Tabgha and Polla Dead Sea displaying the most negative values probably reflect the addition of CO₂ deriving from methane oxidation. This process has been evidenced in other sites of the same area by Avrahamov et al. (2015). Our study shows that waters with higher dissolved CO₂ levels (Group 1 waters and part of the samples of Group 2) are consistent with an upper-mantle isotopic signature suggesting the addition of deeply derived CO₂ (Fig. 8.8). While Yuce et al. (2015) whose data display a distribution comparable to our data (fig. 8.8), also evidenced the contribution of a mantle component for CO₂ along the Turkish part of DST, Torfstein et al. (2013) and Avrahamov et al. (2015) excluded such possibility along the Israeli part.

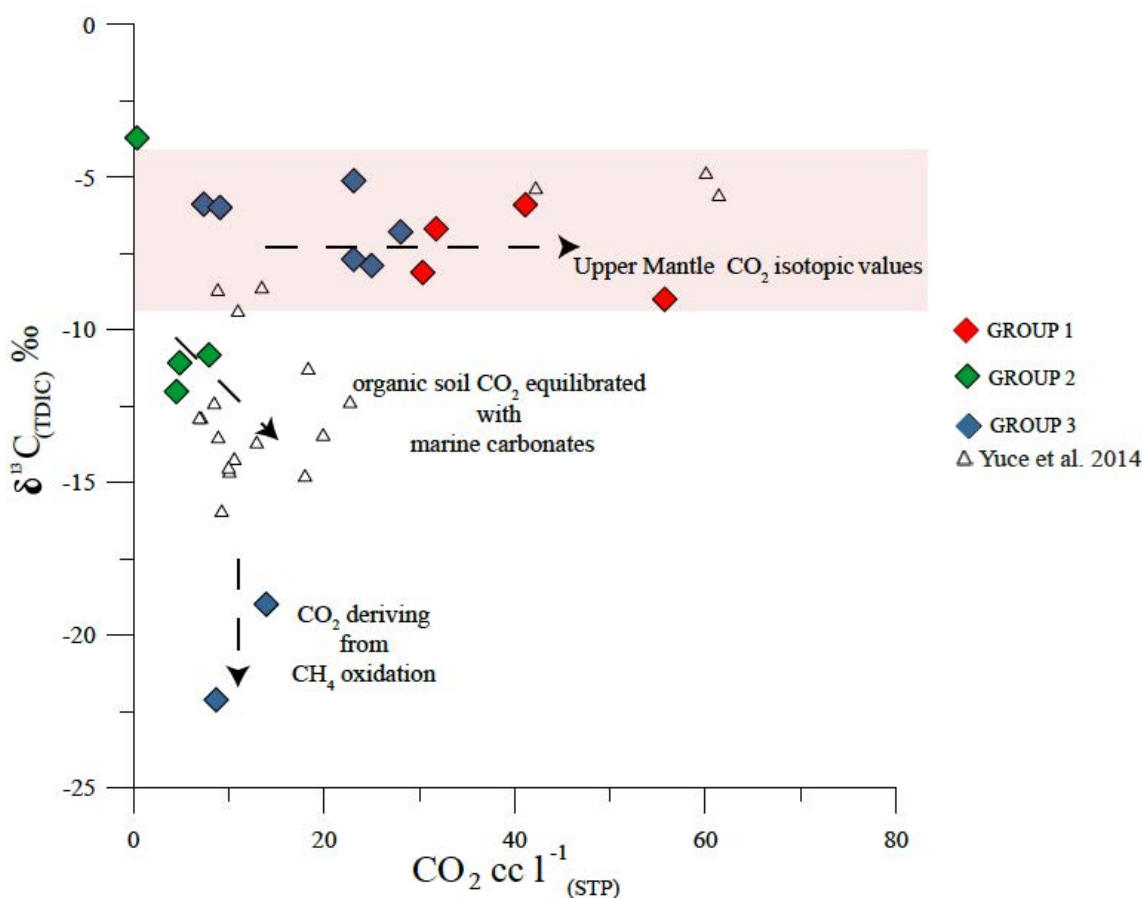


Fig. 8.8 - Co-variation of $\delta^{13}\text{C}$ (TDIC) and dissolved CO_2 (cc l^{-1} STP). The arrows indicate the different processes involving CO_2 in the investigated waters.

The carbon isotopic composition of $\text{CO}_{2(\text{gas})}$ coupled with $\text{CO}_2/{}^3\text{He}$ ratio, is used to better identify the origin of CO_2 (Barry et al., 2013). Three potential end-members which can provide CO_2 are: mantle (M) limestone (L) and organic sediments (S). The considered composition for the end-members are: $\text{CO}_2/{}^3\text{He}=2*10^9$ and $\delta^{13}\text{C}=-6.5\text{‰}$ for Mantle, $\text{CO}_2/{}^3\text{He}=1*10^{13}$ for Limestone and Sediments and $\delta^{13}\text{C}$ values of 0 and -30‰ , respectively (Sano and Marty, 1995 and references therein). The $\delta^{13}\text{C}_{\text{CO}_2}$ vs. $\text{CO}_2/{}^3\text{He}$ graph was initially used to display different fluid contributions along volcanic arcs (Sano and Marty, 1995) but has been later used also in different geodynamic settings and also in areas affected by deep-rooted transform faults (Mutlu et al., 2008; Kulongoski et al., 2013; D'Alessandro et al., 2014). To plot our data in such a graph, the carbon isotopic composition of $\text{CO}_{2(\text{gas})}$ in equilibrium with the investigated waters was calculated at the outlet temperature, taking into account: the amount of CO_2 and HCO_3^- dissolved in water, the values of

$\delta^{13}\text{C}_{\text{TDIC}}$ and the enrichment factor ε_a ($\text{CO}_{2\text{dissolved}}-\text{CO}_{2\text{gas}}$) and ε_b ($\text{CO}_{2(\text{gas})}-\text{HCO}_3^-$) (Zhang et al., 1995).

Figure 8.9 shows that all the investigated waters fall in the field belonging to the contribution of the three end-members before mentioned. The waters are characterized by interaction with mantle-CO₂ in different proportion, calculated following the equation of Sano and Marty (1995). In particular, Hamat Gader and Hammei Teveria (belonging to Group 1) located in the northern part of the investigated area with highest mantle-CO₂ contribution (97.4 and 70.2%, respectively) and Qedem to the west of Dead Sea fall in Fig. 8.9 close to the mantle end-member with a significant mantle-CO₂ contribution (36.4%). The other water samples located in the southern part of the studied area show a shift towards the organic and limestone end-members, with a lower mantle-CO₂ component ranging from 1.2 to 11.1. In particular, the waters of Group 3 (En Gedi Spring, Baniyas and Zukym) and Tabgha belonging to Group 1 have prevalingly organic CO₂ contribution.

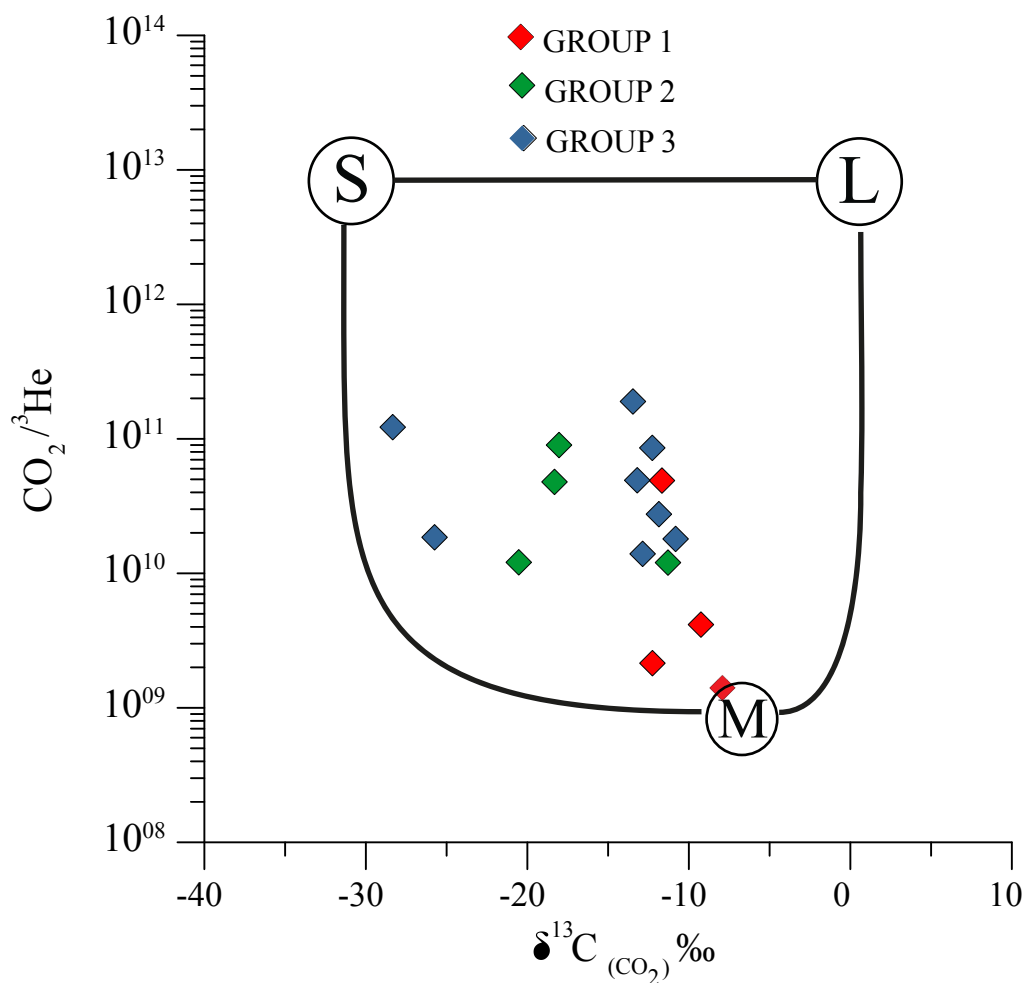


Fig. 8.9 - CO₂/³He plotted vs. δ¹³C_{CO₂} shows a different proportion of CO₂ mixing between fluids of crust and mantle origins. Mantle carbon (M), Marine limestone (L) and Organic sediment (S) fields are reported as reference.

Contrarily to the claim of Torfstein et al. (2013) suggesting that CO₂ is associated to an atmospheric component, our study affirms that the waters along DST strongly interact with non-atmospheric CO₂ as testified by the amount of CO₂ dissolved in the waters, which is always in excess with respect to the equilibrium value with the atmosphere, and the isotopic composition of carbon, previously discussed. Also Avrahamov et al. (2015) exclude that mantle-derived CO₂ rises up along the Israeli sector of DST but their paper is focused on the origin of CH₄ in the sampled fluids and does not discuss the origin of CO₂. We agree that from their data a contribution of mantle-CH₄ is not recognizable but their δ¹³C_{TDIC} and δ¹³C_{CO₂} values are compatible with a mantle

contribution for CO₂.

It is generally assumed that the injection of mantle-He within the crust happens either through intrusion and consequent degassing of mantle-derived magmas or through diffusion of mantle-fluids across the ductile mantle-crust boundary (Kennedy and Van Soest, 2007). Both processes could be invoked at least for the northern sector of the investigated area. But in both cases the injection of mantle-He cannot happen without the involvement of important quantities of mantle-CO₂ (Kennedy and van Soest, 2007). The latter, being more reactive than He, can be involved in many chemico-physical processes that could significantly change its isotopic composition and the CO₂/³He ratio. Such changes may sometimes partially or totally mask its origin, but basing on the present data its mantle-derivation can be easily recognised.

8.4 IMPLICATIONS

The results of this study improved the knowledge about the origin of fluids interacting with the aquifers along DST, providing important information about the sources of helium and CO₂ and the processes affecting these gases during its path towards the earth's surface. The up-rise of deep hot fluids interacting with the shallow aquifer, can be considered responsible of the high temperature of some water sources along the Dead Sea Transform. Different amount of He and CO₂ dissolved in the waters are the result of a different mixing between Mantle and Crustal components, which reflects different tectonic configurations along DST. Geochemical data agree with the heat flux reported by Shalev et al. (2008; 2013), showing that higher contents of mantle helium (³He) and mantle-CO₂ occur in the northern area, where the highest heat flux of the investigated area was recognized (70 mW/m²). Similar relationships between heat fluxes and ³He/⁴He in thermal areas were found by Umeda et al. (2007) in the thermal waters and dissolved gas phase in Kii Peninsula, Japan. These results suggest that ascending deep fluids enriched in CO₂ and helium fuel deep hydrothermal systems.

As previously shown by Torfstein et al. (2013), the geographical distribution of isotopic values

(R/Ra) along the DST is in agreement with the different tectonic conditions. In particular, a mantle up-rise and/or deeper fault systems could justify an easier ascent of mantle fluids with a larger ³He signature in the northern part of the studied area, in agreement with Segev et al. (2006). Moreover, considering that the last magmatic activity in this area has been dated at 0.1 Ma (Mor, 1993), a source of ³He due to the presence of magma bodies intruded into the crust releasing fluids rich in mantle-He cannot be excluded. This could also explain the anomalous heat flux recognised by Shalev et al. (2008) near Galilee Sea. These evidences suggest that in the northern part the fault system is connected at depth, in particular near Hammei Teveria and Hamat Gader where the highest proportion of mantle-He and Mantle-CO₂ are recognized. Finally, the present study remarks that deep regional transform faults are important pathways for mantle fluids either directly or through the intrusion of magmatic batches. Examples can be found both in the Middle-east region (Gülec et al., 2002; Italiano et al., 2013; Torfstein et al., 2013; Yuce et al., 2014) and worldwide (Kulongoski et al., 2013; Klemperer et al., 2013; D'Alessandro et al., 2014).

8.5 CONCLUDING REMARKS

Data of chemical and isotopic composition of He and CO₂ dissolved in waters were measured to investigate the origin of fluids interacting with the waters along the DST.

Values of R/Ra coupled with ⁴He/²⁰Ne show a dominant radiogenic component with a geographical distribution of samples (North-Center-South families) highlighting higher contributions of mantle-helium in waters located in the northern part of the area, where an anomalous heat zone has been previously identified.

High CO₂ amounts dissolved in water are recognized along DST, with maximum values in the northern part close to the Sea of Galilee (Hammei Teveria and Hamat Gader). Moreover, CO₂/³He ratios coupled to δ¹³C(CO₂) allowed to discriminate the contribution of different end-members, showing higher mantle CO₂ contribution in the northern part of investigated area.

As for other similar tectonic structures around the world, the DST fault system allows the rise of

fluids of mantle origin. Such uprise is favoured in the northern part of the investigated area where a shallower Moho discontinuity is present. The contemporaneous presence of the products of recent magmatic activity in the same area does not allow to discriminate if these mantle fluids derives from degassing of magma batches intruded in the crust or from diffusion of mantle-fluids across the ductile mantle-crust boundary.

CHAPTER 9

REFERENCES

- Aiuppa, A., D'Alessandro, W., Gurrieri, S., Madonia, P., Parello, F., 2007. Hydrologic and geochemical survey of the lake "Specchio di Venere" (Pantelleria island, Southern Italy). *Environ. Geol.* DOI 10.1007/s00254-007-0702-1
- Alibo, D.S., Nozaki, Y., 1999. Rare earth elements in seawater: particle association, shalenormalization, and Ce oxidation. *Geochimica et Cosmochimica Acta* 63, 363–372.
- Avrahamov, N., Gelman, F., Yecheli, Y., Aizenshtat, Z., Nissenbaum, A., Sivan, O., 2015. Proposed sources of methane along the Dead Sea Transform. *Chem. Geol.* 395, 165-175.
- Ayers, G. 2012. Behaviour of the REE during water rock interaction and alteration processes in volcanic lake systems. Ms thesis, Utrecht University, The Netherlands, 1-108.
- Azzaro, E., Badalamenti, F., Dongarra, G., Hauser, S., 1983. Geochemical and mineralogical studies of lake Specchio di Venere, Pantelleria island, Italy. *Chem Geol* 40, 149–165
- Bao, S., Zhou, H., Peng, X., Ji, F., Yao, H., 2008. Geochemistry of REE and Yttrium in hydrothermal fluids from the Endeavour segment, Juan de Fuca Ridge. *Geochemical Journal* 42, 359-370.
- Barry, P.H., Hilton, D.R., Fischer, T.P., de Moor, J.M., Mangasini, F, Ramirez, C.J., 2013. Helium and carbon isotope systematics of cold "mazuku" CO₂ vents and hydrothermal gases and fluids from Rungwe Volcanic Province, southern Tanzania. *Chem. Geol.*, 339, 141-156.
- Bau, M., 1991. Rare-earth element mobility during hydrothermal and metamorphic fluid-rock interaction and the significance of the oxidation state of europium. *Chemical Geology* 93, 219-230.
- Bau, M., Moller, P., 1993. Rare-Earth Element Systematics of the Chemically Precipitated Component in Early Precambrian Iron Formations and the Evolution of the Terrestrial Atmosphere-Hydrosphere-Lithosphere System. *Geochimica et Cosmochimica Acta* 57, 2239-2249.
- Bau, M., 1996. Controls on the fractionation of isovalent trace elements in magmatic and aqueous systems: Evidence from Y/Ho, Zr/Hf, and lanthanide tetrad effect. *Contributions to Mineralogy and Petrology* 123, 323-333.
- Bau, M., 1999. Scavenging of dissolved yttrium and rare earths by precipitating iron oxyhydroxide:

Experimental evidence for Ce oxidation, Y-Ho fractionation, and lanthanide tetrad effect, *Geochimica et Cosmochimica Acta* 63(1), 67-77.

Bau, M., Dulski, P., 1999. Comparing yttrium and rare earth in hydrothermal fluids from the Mid-Atlantic Ridge: implications for Y and REE behaviour during near-vent mixing and for the Y/Ho ratio of Proterozoic Seawater. *Chem. Geol.* 155, 77-90.

Bau, M., Koschinsky, A., 2009. Oxidative scavenging of cerium on hydrous Fe oxide: Evidence from the distribution of rare earth elements and yttrium between Fe oxides and Mn oxides in hydrogenetic ferromanganese crusts. *Geochemical Journal* 43, 37-47.

Borrero, C., Toro, L. M., Alvaràn, M., Castillo, H., 2009. Geochemistry and tectonic controls of the effusive activity related with ancestral Nevado del Ruiz volcano, Colombia *Geofísica internacional* 1, 149-169.

Byrne, R.H., 2002. Inorganic speciation of dissolved elements in seawater: The influence of pH on concentration ratios. *Geochemical Transactions* 3, 11-16.

Capasso, G., Favara, R., Inguaggiato, S., 1997. Chemical features and isotopic of gaseous manifestations on Vulcano island, Aeolian Islands, Italy: An interpretative model of fluid circulation. *Geochim. Cosmochim. Acta* 61(16), 3425-3440.

Capasso, G., and Inguaggiato, S., 1998. A simple method for the determination of dissolved gases in natural waters. An application to thermal waters from Vulcano Island. *Appl. Geochem.* 13, 631-642.

Capasso, G., Favara, R., Grassa, F., Inguaggiato, S., Longo, M., 2005. On-line technique for preparation and measuring stable carbon isotope of total dissolved inorganic carbon in water samples ($\delta^{13}\text{C}_{\text{TDIC}}$). *Ann. Geophys.* 48, 159-166.

Censi, P., Mazzola, S., Sprovieri, M., Bonanno, A., Patti, B., Punturo, R., Spoto, S. E., Saiano, F., 2004. Rare earth elements distribution in seawater and suspended particulate of the central Mediterranean Sea. *Chemistry and Ecology* 20, 323-343.

Censi, P., Sprovieri, M., Saiano, F., Di Geronimo, S., I., Larocca, D., Placenti, F., 2007. The behaviour of REEs in Thailand's Mae Klong estuary: Suggestions from the Y/Ho ratios and lanthanide tetrad effects. *Estuarine Coastal and Shelf Science*, 71, 569-579.

Censi, P., Zuddas, P., Larocca, D., Saiano, F., Placenti, F., Bonanno, A., 2007. Recognition of water masses according to geochemical signatures in the Central Mediterranean sea: Y/Ho ratio and rare

earth element behaviour. *Chemistry and Ecology* 23(2), 139-155.

Censi, P., Saiano, F., Zuddas, P., Nicosia, A., Mazzola, S., Raso, M., 2014. Authigenic phase formation and microbial activity control Zr, Hf, and rare earth element distributions in deep-sea brine sediments. *Biogeosciences* 11 (4), 1125-1136.

Censi, P., Cangemi, M., Brusca, L., Madonia, P., Saiano, F., Zuddas, P., 2015. The behavior of rare-earth elements, Zr and Hf during biologically-mediated deposition of silica-stromatolites and carbonate-rich microbial mats. *Gondwana Research* 27, 209-215.

Chiodini, G., Frondini, F., Cardellini, C., Parello, F., Peruzzi, L., 2000. Rate of diffuse carbon dioxide Earth degassing estimated from carbon balance of regional aquifers: the case of central Apennine, Italy. *J. Geophys. Res.* 105, 8423–8434.

Choi, H., Yun, S., Koh, Y., Mayer, B., Park, S., Hutcheon, I., 2009. Geochemical behavior of rare earth elements during the evolution of CO₂-rich groundwater: A study from the Kagwon district, South Korea. *Chemical Geology* 262, 318-327.

Civetta, L., Cornette, Y., Gillot, P.Y., Orsi, G., 1988. The eruptive history of Pantelleria (Sicily Channel) in the last 50 ka. *Bull. Volcanol.* 50, 47-57.

Colvin, A., Rose, W. I., Varekamp, J. C., Palma, J. L., Escobar, D., Gutierrez, E., Montalvo, F., Maclean, A. 2013. Crater lake evolution at Santa Ana Volcano (El Salvador) following the 2005 eruption. *The Geological Society of America Special Paper*, 498, 23-44.

D'Alessandro, W., Brusca, L., Kyriakopoulos, K., Bellomo, S., Calabrese, S., 2014. A geochemical traverse along the "Sperchios Basin - Evoikos Gulf" Graben (Central Greece): origin and evolution of the emitted fluids. *Mar. Pet. Geol.* 55, 295-308.

Deines, P., Langmuir, D., Harmon, R., S., 1974. Stable carbon isotope ratios and the existence of a gas phase in the evolution of carbonate ground water. *Geochim. Cosmochim. Acta* 38 (7), 1147-1164.

Desert Group, Weber, M., et al., 2004. The crustal structure of the Dead Sea Transform. *Geophys. J. Int.* 156, 655–681.

Dongarra, G., Hauser, S., Alaimo, R., Carapezza, M., Tonani, F., 1983. Hot waters on Pantelleria island. Geochemical features and preliminary geothermal investigation *Geothermics* 12, 49–63.

Du, J., Cheng, W., Zhang, Y., Jie, C., Guan, Z., Liu, W., Bai, L., 2006. Helium and isotopic compositions of thermal springs in the earthquake zone of Sichuan, Southwestern China. *Journal of*

Asian Earth Sciences 26, 533-539.

Elderfield, H., Upstillgoddard, R., Sholkovitz, E.R., 1990. The Rare-Earth Elements in Rivers, Estuaries, and Coastal Seas and Their Significance to the Composition of Ocean Waters. *Geochim. Cosmochim. Acta* 54, 971-991.

Favara, R., Giammanco, S., Inguaggiato S., Pecoraino, G., 2001. Preliminary estimate of CO₂ output from Pantelleria island volcano (Sicily, Italy): evidence of active mantle degassing. *Appl Geochem* 16, 883–894.

Feng, J. L., 2010. Behaviour of rare earth elements and yttrium in ferromanganese concretions, gibbsite spots, and the surrounding terra rossa over dolomite during chemical weathering. *Chem. Geol.* 271, 112-132.

Feng, J.L., Zhao, Z.H., Chen, F., Hi, P.H., 2014. Rare earth elements in sinters from the geothermal waters (hot spring) on the Tibetan Plateau, China. *Journal of Volcanology and Geothermal Research* 287, 1-11.

Firdaus, M.L., Minami, T., Norisuye, K., Sohrin, Y., 2011. Strong elemental fractionation of Zr-Hf and Nb-Ta across the Pacific Ocean. *Nat. Geosci.* 4, 227-230.

Forero, J., Zuluaga, C., Mojica, J., 2011. Alteration related to hydrothermal activity of the Nevado del Ruiz volcano (NRV), Colombia. *Boletín de Geología* 33, 59-67.

Frank, M., 2011. Oceanography: Chemical twins, separated. *Nat. Geosci.* 4, 220-221.

Fulignati, P., Gioncada, A., Sbrana A., 1999 Rare-earth element (REE) behaviour in the alteration facies of the active magmatic–hydrothermal system of Vulcano (Aeolian Islands, Italy). *Journal of Volcanology and Geothermal Research*

Gammons, C., Wood, S., Pedrozo, F., Varekamp, J., C., Nelson., B., J., Shope, C., L., Baffico, G., 2005. Hydrogeochemistry and rare earth element behaviour in a volcanically acidified watershed in Patagonia, Argentina. *Chem. Geol.* 222, 249-267.

Ganor, E., Foner, H. A. and Gravenhorst G., 2003. The amount and nature of the dustfall on Lake Kinneret (the Sea of Galilee) Israel: Flux and fractionation. *Atmospheric Environment* 37(30), 4301-4315.

Garfunkel, Z., Zak, I., Freund, R., 1981. Active faulting in the Dead Sea rift. *Tectonophysics* 80, 1-26.

Giammanco, S., Inguaggiato, S., Valenza, M., 1998. Soil and fumarole gases of Mount Etna:

geochemistry and relations with volcanic activity. *J. V. Geotherm. Res.* 81, 297-310.

Giggenbach, W., F., Garcia, N., Londono, A., Rofriguez, L., Rojas, N., Calvache, M., L., 1990. Chemistry of fumarolic vapor and thermal-spring discharges from the Nevado del Ruiz volcanic-magmatic-hydrothermal system, Colombia. *Journal of Volcanology and Geothermal Research* 42, 13-39.

Ginzburg, A., Gvirtzman, G., 1979. Changes in the crust and in the sedimentary cover across the transition from the Arabian Platform to the Mediterranean Basin: evidence from seismic refraction and sedimentary studies in Israel and in Sinai. *Sedimentary Geology* 23, 19-36.

Godfrey, L.V., White, W.M., Salters, V.J.M., 1996. Dissolved zirconium and hafnium distributions across a shelf break in the northeastern Atlantic Ocean. *Geochim. Cosmochim. Acta* 60, 3995-4006.

Godfrey, L. V., Field, M. P., 2008. Estuarine distributions of Zr, Hf, and Ag in the Hudson River and the implications for their continental and anthropogenic sources to seawater. *Geochem. Geophys. Geosyst.* 9, 359-370.

Godfrey L.V., Zimmermann, B., Lee, D.C., King, R.L., Vervoort, J.D., Sherrell, R.M., 2009. Hafnium and neodymium isotope variations in NE Atlantic seawater. *Geochemistry, Geophysics, Geosystems* 10(8), 1-13.

Goldsmith, Y., M. Stein, and Y. Enzel (2014), From dust to varnish: Geochemical constraints on rock varnish formation in the Negev Desert, Israel, *Geochimica et Cosmochimica Acta*, 126, 97-111.

Goldstein, S. J., Jacobsen, S. B., 1988. Rare earth elements in river waters. *Earth Planet. Sci. Lett.* 89, 35-47.

Greaves, M.J., Rudnicki, M., Elderfield, H., 1991. Rare earth elements in the Mediterranean Sea and mixing in the Mediterranean outflow. *Earth Planet. Sci. Lett.* 103, 169-181.

Greaves, M.J., Statham, P.J., Elderfield, H., 1994. Rare earth element mobilization from marine atmospheric dust into seawater. *Marine Chem.* 46, 255-260.

Greaves, M.J., Elderfield, H., Sholkovitz, E.R., 1999. Aeolian sources of rare earth elements to the Western Pacific Ocean. *Marine Chem.* 68, 31-38

Gülec, N., Hilton D.R., Mutlu, H., 2002. Helium isotope variations in Turkey: relationship to tectonics, volcanism and recent seismic activities. *Chem. Geol.* 187, 129–142.

Herut, B., Gavrieli, I., and Halicz L., 1998. Coprecipitation of trace and minor elements in modern

authigenic halites from the hypersaline Dead Sea brine, *Geochimica et Cosmochimica Acta*, 62(9), 1587-1598.

Hikov, A., 2011. Rare earth element mobility during hydrothermal alteration in Asarel porphyry copper deposit, central Srednogie. *Comptes rendus de l'Academie bulgare des Sciences*, 64 (8), 2011.

Hilton, D., Hammerschmidt, Teufel, S., Friedrichsen, H., 1993. Helium isotope characteristics of Andean geothermal fluids and lavas. *Earth Planet. Sci. Lett.*, 120, 265-282.

Hoefs, J., 2009. *Stable Isotope Geochemistry*. Springer.

Inguaggiato, S., Rizzo, A., 2004. Dissolved helium isotope ratios in ground-waters: a new technique based on gas–water re-equilibration and its application to Stromboli volcanic system. *Appl. Geochem.* 19, 665-673

Inguaggiato, S., Martin-Del Pozzo, A., L., Aguayo, A., Capasso, G., Favara, R., 2005. Isotopic chemical and dissolved gas constraints on spring water from Popocatepetl volcano (Mexico): evidence of gas–water interaction between magmatic component and shallow fluids. *J. V. Geotherm Res.* 141, 91-108.

Inguaggiato, S., Hidalgo, S., Bernardo, B., Bourquin, J., 2010. Geochemical and isotopic characterization of volcanic and geothermal fluids discharged from the Ecuadorian volcanic arc. *Geofluids* 50, 525-541.

Inguaggiato, S., Calderone, L., Inguaggiato, C., Morici, S., Vita, F., 2011. Dissolved CO₂ in natural waters: development of an automated monitoring system and first application to Stromboli volcano (Italy). *Ann. Geophys.*, 54(2), 209-218.

Inguaggiato C., Censi P., Zuddas P., Londoño J. M., Chacón Z., Alzate D., Brusca L., D'Alessandro W. 2015 Geochemistry of REE, Zr and Hf in a wide range of pH and water composition: The Nevado del Ruiz volcano-hydrothermal. *Chemical Geology* 417, 125-133.

Italiano, F., Sasmaz, A., Yuce, G., Okan, O.O., 2013. Thermal fluids along the East Anatolian Fault Zone (EAFZ): Geochemical features and relationships with the tectonic setting. *Chem. Geol.* 339, 103–114, doi: 10.1016/j.chemgeo.2012.07.027.

Jochum K. P., Seufert H. M., Spettel B., Palme H., 1986. The solar-system abundances of Nb, Ta, and Y, and the relative abundances of refractory lithophile elements in differentiated planetary bodies. *Geochimica et Cosmochimica Acta* 50, 1173-1183.

Johannesson, K. H., Lyons, B. W. 1994 The rare earth elements geochemistry of Mono Lake water and the importance of carbonate complexing. *Limnol. Oceanogr* 39 (5), 1141-1154.

Kalacheva, E., Taran, Y., Kotenko, T., 2015. Geochemistry and solute fluxes of volcano-hydrothermal system of Shishkotan, Kuril Islands. *Journal of Volcanology and Geothermal Research* 296, 40-54.

Katz, A., and Starinsky, A., 2009. Geochemical History of the Dead Sea, *Aquat Geochem*, 15(1-2), 159-194.

Kennedy M.B. and van Soest M.C. 2007. Flow of mantle fluids through the ductile lower crust: Helium isotope trends. *Science*, 318, 1433-1436

Klein-Bendavid, O., Sass, E., Katz, A., 2004. The evolution of marine evaporitic brines in inland basins: the Jordan–Dead Sea rift valley. *Geochim. Cosmochim. Acta*, 68, 1763–1775.

Klemperer, S.L., Kennedy, B.M., Sastry, S.R., Makovsky, Y., Harinarayana, T., Leech, M.L., 2013. Mantle fluids in the Karakoram fault: Helium isotope evidence. *Earth Planet. Sci. Lett.* 366, 59–70, doi: 10.1016/j.epsl.2013.01.013.

Koschinsky, A., Hein J., R., 2003. Uptake of elements from seawater by ferromanganese crusts: solid-phase associations and seawater speciation. *Mar. Geol.* 198, 331–351.

Kosmulski, M., 2012. IEP as a parameter characterizing the pH-dependent surface charging of materials other than metal oxides. *Advances in Colloid and Interface Science* 171-172, 77-86.

Kulongoski, J., T., Hilton, D., Barry, P., B., Esser, B., J., Hillegonds, D., Belitz, K., 2013. Volatile fluxes through the Big Bend section of the San Andreas Fault, California: Helium and carbon-dioxide. *Chem. Geol.* 339, 92-102.

Lazar, M., Ben-Avraham, Z., Garfunkel, Z., 2012. The Red Sea–New insights from recent geophysical studies and the connection to the Dead Sea fault. *Journal of African Earth Sciences* 68, 96-110.

Lensky, N. G., Y. Dvorkin, V. Lyakhovsky, I. Gertman, and I. Gavrieli (2005), Water, salt, and energy balances of the Dead Sea, *Water Resour Res*, 41(12).

Lewis, A. J., Palmer, M. P., Sturchio, C., Kemp, A. J., 1997. The rare earth element geochemistry of acid sulphate and acid sulphate-chloride geothermal system from Yellowstone National Park, Wyoming, USA. *Geochim et Cosmochim. Acta* 61, 695-706.

Lewis, A., J., Komninou, A., Yardley, B., W., Palmer, M., R., 1998. Rare earth element speciation

in geothermal fluids from Yellowstone National Park, Wyoming, USA. *Geochim et Cosmochim. Acta* 62, 657–663.

Luo, Y.R., Byrne, R.H., 2004. Carbonate complexation of yttrium and the rare earth elements in natural waters. *Geochimica et Cosmochimica Acta* 68, 691-699.

Lustrino M., Wilson M., 2007. The circum-Mediterranean anorogenic Cenozoic igneous province. *Earth-Science Reviews* 81, 1-65.

Mahood, G.A. and Hildreth, W. (1986). Geology of the peralkaline volcano at Pantelleria, Strait of Sicily. *Bulletin of Volcanology* 48, 143-172.

Marty, B., Jambon, A., 1987. C^3He in volatile fluxes from the solid Earth: implications for carbon geodynamics. *Earth Planet. Sci. Lett.* 83, 16-26.

Mattia, M., Bonaccorso, A., Guglielmino, F., 2007 Ground deformations in the Island of Pantelleria (Italy): Insights into the dynamic of the current intereruptive period. *Journal of Geophysical Research* 112, 1-11.

McDonough W. F., and Sun S. S., 1995. The composition of the earth. *Chem. Geol.* 120, 223–253.

McKelvey B. A., Orians K. J., 1993. Dissolved zirconium in the North Pacific Ocean. *Geochimica et Cosmochimica Acta* 57, 3801-3805.

Mechie J., Ben-Avraham Z., Weber M. H., Götze H.J., Koulakov I., Mohsen A., 2013. The distribution of Moho depths beneath the Arabian plate and margins. *Tectonophysics* 609, 234-249.

Michard, A., 1989. Rare earth element systematics in hydrothermal fluids. *Geochim et Cosmochim. Acta* 53, 745–750.

Millero, F.J., 1992. Stability-Constants for the Formation of Rare-Earth Inorganic Complexes as a Function of Ionic-Strength. *Geochim Cosmochim Acta* 56, 3123-3132.

Moller, P., Rosenthal, E., Dulski, P., Geyer, S., Guttman, Y., 2003. Rare earths and yttrium hydrostratigraphy along the Lake Kinneret-Dead Sea-Arava transform fault, Israel and adjoining territories. *Applied Geochemistry* 18, 1613-1628.

Moller, P., Rosenthal E., Geyer S., Guttman J., Dulski, P., Rybakov, M., Zilberbrand, M., Jahnke, C., Flexer, A., 2007. Hydrochemical processes in the lower Jordan valley and in the Dead Sea area, *Chemical Geology* 239(1-2), 27-49.

Moller, P., Rosenthal, W., Geyer, A., Flexer, A., 2007. Chemical evolution of saline waters in the

Jordan-Dead Sea transform and in adjoining areas. *Int. J. Earth Sci.*, 96, 541-566.

Monroy-Guzman F., Trubert D., Brillard L., Hussonnois M., Constantinescu O. and Le Naour C., 2010. Anion Exchange Behaviour of Zr, Hf, Nb, Ta and Pa as Homologues of Rf and Db in Fluoride Medium. *J. Mex. Chem. Soc.*, 54(1), 24-33.

Mor, D., 1993. A time-table for the levant volcanic province, according to K-Ar dating in the golan heights, Israel. *Journal of African Earth Sciences (and the Middle East)*, 16, 223-234.

Mutlu H., Gülec N., Hilton D.R., 2008. Helium-carbon relationships in geothermal fluids of western Anatolia, Turkey. *Chem. Geol.* 247, 305-321.

Négre, Ph., Guerrot, C., Cocherie, A., Azaroual, A., Brash, M., Fouillac, Ch., 2000. Rare earth elements, neodymium and strontium isotopic systematics in mineral waters: evidence from the Massif Central, France. *Appl. Geochem.* 15, 1345–1367.

O'Nions, R.,K., and Oxburgh, E.,R., 1988. Helium, volatile fluxes and the development of continental crust. *Earth Planet. Sci. Lett.*, 90, 331-347.

Parello F, Allard P, D'Alessandro W, Federico C, Jean-Baptiste P, Catani O., 2000. Isotope geochemistry of Pantelleria volcanic fluids, Sicily Channel rift: a mantle volatile end-member for volcanism in southern Europe. *Earth Planet Sci Lett* 180, 325– 339

Parkhurst, D.L., Appelo, C.A.J., 2010. User's Guide to PHREEQC (Version 2.17.5)-A Computer program for Speciation, Batch- Reaction, One-Dimensional Transport and Inverse Geochemical Calculations. Available at: http://www.brr.cr.usgs.gov/projects/GWC_coupled/phreeqc/index.html.

Peiffer, L., Taran, Y. A., Lounejeva, E., Solís-Pichardo, E., Rouwet, D., Bernard-Romero, R.A. 2011. Tracing thermal aquifers of El Chichónn volcano-hydrothermal system (Mexico) with $^{87}\text{Sr}/^{86}\text{Sr}$, Ca/Sr and REE. *Journal of Volcanology and Geothermal Research* 205, 55-66.

Pershina V., Trubert D., Le Naour C. and Kratz J.V., 2002. Theoretical predictions of hydrolysis and complex formation of group-4 elements Zr, Hf and Rf in HF and HCl solutions. *Radiochim. Acta*, 90, 869–877.

Pik, R., Marty, B., 2009. Helium isotopic signature of modern and fossil fluids associated with the Corinth rift fault zone (Greece): Implication for fault connectivity in the lower crust. *Chem. Geol.* 266, pp. 67-65.

- Piper, D.Z., Bau, M., 2013. Normalized Rare Earth Elements in Water, Sediments, and Wine: Identifying Sources and Environmental Redox Conditions. *American Journal and Analytical Chemistry* 4, 69-83.
- Qu, C.L., Liu, G., Zhao, Y.F., 2009. Experimental study on the fractionation of yttrium from holmium during the coprecipitation with calcium carbonates in seawater solutions, *Geochem. J.* 43, 403–414.
- Raso, M., Censi, P., Saiano, F., 2013. Simultaneous determinations of zirconium, hafnium, yttrium and lanthanides in seawater according to a co-precipitation technique onto iron-hydroxide. *Talanta* 116, 1085-1090.
- Roded, R., Shalev, E., Katoshevski, D., 2013. Basal heat flow and hydrothermal regime at the Golan-Ajloun hydrological basins. *J. Hydrol.* 476, 200-211.
- Rouwet, D., Inguaggiato, S., Taran, Y., Varley, N., Santiago, J., A., 2008. Chemical and isotopic compositions of thermal springs, fumaroles and bubbling gases at Tacaná Volcano (Mexico–Guatemala): implications for volcanic surveillance. *Bull. Volcanol.* 71, 319-335.
- Rybakov, M., Segev, A., 2004. Top of the crystalline basement in the Levant. *Geochemistry Geophysics Geosystems* 5(9), 1-8.
- Sano, Y., Marty, B. 1995. Origin of carbon in fumarolic gas from island arcs. *Chem. Geol.* 119, 265-274.
- Sano, Y., Wakita, H., 1985. Geographical Distribution of $^3\text{He}/^4\text{He}$ Ratios in Japan: Implications on Arc Tectonics and Incipient Magmatism. *J. Geophys. Res.* 90, 8279-8741.
- Schmidt, K., Bau, M., Hein J. R., Koschinsky, A., 2014. Fractionation of the geochemical twins Zr-Hf and Nb-Ta during scavenging from seawater by hydrogenetic ferromanganese crusts. *Geochim et Cosmochim. Acta* 140, 468-487.
- Segev, A., Rybakov, M., Lyakhovsky, V., Hofstetter, A., Tibor, G., Goldshmidt, V., 2006. The structure, isostasy and gravity field of the Levant continental margin and the southeast Mediterranean area. *Tectonophysics* 425, 137-157.
- Seto, M., Tsaku, A., 2008. Chemical condition for the appearance of a negative Ce anomaly in stream waters and groundwaters. *Geochemical journal* 42, 371-38.
- Shalev, E., Levitte, D., Gabay, R., Zemach, E., 2008. Assessment of Geothermal Resources in Israel. GSI Rep. GSI/29/2008, Jerusalem, 1-23.

Shalev, E., Lyakhosky, V., Weinstein, Y., Ben-Avraham, Z., 2013. The thermal structure of Israel and Dead Sea Fault. *Tectonophysics* 602, 69-77.

Shannon, R.D., 1976. Revised effective ionic radii and systematic studies of interatomic distances in halides and chalcogenides. *Acta Cryst.*, A32:751–767.

Reisfeld, R. and Jorgensen, C.K., 1977. *Lasers and excited states of rare earths*, Springer-Verlag, Berlin, 226 pp.

Jofrgensen, C.K., 1979. Theoretical chemistry of rare earths. In *Handbook on the Physics And chemistry of Rare Earths*. vol. 3, (eds. Gschneidner, K. A. Jr. And L. Eyring), 111-169, North-Holland, Amsterdam.

Shaw, A., M., Hilton D., R., Fischer, T., P., Walker, J., A., Alvarado, G., E., 2003. Contrasting He-C relationship in Nicaragua and Costa Rica: insights into C cycling through subduction zones. *Earth Planet. Sci. Lett.* 214, 499-513.

Siebert C, Rosenthal E, Moller P, Rodiger T, Meiler M., 2012. The hydrochemical identification of groundwater flowing to the Bet She'an-Harod multiaquifer system (Lower Jordan Valley) by rare earth elements, yttrium, stable isotopes (H, O) and Tritium. *Applied Geochemistry* 27, 703-714.

Steinhorn, I., 1983. In situ salt precipitation at the Dead Sea. *Limnology & Oceanography* 28(3), 580-583.

Takano, B., Suzuki, K., Sugimori, K., Ohba, T., Fazlullin, S.M., Bernard, A., Sumarti, S., Sukhyar, R., Hirabayashi, M., 2004. Bathymetric and geochemical investigation of Kawah Ijen Crater Lake, East Java. Indonesia. *J. Volcanol. Geotherm. Res.* 135, 299–329.

Tanaka, K., Ohta, A., Kawabe, I., 2004. Experimental REE partitioning between calcite and aqueous solution at 25°C and 1 atm: Constraints on the incorporation of seawater REE into semount-type limestones. *Geochemical Journal* 38, 19-32.

Tanaka, K., Takahashi, Y., Shimizu, H., 2008. Local structure of Y and Ho in calcite and its relevance to Y fractionation from Ho in partitioning between calcite and aqueous solution. *Chemical Geology* 248, 104-113.

Taran, Y., Rouwet, D., Inguaggiato, S., Aiuppa, A., 2008. Major and trace element geochemistry of neutral and acidic thermal springs at El Chichón volcano, Mexico: implication for monitoring of the volcanic activity. *J. Volcanol. Geotherm. Res.* 178, 224-236

Taylor, S.R., and McLennan, S.M., 1995. *The geochemical evolution of the continental crust*,

Reviews of Geophysics 33(2), 241-265.

Thiagarajan, N., and Lee, C.T.A., 2004. Trace-element evidence for the origin of desert varnish by direct aqueous atmospheric deposition, *Earth and Planetary Science Letters* 224(1-2), 131-141.

Torfstein, A., Hammerschmidt, K., Friedrichsen, H., Starinsky, A., Garfunkel, Z., Kolodny, Y., 2013. Helium isotopes in Dead Sea Transform waters. *Chem. Geol.* 352, 188-201.

Toulkeridis, T., Podwojewski, P., Còauer, N., 1998. Tracing the source of gypsum in New Caledonia soils by REE contents and S-Sr isotopic composition.

Umeda, K., Sakagawa, Y., Ninomiya, A., Asamori, K., 2007. Relationship between helium isotopes and heat flux from hot springs in a non-volcanic region, Kii Peninsula, southwest Japan. *Geophys. Res. Lett.* doi:10.1029/2006GL028975.

Varekamp, J. C., 2015. The Chemical Composition and Evolution of Volcanic Lakes. In: Rouwet, D., Christenson, B., Tassi, F., Vandemeulebrouck, J. eds, *Volcanic Lakes*, 93-123.

Varekamp, J. C., Ouimette, A. P., Herman, S. W., Flynn, K. S., Bermudez, A., Delpino, D., 2009. Naturally acid waters from Copahue volcano, Argentina. *Applied Geochemistry* 24, 208-220.

Vergouw JM, Difeo A, Xu Z, Finch JA. An agglomeration study of sulphide minerals using zeta-potential and settling rate. Part I: Pyrite and galena. *Minerals Engineering* 1998; 11: 159-169.

Weinberger, R., Sneth, M., Harlavan, Y., 2003. The occurrence of Middle-Miocene volcanism at Mount Hermon, northern Israel. *Isr. J. Earth Sci.* 52, 179–184.

Weinstein R, Paldor N, Anati DA, Hecht A. 2000. Internal seiches in the strongly stratified Dead Sea. *Israel Journal of Earth Sciences* 49, 45-53.

Weinstein, Y., 2000. Spatial and temporal geochemical variability in basin-related volcanism, northern Israel. *Journal of African Earth Sciences* 30, 865-886.

White, J.C., Parker, D.F., Minghua, R., 2009. The origin of trachyte and pantellerite from Pantelleria, Italy: Insights from major element, trace element, and thermodynamic modelling. *Journal of Volcanology and Geothermal Research* 189, 33-55.

Wood, S. A., 1990. The aqueous geochemistry of the rare-earth elements and yttrium 1. Review of available low-temperature data for inorganic complexes and the inorganic REE speciation of natural waters. *Chem. Geol.* 82, 159-186.

Wood, S.A., 2003. *The geochemistry of Rare Earth Elements and Yttrium in Geothermal Waters.*

Society of Economic Geologists Special Publication 10, 133-158.

Wood, D.A., Gammons, C.H., Parker, S., R., 2006. The behavior of rare earth elements in naturally and anthropogenically acidified waters. *Journal of Alloys and Compounds* 418, 161-165.

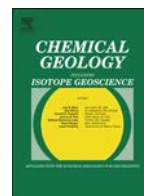
Yuce G., Italiano F., D'Alessandro W., Yalcin T.H., Yasin D.U., Gulbay A.H., Ozyurt N.N., Rojay B., Karabacak V., Bellomo S., Brusca L., Yang T., Fu C.C., Lai C.W., Ozacar, A., Walia, V., 2014. Origin and interactions of fluids circulating over the Amik Basin (Hatay-Turkey) and relationships with the hydrologic, geologic and tectonic settings. *Chem. Geol.* 388, 23-39.

Yui, M., Kikawada, Y., Oi, T., Nozaki, T., 1998. Abundance of lanthanoids in rock salts determined by neutron activation analysis. *Journal of radioanalytical and nuclear chemistry* 238(1), 3-6

Zak, I., *The Geology of Mt. Seom*. Hebrew University 1967. (Ph.D., in Hebrew, Engl. abstract).

Zhang J., Quay P. D., and Wilbur D. O., 1995. Carbon isotope fractionation during gas-water exchange and dissolution of CO₂. *Geochim. Cosmochim. Acta* 59, 107-114.

APPENDIX



Geochemistry of REE, Zr and Hf in a wide range of pH and water composition: The Nevado del Ruiz volcano-hydrothermal system (Colombia)



C. Inguaggiato^{a,b,d,*}, P. Censi^a, P. Zuddas^b, J.M. Londoño^c, Z. Chacón^c, D. Alzate^c, L. Brusca^d, W. D'Alessandro^d

^a Dipartimento di Scienze della Terra e del Mare, Università degli Studi di Palermo, Via Archirafi, 22, 90123 Palermo, Italy

^b UPMC-Sorbonne Universités, Institut des Sciences de la Terre de Paris, 4 place Jussieu, F75005 Paris, France

^c Servicio Geológico Colombiano, Observatorio Vulcanológico y Sismológico de Manizales, Avenida 12 de Octubre, 15–47 Manizales, Colombia

^d Istituto Nazionale di Geofisica e Vulcanologia, Sezione di Palermo, Via U. La Malfa, 153, 90146 Palermo, Italy

ARTICLE INFO

Article history:

Received 25 May 2015

Received in revised form 25 September 2015

Accepted 30 September 2015

Available online 3 October 2015

Keywords:

Zirconium

Hafnium

Rare earth elements

Ionic complexes

Acidic waters

Fe–Al oxyhydroxides

ABSTRACT

The geochemical behaviour of Rare Earth Elements, Zr and Hf was investigated in the thermal waters of Nevado del Ruiz volcano system. A wide range of pH, between 1.0 and 8.8, characterizes these fluids. The acidic waters are sulphate dominated with different Cl/SO₄ ratios. The important role of the pH and the ionic complexes for the distribution of REE, Zr and Hf in the aqueous phase was evidenced. The pH rules the precipitation of authigenic Fe and Al oxyhydroxides producing changes in REE, Zr, Hf amounts and strong anomalies of Cerium. The precipitation of alunite and jarosite removes LREE from the solution, changing the REE distribution in acidic waters. Y–Ho and Zr–Hf (twin pairs) have a different behaviour in strong acidic waters with respect to the water with pH near-neutral. Yttrium and Ho behave as Zr and Hf in waters with pH near neutral-to-neutral, showing superchondritic ratios. The twin pairs showed to be sensitive to the co-precipitation and/or adsorption onto the surface of authigenic particulate (Fe-, Al-oxyhydroxides), suggesting an enhanced scavenging of Ho and Hf with respect to Y and Zr, leading to superchondritic values. In acidic waters, a different behaviour of twin pairs occurs with chondritic Y/Ho ratios and sub-chondritic Zr/Hf ratios. For the first time, Zr and Hf were investigated in natural acidic fluids to understand the behaviour of these elements in extreme acidic conditions and different major anion chemistry. Zr/Hf molar ratio changes from 4.75 to 49.29 in water with pH < 3.6. In strong acidic waters the fractionation of Zr and Hf was recognized as function of major anion contents (Cl and SO₄), suggesting the formation of complexes leading to sub-chondritic Zr/Hf molar ratios.

© 2015 Elsevier B.V. All rights reserved.

1. Introduction

In the last 30 years, an extensive literature about the distribution of REE (lanthanides and yttrium) and the Y/Ho ratios during fractionation processes between different phases was developed (Bau, 1996, 1999; Bau and Dulski, 1999; Ruberti et al., 2002; Censi et al., 2007, 2014, 2015; Piper and Bau, 2013). The REE abundances provide insight into water–rock interaction processes. The REE geochemistry in geothermal fluids is complex and depends on the pH, the stability of solid phases, the concentrations of anionic ligands complexing the REE and adsorption of mineral surfaces (Wood, 1990, 2003; Lewis et al., 1997, 1998, and references therein; Gammons et al., 2005; Bao et al., 2008; Peiffer et al., 2011). The concentration of total dissolved REE in near neutral pH waters and in seawater is low and their dissolved species are dominated by carbonate complexes (Byrne, 2002), whereas in acidic waters

(pH < 3.6) carbonate and hydroxide can be considered negligible. The geothermal waters with very acidic pH values have higher contents of REE dissolved in waters up to 10⁴ times compared to seawater (Wood, 2003 and references therein). The REE contents of hydrothermal fluids usually increase with decreasing pH, independently from the temperature and the type of local rock (Michard, 1989). During the mixing between fluids discharged from the hydrothermal vent on the marine floor and seawater, the REE are scavenged by Fe and Mn oxyhydroxides (Bau and Dulski, 1999; Wood, 2003 and references therein). The geothermal systems are characterized by a wide variety of REE patterns; in particular the acid sulphate waters have high REE contents sometimes with Light Rare Earth Elements (LREE) depleted with respect to the local rock (Wood, 2003 and references therein).

Recent studies investigated isoivalent elements Zr–Hf, Y–Ho and their fractionation during processes involving solid phases. The Y–Ho and Zr–Hf are characterized by similar ionic radius and by the same charge +3 and +4 respectively. The twin pairs are characterized by negligible fractionation during processes occurring at high temperature in silicate melt and are controlled by charge and radius. A different

* Corresponding author at: Dipartimento di Scienze della Terra e del Mare, Università degli Studi di Palermo, Via Archirafi, 36, 90123 Palermo, Italy.

E-mail address: claudio.inguaggiato@unipa.it (C. Inguaggiato).

behaviour of Y–Ho and Zr–Hf was recognized in processes that take place in aqueous system, showing values which deviate from the chondritic ratio, due to fractionation processes ruled by the electronic configurations of elements (Bau, 1996). In seawater, continental is the main source of Zr–Hf, showing a larger removal of Hf with respect to Zr, due to the different sorption of these elements onto Fe and/or Mn oxyhydroxides (Godfrey et al., 1996; Godfrey and Field, 2008; Firdaus et al., 2011; Frank, 2011; Censi et al., 2015; Schmidt et al., 2014). Moreover, Zr and Hf form complexes with hydroxyl groups in waters with pH from near neutral to neutral (Byrne, 2002). However, the fractionation of these elements has never been studied in extreme acidic environments.

In this research we investigate the behaviour of REE, Zr and Hf in waters circulating within the Nevado del Ruiz (NDR) volcano–hydrothermal system. This natural system is considered a laboratory for better understanding of the processes involving these elements within a wide spectrum of pH values and chemical composition of waters.

2. Geo-lithologic aspects

Nevado del Ruiz is one of the active volcanoes belonging to the great chain of the Andes (located a few km west of Bogota), connected with the active subduction of Nazca Plate below the South American plate. The last plinian eruption occurred in 1985, generating a huge lahar that buried Armero town killing approximately 23,000 people. The NDR volcano is a large edifice mainly constructed during three major phases over the past 600 to 1200 ka, with a summit elevation of 5389 m (Forero et al., 2011 and references therein). The volcanic complex is mainly built by andesitic lava, whereas pyroclastic deposits belonging to the last eruptive phase overlay the lava flows. This volcanic system is characterized by calc-alkaline rocks ranging from andesitic to dacitic in composition with quite constant distribution of REE, Zr and Hf in different magmatic suites (Borrero et al., 2009). Fig. 1 shows the REE distribution of average local rock normalized to chondrite, displaying a decreasing pattern from La to Lu and lack of a significant Eu anomaly (Borrero et al., 2009 and reference therein). Borrero et al. do not show different trends for a range of magmatic suites, affirming that the evolution of magma is mainly controlled by the fractional crystallization.

The NDR rocks have quite constant Y/Ho and Zr/Hf molar ratios of 58.3 and 66.8 respectively (Borrero et al., 2009 and reference therein), falling in the field of processes controlled mainly by charge and radius (Bau, 1996).

3. Materials and methods

Hot and cold waters were collected in the area close to NDR volcano (Fig. 2). Temperature, pH, Eh and electrical conductivity of waters were measured in the field with an ORION 250+. The sample waters collected to determine major cations and trace elements were filtered through

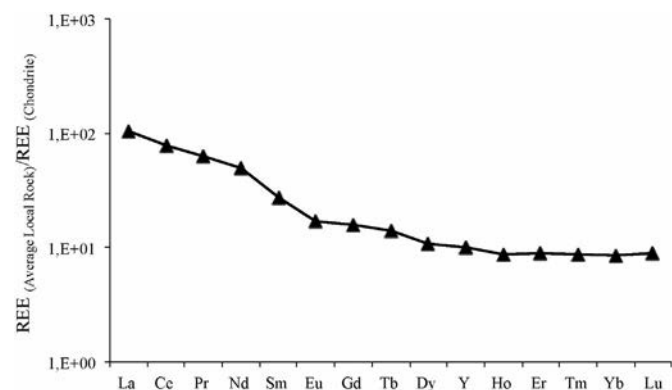


Fig. 1. Chondrite-normalized REE patterns in average local rock.

0.45 µm MILIPORE cellulose acetate filters into 250 ml Nalgene bottles and acidified in the field with ultrapure HNO₃. The sample waters to determine major anions were filtered with 0.45 µm filters in the field into LDPE plastic bottle. The major elements were analysed by Dionex ICS 1100 chromatograph. A Dionex CS-12A column was used for cations (Na, K, Mg and Ca) and a Dionex AS14A column for anions (F, Cl, and SO₄). Alkalinity was determined in the field by titration with HCl 0.1 M.

Trace elements, including also REE, Zr and Hf, were analysed by Q-ICP-MS (Agilent 7500ce) equipped with a Micromist nebulizer, a Scott double pass spray chamber, a three-channel peristaltic pump, an auto sampler (ASX-500, Cetac) and a Octopole Reaction System (ORS) for removing interferences of polyatomic masses and isobaric isotopes. The mass spectrometer was calibrated with a multi-element standard solution, daily prepared and diluted 10 times to obtain a curve with 11 calibration points. The sensitivity variations were monitored using ¹⁰³Rh, ¹¹⁵In, and ¹⁸⁵Re at a final concentration of 8 µg/l for each as internal standards added directly online by an appropriate device that mixes an internal standard solution to the sample just before the nebulizer. Sixty second rinse using 0.5% HCl and 2% of HNO₃ solution plus 60-s rinse using 2% of HNO₃ solution reduced memory interferences between samples. The precision of analysis was checked by running 5 replicates of every standard and sample, it was always within ± 10%. Data accuracy was evaluated analysing standard reference materials (Spectrapure Standards SW1 and 2, SLRS4, NIST 1643e, Environment Canada TM 24.3 and TM 61.2) for each analytical session and error for each element was < 15%. Fe, Al with high concentrations (> 1 mg/l) and Si were analysed by ICP-OES Horiba Ultima 2 at wavelength of 259.940 nm, 396.152 nm and 251.611 nm respectively.

The saturation indexes (SI) of solid phases and ion speciation were calculated using Phreeqc software package (version 3.0.6; Parkhurst and Appelo, 2010). The simulations were carried out using the database LLNL at the chemical–physical conditions measured in the field.

Scanning Electronic Microscopy (SEM) observations and Energy Dispersive X-ray Spectra (EDS) were carried out on the suspended particulate matter (SPM) collected during the filtration from the investigated waters, in order to get information about the nature of suspended solids. The filters with the SPM were assembled on the aluminium stub and coated with gold. The analysis were performed with LEO 440 SEM equipped with an EDS system OXFORD ISIS Link and Si (Li) PENTAFET.

Anomalies of Cerium and Europium in waters were calculated with respect to the neighbouring elements normalized to the average local rock, using the equation proposed by Alibo and Nozaki (1999):

$$\text{REE}_n/\text{REE}_{n^*} = 2 * (\text{REE})_n / [(\text{REE})_{n-1} + (\text{REE})_{n+1}]$$

(REE)_n is the concentration of the element chosen to calculate the anomaly, while (REE)_{n-1} and (REE)_{n+1} represent the previous and the subsequent element along the REE series, respectively.

4. Results

4.1. General aspects

NDR waters cover a wide spectrum of pH, ranging from 1 to 8.8. Temperature ranges from 6.8 to 79.5 °C, electrical conductivity values span from 0.2 to 33.5 mS/cm and Eh values range between – 31 and + 325.4 mV (Table 1). The acidity recorded in the investigated waters is due to the interaction of magmatic gases, such as HCl, SO₂, and their dissolution and dissociation in groundwater (e.g., Giggerbach et al., 1990). According to the pH, the waters were classified into two groups: Group 1 (near neutral-to-neutral) is characterized by pH values ranging between 5.9 and 8.8, Group 2 (acidic) has pH values between 1.0 and 3.6. Considering the major anion contents, the groups were further subdivided. Group 1a with the highest amount in HCO₃, Group 1b with chloride dominant composition. The fluids belonging to Group 2 are acid sulphate waters with composition plotting near the SO₄ corner

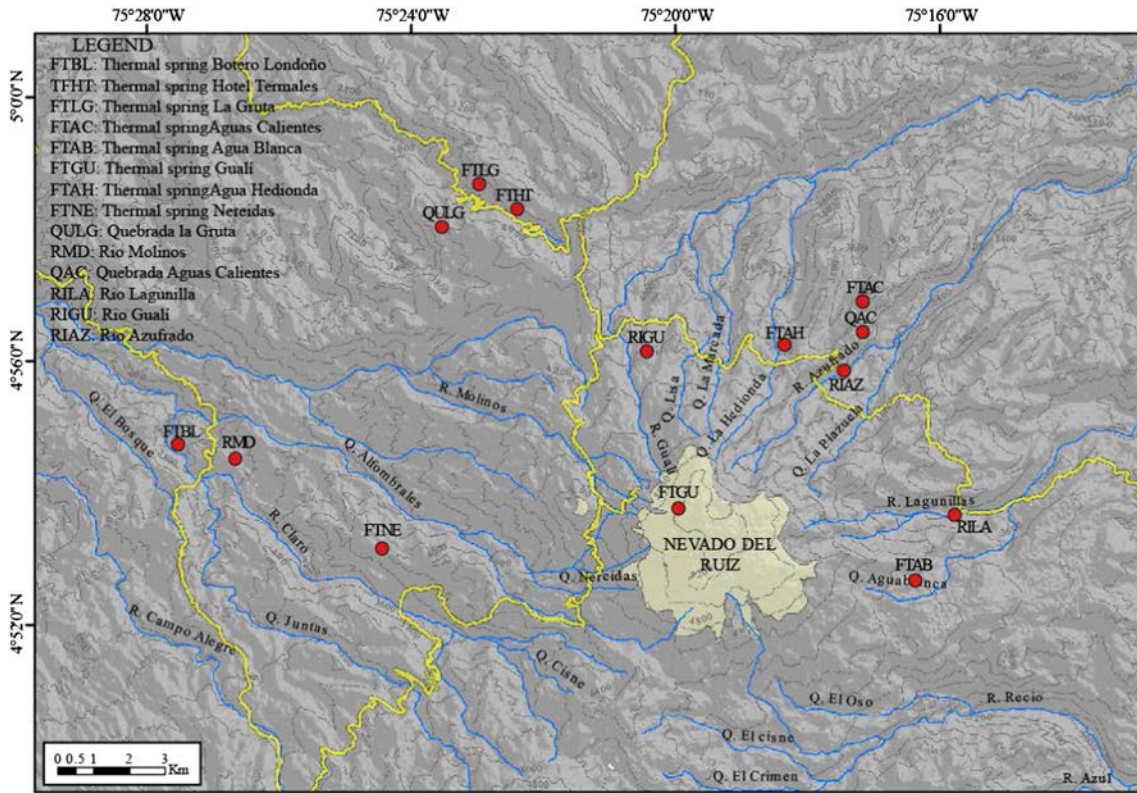


Fig. 2. Location map of sampled waters.

in the ternary anion diagram (Fig. 3). The latter group can be subdivided according to the Cl content: Group 2a with lower Cl/SO₄ ratios (<0.13) and Group 2b with higher Cl/SO₄ ratios (>0.32).

Fe and Al contents are several orders of magnitude higher (up to 4.14 and 30.23 mmol/l respectively) in Group 2 compared to Group 1 (up to 2.85 * 10⁻⁴ and 5.44 * 10⁻⁴ mmol/l respectively). The water groups have different mineral saturation state (Table 2). Group 1 waters are oversaturated with respect to iron and aluminium oxyhydroxides, while the waters of Group 2 are undersaturated with respect to those minerals. SEM-EDS analyses of SPM show amorphous silica in all the investigated waters, sometimes silica sphere probably encrusting organic matter (Fig. 4b). Moreover, different solid phases were found in the groups of waters classified previously: in Group 1a Fe-, Al-oxyhydroxides encrusting amorphous silica are present (Fig. 4a); in Group 2a waters Fe–Al–Ca solid phases (probably sulphates) onto amorphous silica are recognized (Fig. 4c; d).

The isosol diagram (log-log compositional plot) was used to evaluate the degree of rock dissolution. This diagram allows to evaluate if the chemical composition of waters is a reflection of the rocks (near-congruent dissolution, under hyperacid conditions) and the possible removal of elements by precipitation of secondary minerals (Taran et al., 2008; Colvin et al., 2013; Varekamp, 2015 and references therein). The hyperacid waters of Group 2 fall between the isosol lines indicating the dissolution of about 5 to 10 g of rock (Fig. 5). The Group 2b waters show to be close to congruent dissolution of the average local rock, for all elements with the exception of Si that is depleted in all samples (Fig. 5), probably due to the precipitation of silica minerals. The major elements of Group 2a deviate from the isosol line, with the exception of Mg and Ca that fall close to the 5–10 g of rock dissolution line (Fig. 5). Strong depletions of Fe, Al, K and minor depletion of Na (Fig. 5) suggest the precipitation of alunite [(K,Na)Al₃(SO₄)₂(OH)₆] and jarosite [(K, Na)Fe₃(SO₄)₂(OH)₆], typical minerals precipitating in

Table 1
Chemical composition of the studied waters expressed in mmol/l.

Group	Sample name	T (°C)	pH	Cond (mS/cm)	Eh (mV)	Na	K	Mg	Ca	F	Cl	SO ₄	HCO ₃	Al	Fe	Si
Group 1	Agua Hedionda	13.9	5.9	0.4	170	0.48	0.07	1.07	0.76	0.01	0.05	1.01	2.30	0.0007	0.0005	1.64
	Rio Molinos	15.9	8.8	0.5	–	2.04	0.20	0.62	1.43	0.02	1.43	1.80	1.20	0.0005	0.0003	1.15
	Nereidas	50.4	6.1	2.0	96	5.35	0.45	1.95	3.25	0.00	0.62	3.10	9.40	0.0008	0.0004	3.06
	Botero Londono	79.5	7.7	6.8	–31	27.06	2.10	0.26	1.20	0.10	28.4	0.68	1.40	0.0353	0.0098	2.78
Group 2	Termal La Gruta	33.5	1.6	8.7	236	14.06	1.41	5.90	4.42	1.47	14.5	36.9	–	11.09	0.53	2.94
	Hotel 1	59.8	1.4	17.0	271	20.93	1.79	9.23	6.03	2.09	20.8	52.1	–	12.00	1.28	3.67
	Hotel 2	62.6	1.4	10.3	115	21.47	1.93	9.72	6.39	2.07	21.9	56.2	–	12.41	1.30	3.75
	Agua caliente	59.3	1.0	33.3	325	14.99	5.78	7.76	6.15	3.10	35.7	110.2	–	30.23	4.14	2.58
	Quebrada La Gruta	15.3	2.1	3.0	207	4.76	0.86	2.08	1.52	0.55	4.93	12.6	–	3.13	0.28	1.53
	Agua Blanca	29.1	3.3	2.5	205	1.81	0.26	2.16	10.38	0.22	1.39	16.1	–	1.86	0.27	2.03
	Rio Lagunillas	6.8	3.6	0.2	171	0.16	0.03	0.28	0.41	0.01	0.09	1.40	–	0.26	0.07	0.55
	Rio Guali	7.2	3.5	1.2	–	1.06	0.16	1.23	2.68	0.13	0.76	5.77	–	0.83	0.14	1.64
	Rio Azufrado	16.0	3.4	1.8	190	4.59	0.39	4.63	6.62	0.19	1.54	16.1	–	1.50	0.35	2.56
	FT Gauli	59.2	2.8	3.5	246	1.81	0.28	2.89	8.67	0.31	1.30	15.7	–	1.78	0.02	3.25

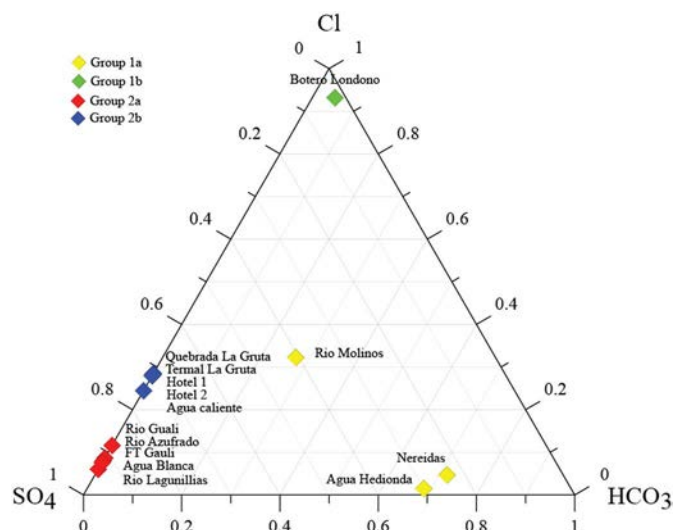


Fig. 3. Triangular plot of major anions dissolved in water.

hyperacid hydrothermal systems (Taran et al., 2008; Varekamp et al., 2009; Colvin et al., 2013). The waters of Group 1 don't reflect the composition of the average local rock, showing the strong depletions in Fe and Al (Fig. 5), particularly in Group 1a waters, where the near-neutral pH allows the precipitation of iron and aluminium oxyhydroxides.

4.2. REE, Zr and Hf

The total amount of REE in NDR waters ranges between 0.8 and 6722 nmol/l (Table 3). We found an inverse correlation between the total amount of REE and pH values (Fig. 6): higher REE contents are recognized in Group 2 (lower pH values) with respect to Group 1 (higher pH values). Great differences in Σ REE are found between the subgroups 1a and 1b with Botero Londono sample (Group 1b) displaying a higher value with respect to the waters of Group 1a (Fig. 6). The correlation between Σ REE and pH values suggests that rock dissolution is occurring more completely under acidic conditions, particularly Group 2b waters showing near-congruent dissolution of up to 10 g of rock per litre (Fig. 5).

Considering the constant distribution of REE in the magmatic rocks of NDR, the studied waters were normalized to the average local rock (Borrero et al., 2009 and reference therein) evaluating processes of water–rock interaction in the hydrothermal system. The rock normalized REE patterns differ among the various water groups (Fig. 7). Group 1a shows patterns increasing from La to Lu, a positive Eu anomaly and negative Ce anomaly (Fig. 7). The Botero Londono water (Group 1b)

shows a slight decrease from La to Lu (Fig. 7). The Group 2b waters show a flat pattern, whereas the waters of Group 2a are characterized by anomalous shape of pattern strongly depleted in LREE compared to the Middle Rare Earth Elements (MREE) and Heavy Rare Earth Elements (HREE) (Fig. 7).

The amount of Y and Ho dissolved in waters ranges from 0.17 to 914 nmol l⁻¹ and from 0.003 to 17.7 nmol l⁻¹ respectively. Y/Ho molar ratios range between 47.8 and 127, with values changing from chondritic to superchondritic in acidic waters and in near-neutral waters respectively (Fig. 8).

The Zr concentration ranges from 0.48 to 35.1 nmol l⁻¹ with Hf from 0.007 to 0.90 nmol l⁻¹. Zr/Hf molar ratios are within the range between 4.7 and 104, showing sub-chondritic values in acidic waters and superchondritic values in near-neutral waters (Fig. 8). Y/Ho and Zr/Hf ratios show simultaneous changes in the waters of Group 1, whereas a different behaviour was recognized in acidic waters of Group 2 (Fig. 8).

5. Discussion

5.1. REE behaviour

The compositional variation of REE is mainly due to 4 processes: (i) the composition of the rocks interacting with water (dissolution of glass and minerals), (ii) the anionic composition of the waters determining the different complexation of REE, (iii) the incorporation into secondary minerals as function of the chemical-physical property of the waters and (iv) adsorption processes onto newly formed phases at higher pH (oxyhydroxide of Fe, Al, and Mn).

In NDR waters, the REE are strongly released by the rocks into acidic waters (Group 2). The pH controls the precipitation of new solid phases, inducing sorption and desorption of REE. The significant positive correlations between the total amount of REE and Fe or Al dissolved in waters (Fig. 9) shows the simultaneous variation of these elements, with the involvement of Fe and Al controlling the abundance of REE dissolved in water. Strong processes of scavenging occur during the co-precipitation and/or adsorption onto the surface of oxide and oxyhydroxide of Fe, Al, and Mn (Censi et al., 2007; Bau and Koschinsky, 2009).

REE-complexes play a role together with other geochemical processes during the fractionation of REE (Lewis et al., 1998). The very low pH of the studied waters (Group 2) suggests that all the inorganic carbon dissolved occurs mainly as dissolved CO₂; consequently, carbonate complexes are negligible in these acidic solutions. However, [REE(CO₃)⁺] and [REE(CO₃)₂⁻] play a role in the waters belonging to Group 1, as they are the only ones with higher amount of carbonate species (HCO₃⁻ and/or CO₃²⁻) dissolved in solution. The assessment of water–rock interaction processes is evaluated by the patterns of REE dissolved in waters normalized to the average local rock (Fig. 7).

In the acidic solutions of Group 2, the speciation of REE is ruled by complexes with SO₄²⁻, F⁻ and Cl⁻, according to the relative abundance of anions dissolved in waters (Lewis et al., 1998). The Group 2b is the only one with flat patterns suggesting that source rocks mainly control the REE distribution, without processes changing the REE distribution in waters (Fig. 8). In Group 2a, the REE-patterns normalized to average local rock (Fig. 8) are characterized by strong LREE depletion. A similar shape of pattern with LREE depletion was already observed in other acid-sulphate waters from Waitapu (New Zealand), Copahue volcano (Argentina), Santa Ana (El Salvador), Kawah Ithen Crater Lake (Indonesia) and Kutomintar and Sinarka volcanoes (Kawah Ijen) (Takano et al., 2004; Wood et al., 2006; Varekamp et al., 2009; Colvin et al., 2013; Kalacheva et al., 2015). Strong REE fractionation occurs during the hydrothermal alteration in very low pH waters with high SO₄²⁻ contents, showing higher LREE contents in alunitic advanced argillic altered rocks compared to the unaltered volcanic rocks (Hikov, 2011). The alteration minerals play an important role taking up the REE from the aqueous solution and/or releasing the elements, as a function of the chemical physical condition of the system that determines

Table 2
Saturation indexes of studied waters.

Group	Sample Name	Goethite FeOOH	Hematite Fe ₂ O ₃	Gibbsite Al(OH) ₃	Boehmite AlO(OH)
Group 1	Agua Hedionda	0.02	0.99	0.80	0.92
	Rio Molinos	3.66	8.27	0.48	0.61
	Nereidas	0.14	1.38	1.59	1.91
	Botero Londono	5.90	13.0	0.89	1.32
	Termal La Gruta	-6.57	-12.2	-3.97	-3.76
Group 2	Hotel 1	-7.07	-13.0	-4.62	-4.26
	Hotel 2	-6.22	-11.3	-4.60	-6.22
	Agua caliente	-7.04	-12.9	-5.50	-5.14
	Quebrada La Gruta	-8.25	-15.6	-5.83	-5.70
	Agua Blanca	-6.57	-12.2	-3.97	-3.76
	Rio Lagunillas	-5.08	-9.20	-2.24	-2.18
	Rio Guali	-6.87	-12.8	-4.64	-4.57
	Rio Azufrado	-7.69	-14.4	-5.26	-5.13
	FT Guali	-8.83	-16.5	-4.83	-4.47

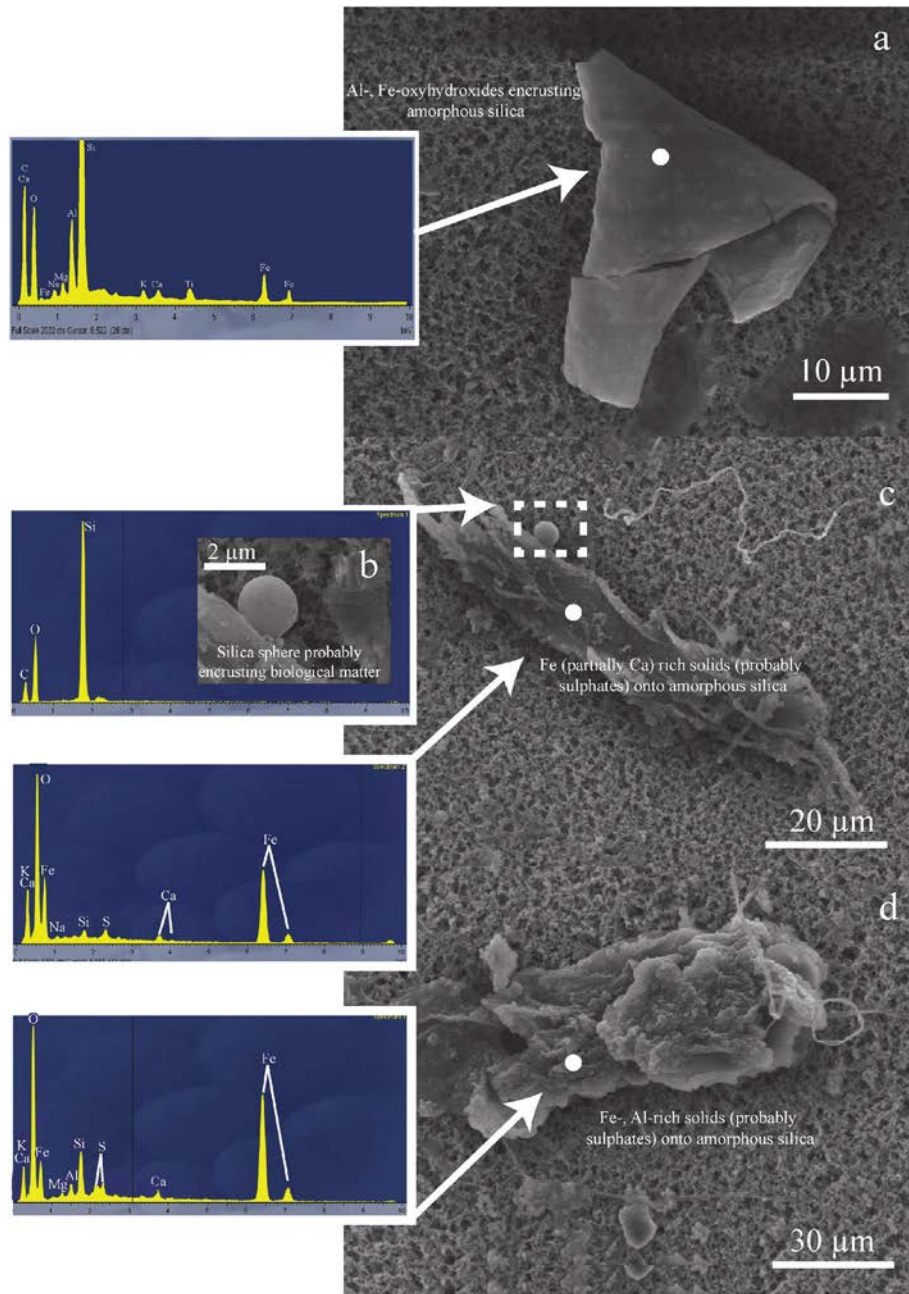


Fig. 4. SEM-EDS observations of SPM showing: in Group 1a Al-, Fe- oxhydroxides encrusting amorphous silica (a); in Group 2a, silica sphere probably encrusting biological matter (b), Fe (partially Ca) rich solids (probably sulphates) onto amorphous silica (c), Fe-, Al-, rich solids.

the stability of the solid phases. In particular, the precipitation of alunite–jarosite, was considered responsible of the LREE depletion in the acid–sulphate waters being the solid phases enriched in LREE (Ayers, 2012; Varekamp, 2015 and references therein). In the isosol diagram, Group 2a waters show depletions in K, Fe, Al, and Na pointing to alunite and jarosite precipitation (Fig. 5). Moreover, Al- and Fe-sulphates were found by SEM-EDS analysis as SPM (Fig. 4c, d). Coupling these information about the chemical propriety of waters and the nature of SPM, the depletion of LREE Group 2a, can be justified by the precipitation of Al- and Fe-sulphates as alunite and jarosite.

REE-patterns (Group 1a) normalized to average local rocks (Fig. 8) show a progressive increase from La to Lu according to the stability constant of $[\text{REE}(\text{CO}_3)]^+$ characterized by a progressive increase along the REE series (Wood, 1990; Millero, 1992). Botero Londono (Group 1b) is the only water with chloride-dominated composition. Considering the stability constant of $[\text{REECl}]^{2+}$ (Wood, 1990), the different patterns

(Botero Londono) compared to other groups of samples is due to REE-chloride complex stability constant, characterized by the same trend recognized for Botero Londono with a slight pattern decreasing along the REE series.

The precipitation of solid phases involving Fe and Al at circum-neutral pH conditions changes the abundance and the distribution of REE in water. Cerium and Europium differ from the other REE for being redox sensitive elements. Cerium is removed from waters during neutralization as CeO_2 and/or from precipitation of Fe, Mn and Al oxyhydroxides in river waters and marine environment (Goldstein and Jacobsen, 1988; Elderfield et al., 1990; Seto and Tsaku, 2008). The Ce and Eu anomalies vary with pH (Fig. 10). In particular, the waters with $\text{pH} < 3.6$ (Group 2) have no significant Ce and Eu anomalies, whereas the waters with $\text{pH} > 5.9$ (except Botero Londono sample) show strong negative anomalies of Ce and strong positive anomalies of Eu. The Ce anomaly can be explained considering the enhanced

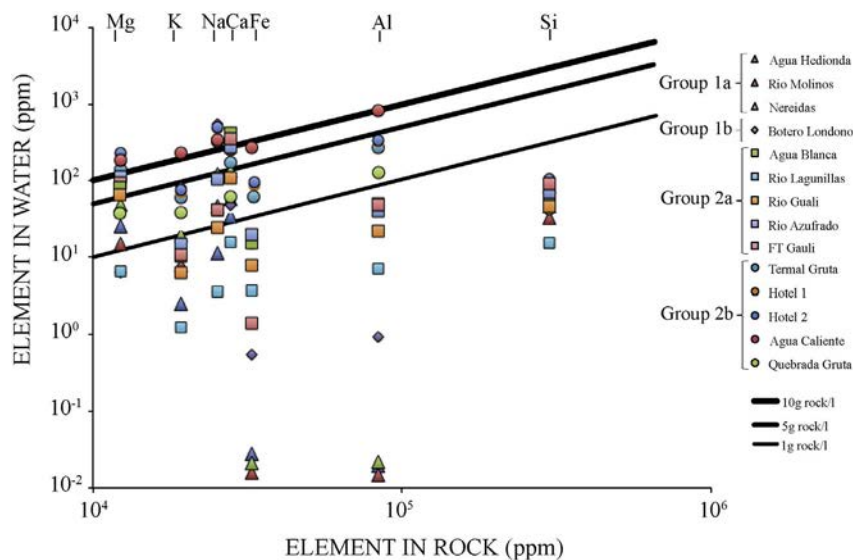


Fig. 5. Isosol diagram is a log-log compositional plot, with the average volcanic rock composition versus the water composition. Isosol lines represent the equal amount of rock dissolved for the element considered. The plot shows the near-congruent dissolution of Group 2b (acid waters) and the depletion in K, Na, Fe, Al, in Group 2a (acid waters). The Group 2 shows a rock dissolution ranging between 5 and 10 g/l. Group 1 (near-neutral pH) is strongly depleted in Fe, Al reflecting the precipitation of Fe, Al- oxyhydroxides. (probably sulphates) onto amorphous silica (d).

removal of Ce with respect to La and Pr, during the processes of coprecipitation and/or adsorption onto the surface of authigenic minerals (Al-, Fe oxyhydroxides).

Ce has a different behaviour in Botero Londono sample compared to the other samples of Group 1, not showing strong Cerium anomaly (Fig. 10a). The main differences of Botero Londono water compared to the other waters belonging of Group 1 are the higher ionic strength and the lower Eh value. These differences could limit the precipitation of Al-, Fe-oxyhydroxide allowing higher amounts of Al and Fe dissolved in water. Moreover, SEM-EDS observations of SPM (Botero Londono) do not show the presence of Al-, Fe-oxyhydroxide solid phases.

Almost all the investigated waters are characterized by a small anomaly of Europium (Fig. 10b), except for the waters of Group 1 where a strong positive anomaly (1.22–7.43) occurs, suggesting additional processes that fractionate the REE. The strong positive Eu anomaly found in the water of Group 1a could be justified by the slow interaction of waters with Eu enriched plagioclase, as already recognized in other hydrothermal systems (Wood, 2003 and references therein; Varekamp et al., 2009; Peiffer et al., 2011).

5.2. The behaviour of twin pairs (Y-Ho; Zr-Hf)

The decoupling of Y–Ho and Zr–Hf in seawater indicated that these elements are not controlled only by charge and ionic radius (Bau,

1996; Godfrey et al., 1996). The behaviour of Zr and Hf in natural waters is limited to the neutral-basic environments (mainly sea water), where super-chondritic Zr/Hf ratio was recognized (Firdaus et al., 2011; Schmidt et al., 2014). The inorganic speciation of Zr and Hf in water with circum-neutral pH is dominated by hydroxyl groups ($Zr(OH)_5^-$, $Hf(OH)_5^-$, $Zr(OH)_4$, $Hf(OH)_4$), whereas Y and Ho are mainly complexed by carbonate species (Byrne, 2002). The different charge of metal complexes determines the adsorption behaviour onto the solid surfaces (Koschinsky and Hein, 2003). Bau and Koschinsky (2009) show that the Y/Ho ratio in marine Fe–Mn hydroxydes is significantly lower than seawater, suggesting an enhanced scavenging of Ho with respect to Y in the Fe–Mn crusts. Recently, Schmidt et al. (2014) investigating the fractionation of Zr–Hf between seawater and Fe–Mn crusts, showed that Zr/Hf ratio is lower in the Fe–Mn oxyhydroxides compared to seawater. These studies indicate that both Hf and Ho are more easily removed than Zr and Y during the formation of marine Fe–Mn oxyhydroxides and that the geochemical behaviour of these twin pairs is not simply ruled by charge and ionic radius.

The near neutral-to-neutral waters of Group 1 have higher values of Y/Ho and Zr/Hf ratios with respect to the acidic waters and the average local rock (Fig. 8). The twin pairs' fractionation in Group 1 is due to the formation of the observed authigenic solid phases (Fe-, Al-oxyhydroxides) stable at neutral pH. The preferential removal of Ho and Hf with respect to Y and Zr is attributed to the enhanced scavenging

Table 3
REE, Zr and Hf dissolved in waters expressed in nmol/l.

Group	Sample	Y	La	Ce	Pr	Nd	Sm	Eu	Gd	Tb	Dy	Ho	Er	Tm	Yb	Lu	Zr	Hf
Group 1	Agua Hedionda	0.52	0.04	0.07	0.013	0.051	0.005	0.017	0.020	0.002	0.025	0.007	0.017	0.005	0.034	0.008	1.30	0.013
	Rio Molinos	0.17	0.02	0.008	0.006	0.029	0.007	0.017	0.009	0.002	0.014	0.003	0.01	0.003	0.008	0.003	5.31	0.057
	Nereidas	1.13	0.04	0.07	0.012	0.074	0.015	0.037	0.045	0.005	0.042	0.009	0.03	0.008	0.054	0.012	0.70	0.007
	Botero Londono	5.24	11.1	19.2	1.85	5.95	0.99	0.31	0.89	0.11	0.48	0.09	0.25	0.04	0.21	0.03	2.21	0.03
	Termal Gruta	642	512	1102	142	545	103	24.5	89.23	11.8	58.8	11.6	32.3	4.36	26.8	3.96	21.7	0.46
	Hotel 1	465	560	1034	119	429	77.9	19.6	71.30	9.07	46.5	9.39	25.8	3.52	21.6	3.16	8.52	0.24
	Hotel 2	483	565	1050	121	439	79.2	20.0	70.37	9.15	47.2	9.57	26.4	3.70	22.3	3.19	14.7	0.33
	Agua Caliente	914	1419	2575	269	944	177	43.8	153	19.1	91.7	17.7	47.6	6.45	38.3	5.62	35.1	0.90
	Quebrada Gruta	147	145	303	35.2	131	24.7	5.89	21.3	2.74	14.3	2.75	8.50	1.04	6.41	0.95	27.7	0.56
	Agua Blanca	629	20.4	108	22.8	177	63.6	19.0	81.6	12.83	64.6	11.7	28.4	3.26	17.5	2.34	3.01	0.28
Group 2	Rio Lagunillas	49.7	9.38	28.5	4.81	23.5	6.01	1.17	7.00	1.02	5.04	1.04	2.59	0.35	1.93	0.30	0.48	0.10
	Rio Guali	204	22.2	65.5	12.0	66.2	20.6	4.25	24.9	3.56	19.3	3.90	10.3	1.29	7.53	1.06	2.17	0.10
	Rio Azufrado	565	8.88	42.6	10.1	94.9	49.6	13.4	65.2	9.83	52.1	10.4	27.4	3.52	20.5	2.99	3.65	0.24
	FT Gauli	599	9.60	47.9	11.0	99.7	39.7	9.61	55.8	9.09	50.6	10.70	28.2	3.72	21.3	3.12	0.74	0.09

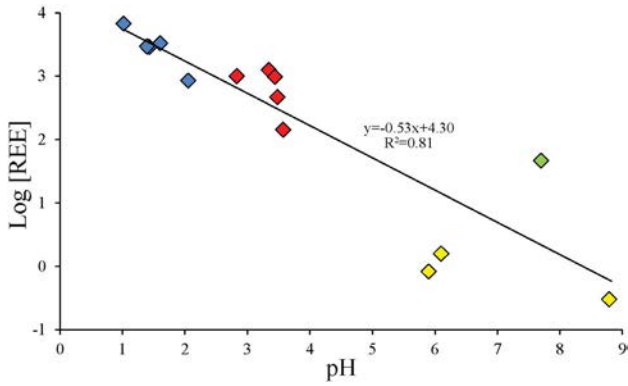


Fig. 6. Variations of total REE dissolved in water as a function of pH. Symbols as in Fig. 3.

during the co-precipitation onto the surfaces of Fe, Al oxyhydroxides (Bau, 1999; Bau and Dulski, 1999; Bao et al., 2008; Censi et al., 2007; Feng, 2010; Schmidt et al., 2014). However, in Botero Londono water (Group 1b), Y–Ho and Zr–Hf do not significantly fractionate and Ce anomaly is negligible (Fig. 10a), in agreement with the limited Fe, Al oxyhydroxide formation. Our data show that Y–Ho and Zr–Hf are removed from the hydrothermal system by Fe-, Al-oxyhydroxides precipitating in water with circum-neutral pH.

In Group 2 (acidic waters), Y–Ho and Zr–Hf twin pairs are characterized by a different behaviour. Y/Ho ratios are close to the average local rock, showing the negligible fractionation of these isovalent elements, while Zr/Hf ratios are sub-chondritic. The behaviour of Zr and Hf in extreme acidic environments has not been studied yet. Only few studies were carried out on the speciation of Zr and Hf with fluoride and chloride ligands, but not in water with very high sulphate contents (Pershina et al., 2002; Monroy-Guzman et al., 2010). Molecular dynamic calculation (Pershina et al., 2002) indicated that in chloride media, chloride complexes are enhanced for Hf with respect to Zr, independently of pH. In Group 2 waters Zr and Hf are decoupled indicating

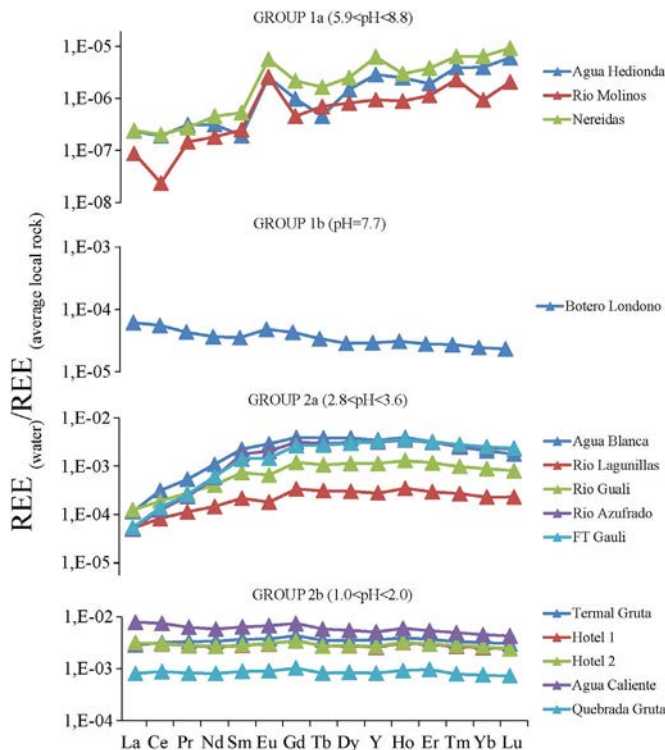


Fig. 7. Average local rock-normalized REE patterns dissolved in water.

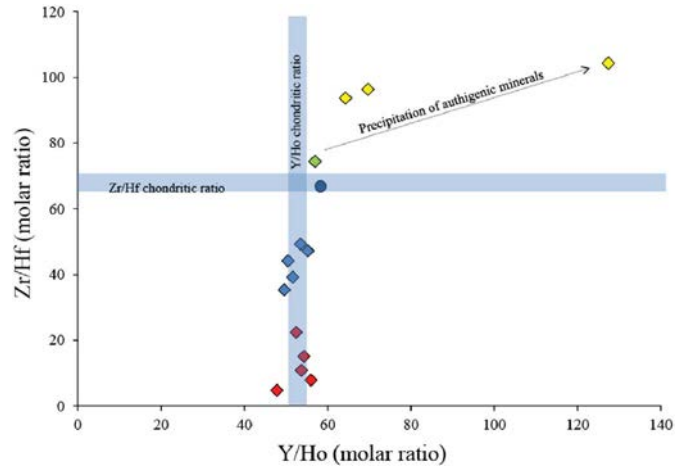


Fig. 8. Zr/Hf and Y/Ho (molar ratios). Symbols as in Fig. 3, blue circle represent Y/Ho and Zr/Hf (molar ratios) in average local rock. (For interpretation of the references to color in this figure legend, the reader is referred to the web version of this article.)

that the geochemical twin is not controlled only by ionic radius and charge. Fig. 11 show that Zr/Hf ratio increases as Cl/SO₄ ratio increases highlighting a different behaviour of isovalent elements as a function of anion contents (Cl and SO₄). The Zr–Hf fractionation observed in this acidic environment may result from different stability constants of Zr and Hf complexes with Cl and SO₄ ligands that in turn determine the relative abundance of these metals in hyper-acid waters.

6. Concluding remarks

The thermal fluids circulating in NDR system have a variety of major chemical composition and cover a wide range of pH values from 1 to 8.8. The concentrations of REE and their patterns normalized to the average

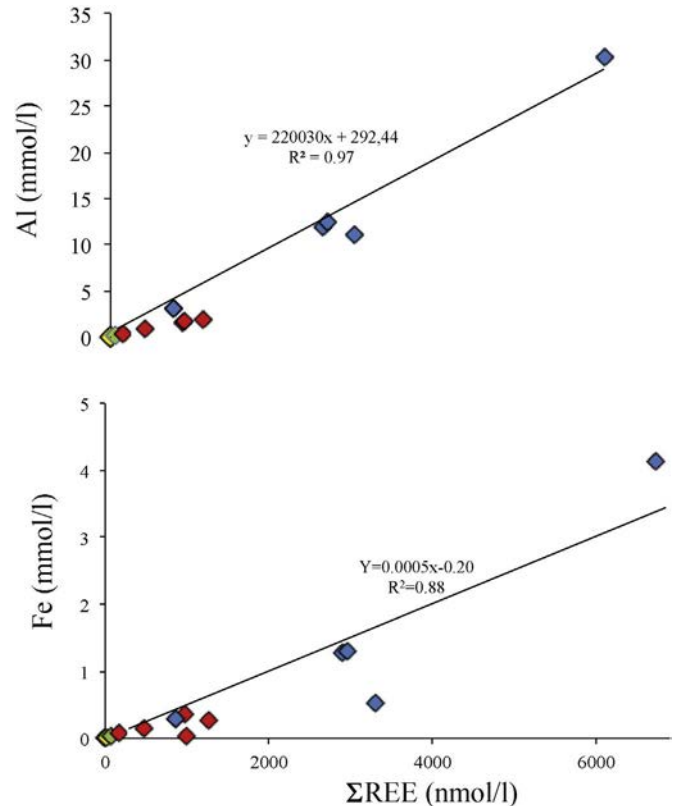


Fig. 9. Total amount of REE versus Fe, Al dissolved in waters. Symbols as in Fig. 3.

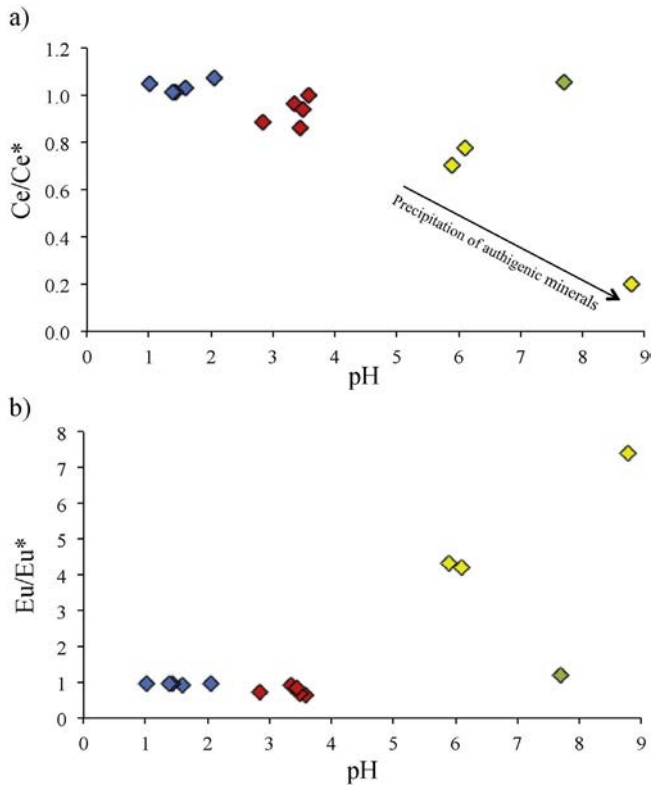


Fig. 10. a) Relationship between Cerium anomaly and pH values. b) Relationship between Europium anomaly and pH values. Symbols as in Fig. 3.

local rock change as function of processes occurring in the shallower and/or deep system. The major anions play an important role on the distribution of REE driven by complexation, whereas the pH values rule the precipitation of solid phases, also fractionating the REE. Negative cerium anomaly in water with near-neutral pH underscores the importance of authigenic minerals (Fe-, Al-oxyhydroxides) on the fractionation of REE, indicating a different behaviour of Ce with respect to the neighbouring elements. Moreover, the precipitation of alunite and jarosite strongly fractionate the REE distribution in Group 2b, depleting the LREE in the aqueous phase.

For the first time, Y–Ho and Zr–Hf behaviour was studied simultaneously in a wide range of pH and chemical composition of major anions. The precipitation of Al-, Fe-oxyhydroxides occurs when pH

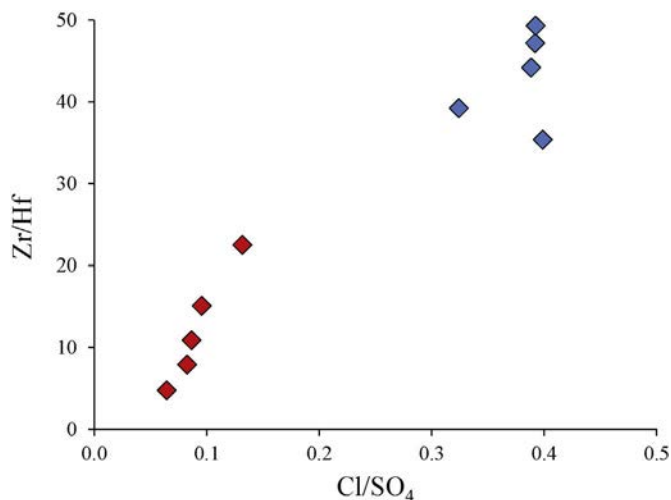


Fig. 11. Zr/Hf versus Cl/SO₄ (molar ratios) in acidic waters (Group 2). Symbols as in Fig. 3.

values are close to neutrality fractionating Y–Ho and Zr–Hf, with a preferential Ho and Hf removal. A different behaviour of Y–Ho and Zr–Hf was identified in acidic sulphate waters with different content of chloride. Y/Ho displays chondritic ratios, showing a negligible fractionation compared to the local rock, whereas Zr/Hf ratios are sub-chondritic, increasing as Cl/SO₄ ratios increase. This evidence suggests a different stability of chemical complexes of Zr and Hf with Cl and SO₄ ligands, leading to sub-chondritic Zr/Hf ratios in strong acid environments.

Acknowledgements

We thank Dr. Yuri Taran and Dr. Johan C. Varekamp for the useful suggestions in an earlier version of the manuscript. We also thank Dr. David R. Hilton for the editorial handling and two anonymous reviewers for constructive comments that improved the quality and the clarity of the manuscript.

This work is part of the doctoral thesis of the first author and was supported by: the Università degli Studi di Palermo, the Université Pierre et Marie Curie, the Università Italo-Francese, the Istituto Nazionale di Geofisica e Vulcanologia (Palermo) and the Servicio Geológico Colombiano.

References

- Alibo, D.S., Nozaki, Y., 1999. Rare earth elements in seawater: particle association, shale normalization, and Ce oxidation. *Geochim. Cosmochim. Acta* 63, 363–372.
- Ayers, G., 2012. Behaviour of the REE During Water Rock Interaction and Alteration Processes in Volcanic Lake Systems (Ms thesis) Utrecht University, The Netherlands, pp. 1–108.
- Bao, S., Zhou, H., Pensg, X., Ji, F., Yao, H., 2008. Geochemistry of REE and yttrium in hydrothermal fluids from the Endeavour segment, Juan de Fuca Ridge. *Geochem. J.* 42, 359–370.
- Bau, M., 1996. Controls on the fractionation of isoivalent trace elements in magmatic and aqueous systems: evidence from Y/Ho, Zr/Hf, and lanthanide tetrad effect. *Contrib. Mineral. Petrol.* 123, 323–333.
- Bau, M., 1999. Scavenging of dissolved yttrium and rare earths by precipitating iron oxyhydroxide: experimental evidence for Ce oxidation, Y–Ho fractionation, and lanthanide tetrad effect. *Geochim. Cosmochim. Acta* 63 (1), 67–77.
- Bau, M., Dulski, P., 1999. Comparing yttrium and rare earth in hydrothermal fluids from the Mid-Atlantic ridge: implications for Y and REE behaviour during near-vent mixing and for the Y/Ho ratio of Proterozoic seawater. *Chem. Geol.* 155, 77–90.
- Bau, M., Koschinsky, A., 2009. Oxidative scavenging of cerium on hydrous Fe oxide: evidence from the distribution of rare earth elements and yttrium between Fe oxides and Mn oxides in hydrogenetic ferromanganese crusts. *Geochem. J.* 43, 37–47.
- Borrero, C., Toro, L.M., Alvarán, M., Castillo, H., 2009. Geochemistry and tectonic controls of the effusive activity related with ancestral Nevado del Ruiz volcano, Colombia. *Geofis. Int.* 1, 149–169.
- Byrne, R.H., 2002. Inorganic speciation of dissolved elements in seawater: the influence of pH on concentration ratios. *Geochem. Trans.* 3, 11–16.
- Censi, P., Sprovieri, M., Saiano, F., Di Geronimo, S.I., Larocca, D., Placenti, F., 2007. The behaviour of REEs in Thailand's Mae klong estuary: suggestions from the Y/Ho ratios and lanthanide tetrad effects. *Estuar. Coast. Shelf Sci.* 71, 569–579.
- Censi, P., Saiano, F., Zuddas, P., Nicosia, A., Mazzola, S., Raso, M., 2014. Authigenic phase formation and microbial activity control Zr, Hf, and rare earth element distributions in deep-sea brine sediments. *Biogeosciences* 11 (4), 1125–1136.
- Censi, P., Cangemi, M., Brusca, L., Madonia, P., Saiano, F., Zuddas, P., 2015. The behavior of rare-earth elements, Zr and Hf during biologically-mediated deposition of silica-stromatolites and carbonate-rich microbial mats. *Gondwana Res.* 27, 209–215.
- Colvin, A., Rose, W.I., Varekamp, J.C., Palma, J.L., Escobar, D., Gutierrez, E., Montalvo, F., Maclean, A., 2013. Crater lake evolution at Santa Ana volcano (El Salvador) following the 2005 eruption. *Geol. Soc. Am. Spec. Pap.* 498, 23–44.
- Elderfield, H., Upstillgoddard, R., Sholkovitz, E.R., 1990. The rare-earth elements in rivers, estuaries, and coastal seas and their significance to the composition of ocean waters. *Geochim. Cosmochim. Acta* 54, 971–991.
- Feng, J.L., 2010. Behaviour of rare earth elements and yttrium in ferromanganese concretions, gibbsite spots, and the surrounding terra rossa over dolomite during chemical weathering. *Chem. Geol.* 271, 112–132.
- Firdaus, M.L., Minami, T., Norisuye, K., Sohrin, Y., 2011. Strong elemental fractionation of Zr–Hf and Nb–Ta across the Pacific Ocean. *Nat. Geosci.* 4, 227–230.
- Forero, J., Zuluaga, C., Mojica, J., 2011. Alteration related to hydrothermal activity of the Nevado del Ruiz volcano (NRV), Colombia. *Bol. Geol.* 33, 59–67.
- Frank, M., 2011. Oceanography: chemical twins, separated. *Nat. Geosci.* 4, 220–221.
- Gammons, C., Wood, S., Pedrozo, F., Varekamp, J.C., Nelson, B.J., Shope, C.L., Baffico, G., 2005. Hydrogeochemistry and rare earth element behaviour in a volcanically acidified watershed in Patagonia, Argentina. *Chem. Geol.* 222, 249–267.
- Giggenbach, W.F., Garcia, N., Londono, A., Rofriguez, L., Rojas, N., Calvache, M.L., 1990. Chemistry of fumarolic vapor and thermal-spring discharges from the Nevado del Ruiz volcanic-magmatic-hydrothermal system, Colombia. *J. Volcanol. Geotherm. Res.* 42, 13–39.

- Godfrey, L.V., White, W.M., Salters, V.J.M., 1996. Dissolved zirconium and hafnium distributions across a shelf break in the northeastern Atlantic Ocean. *Geochim. Cosmochim. Acta* 60, 3995–4006.
- Godfrey, L.V., Field, M.P., 2008. Estuarine distributions of Zr, Hf, and Ag in the Hudson River and the implications for their continental and anthropogenic sources to seawater. *Geochim. Geophys. Geosyst.* 9, 359–370.
- Goldstein, S.J., Jacobsen, S.B., 1988. Rare earth elements in river waters. *Earth Planet. Sci. Lett.* 89, 35–47.
- Hikov, A., 2011. Rare earth element mobility during hydrothermal alteration in Asarel porphyry copper deposit, central Srednogie. *C. R. Acad. Bulg. Sci.* 64 (8), 2011.
- Kalacheva, E., Taran, Y., Kotenko, T., 2015. Geochemistry and solute fluxes of volcano-hydrothermal system of Shiashkotan, Kuril Islands. *J. Volcanol. Geotherm. Res.* 296, 40–54.
- Koschinsky, A., Hein, J.R., 2003. Uptake of elements from seawater by ferromanganese crusts: solid-phase associations and seawater speciation. *Mar. Geol.* 198, 331–351.
- Lewis, A.J., Palmer, M.P., Sturchio, C., Kemp, A.J., 1997. The rare earth element geochemistry of acid sulphate and acid sulphate–chloride geothermal system from Yellowstone National Park, Wyoming, USA. *Geochim. Cosmochim. Acta* 61, 695–706.
- Lewis, A.J., Komninou, A., Yardley, B.W., Palmer, M.R., 1998. Rare earth element speciation in geothermal fluids from Yellowstone National Park, Wyoming, USA. *Geochim. Cosmochim. Acta* 62, 657–663.
- Michard, A., 1989. Rare earth element systematics in hydrothermal fluids. *Geochim. Cosmochim. Acta* 53, 745–750.
- Millero, F.J., 1992. Stability-constants for the formation of rare-earth inorganic complexes as a function of ionic-strength. *Geochim. Cosmochim. Acta* 56, 3123–3132.
- Monroy-Guzman, F., Trubert, D., Brillard, L., Hussonnois, M., Constantinescu, O., Le Naour, C., 2010. E Anion Exchange Behaviour of Zr, Hf, Nb, Ta and Pa as Homologues of Rf and Db in Fluoride. *Medium. J. Mex. Chem. Soc.* 54 (1), 24–33.
- Parkhurst, D.L., Appelo, C.A.J., 2010. User's guide to PHREEQC (Version 2.17.5)—a computer program for speciation, batch-reaction, One-Dimensional Transport and Inverse Geochemical Calculations (Available at: http://www.brr.cr.usgs.gov/projects/GWC_coupled/phreeqc/index.html).
- Piper, D.Z., Bau, M., 2013. Normalized rare earth elements in water, sediments, and wine: identifying sources and environmental redox conditions. *Am. J. Anal. Chem.* 4, 69–83.
- Peiffer, L., Taran, Y., Lounejeva, E., Solís-Pichardo, E., Rouwet, D., Bernard-Romero, R.A., 2011. Tracing thermal aquifers of El Chichón volcano-hydrothermal system (Mexico) with $^{87}\text{Sr}/^{86}\text{Sr}$, Ca/Sr and REE. *J. Volcanol. Geotherm. Res.* 205, 55–66.
- Pershina, V., Trubert, D., Le Naour, C., Kratz, J.V., 2002. Theoretical predictions of hydrolysis and complex formation of group-4 elements Zr, Hf and Rf in HF and HCl solutions. *Radiochim. Acta* 90, 869–877.
- Ruberti, E., Castorina, F., Censi, P., Comin-Chiaromonti, P., Gomes, C.B., Antonini, P., Andrade, F.R.D., 2002. The geochemistry of the Barra do Itaipirapua carbonatite (Ponta Grossa Arch, Brazil): a multiple stockwork. *J. S. Am. Earth Sci.* 15 (2), 215–228.
- Schmidt, K., Bau, M., Hein, J.R., Koschinsky, A., 2014. Fractionation of the geochemical twins Zr–Hf and Nb–Ta during scavenging from seawater by hydrogenetic ferromanganese crusts. *Geochim. Cosmochim. Acta* 140, 468–487.
- Seto, M., Tsaku, A., 2008. Chemical condition for the appearance of a negative Ce anomaly in stream waters and groundwaters. *Geochem. J.* 42, 371–438.
- Takano, B., Suzuki, K., Sugimori, K., Ohba, T., Fazlullin, S.M., Bernard, A., Sumarti, S., Sukhyar, R., Hirabayashi, M., 2004. Bathymetric and geochemical investigation of Kawah Ijen Crater Lake, East Java, Indonesia. *J. Volcanol. Geotherm. Res.* 135, 299–329.
- Taran, Y., Rouwet, D., Inguaggiato, S., Aiuppa, A., 2008. Major and trace element geochemistry of neutral and acidic thermal springs at El Chichón volcano, Mexico: implications for monitoring of the volcanic activity. *J. Volcanol. Geotherm. Res.* 178, 224–236.
- Varekamp, J.C., Ouimette, A.P., Herman, S.W., Flynn, K.S., Bermudez, A., Delpino, D., 2009. Naturally acid waters from Copahue volcano, Argentina. *Appl. Geochem.* 24, 208–220.
- Varekamp, J.C., 2015. The chemical composition and evolution of volcanic lakes. In: Rouwet, D., Christenson, B., Tassi, F., Vandemeulebrouck, J. (Eds.), *Volcanic Lakes*, pp. 93–123.
- Wood, S.A., 1990. The aqueous geochemistry of the rare-earth elements and yttrium 1. Review of available low-temperature data for inorganic complexes and the inorganic REE speciation of natural waters. *Chem. Geol.* 82, 159–186.
- Wood, S.A., 2003. The geochemistry of rare earth elements and yttrium in geothermal waters. *Soc. Econ. Geol. Spec. Publ.* 10, 133–158.
- Wood, D.A., Gammons, C.H., Parker, S.R., 2006. The behavior of rare earth elements in naturally and anthropogenically acidified waters. *J. Alloys Compd.* 418, 161–165.